## ABSTRACT

TERRY, JASON CHARLES. Fundamental Studies in Flameless Combustion and Implications to Reaction Zone Structure and Pollutants Formation. (Under the direction of Dr. Tarek Echekki.)

The objective of this study is to investigate numerically the effects of strain rate, methane dilution by nitrogen, and air-side preheat on pollutant and molecular hydrogen production and the reaction zone structure during flameless and flame-based combustion in a non-premixed counter-flow geometry of diluted methane with preheat air. Fundamental flameless and lean flame-based combustion studies are useful in shedding light on their possible uses in fuel reforming, especially as it pertains to the production of cleaner fuels for fuel cell operation, or partial oxidation. The study centers on fuel concentrations from 5 to 15% (by volume) in intervals of 2% along with both varying inlet velocities (the relation to strain rate is described below) of 10 to 60 cm/s in intervals of 10 cm/s, and oxidizer preheat temperatures from 1100 to 2100 K in intervals of 200 K. The geometry is based on axisymmetric counterflow of fuel and oxidizer jets, which are separated by a distance of 5 cm at their inlets. Parametric studies of different fuel dilution rates show that $NO_x$ mass fractions decrease with an increasing strain rate as well as decreasing fuel concentration in both flameless and flame-based combustion, while $NO_x$ mass fractions increased with the air-side preheat temperature. The intermediate species, $H_2$, is found to follow a similar trend to $NO_x$ as preheat temperatures and fuel concentrations were increased; however, varying strain rate has little or no effect on $H_2$ concentrations. The distinct differences in behavior between $NO_x$ and $H_2$ may be attributed primarily to the conflicting roles of strain in both increasing reactants' delivery to the reaction zone and its reduction of chemical residence time. Reaction flux analysis, which elucidates the chemical mechanisms governing the flameless and flame-based modes of burning concerning $NO_x$, shows an important shift in the dominant mechanisms producing NO, from the thermal $NO_x$ mechanism at high preheat temperatures, and to prompt $NO_x$ at lower preheat temperatures.

# FUNDAMENTAL STUDIES IN FLAMELESS COMBUSTION AND IMPLICATIONS TO REACTION ZONE STRUCTURE AND POLLUTANTS FORMATION

by

**JASON CHARLES TERRY**

A thesis submitted to the Graduate Faculty of
North Carolina State University
in partial fulfillment of the
requirements for the Degree of
Master of Science

**MECHANICAL AND AEROSPACE ENGINEERING**

Raleigh

2003

**APPROVED BY:**

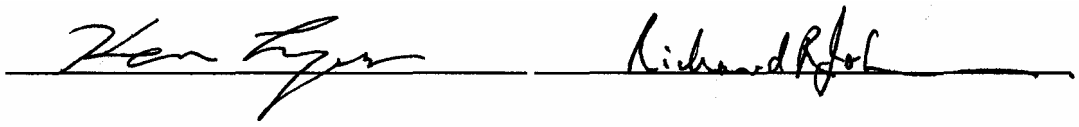

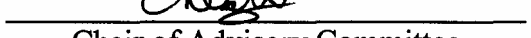

Chair of Advisory Committee

## BIOGRAPHY

Jason Terry was born in South Carolina on June 12, 1977. He is the son of Mike and Ann Terry of Kershaw, SC. He has one brother, Kevin Terry. Jason attended North Central High School, graduating in June, 1995.

Following high school, Jason enrolled in the Mechanical Engineering program at The University of South Carolina at Columbia. While dutifully attending classes and working towards a Bachelor of Science in Mechanical Engineering, he worked part-time and completed three semesters of co-op and intern experience. In May of 2000, he graduated from The University of South Carolina with a Bachelor of Science degree in Mechanical Engineering.

Following graduation, Jason began work in New Hill, North Carolina at the Shearon Harris Nuclear Power Plant as a Mechanical Design Engineer where he worked for 1½ years before enrolling in Graduate School at North Carolina State University. While pursuing a Master's of Science in Mechanical Engineering at NC State, Jason worked part time as a Mechanical Design Engineer at the Shearon Harris Nuclear Power Plant as well as a Teaching Assistant for NC State University's Department of Mechanical and Aerospace Engineering.

Jason has now graduated from NC State University and his stress level has been drastically reduced.

## ACKNOWLEDGEMENTS

First of all, I would like to thank God for giving me the ability to achieve all that I have and to strive for success in life. I also would like to thank my family for the constant support through friendship, guidance, and most importantly…love. I would like to thank Dr. Tarek Echekki who has made it possible through his calming guidance (however much we frustrated each other at times) for me to complete this work while still retaining my sanity. I would also like to thank my various professors and mentors here at NC State and The University of South Carolina for providing me with a strong fundamental knowledge of Mechanical Engineering, without which, I would be lost in a sea of reaction mechanisms, radiation view factors, and conservation equations. And last, but definitely not least, I would like to thank my friends and in particular my girlfriend…without these guys (and gals), I'd be lost in a sea of happy hours, one room apartments, and lonely Friday nights.

## TABLE OF CONTENTS

## LIST OF FIGURES

### CHAPTER 3



### CHAPTER 4

# CHAPTER I

# INTRODUCTION

## 1.1. Motivation

The power density of hydrocarbon fuels is widely known to be high in comparison to that of a battery and has been seen to be as high as 100 times that of standard batteries. With this in mind, the logical choice of power sources for electronic devices would be those with combustion based power sources. However, it is also well know that the combustion process (using almost all available hydrocarbon fuels) produces harmful pollutants. Gases such as NO, $NO_2$, and $NO_3$ (generally known as $NO_x$) along with CO and unburned hydrocarbons such as $CH_4$, $CH_3OH$, and $C_2H_6$ have all been found in one way or another to adversely affect our environment and our health. Through research and modeling, it has been found that depending upon the type of fuel, the levels of these pollutants can be lowered when the combustion temperature is lowered. This is demonstrated in the use of EGR in a normal internal combustion engine to lower $NO_x$ production. An important obstacle in the development for mass production and use of both micro scale (on the order of a millimeter) and macro scale (on the order of a centimeter) combustion is the lowering of harmful pollutants while still obtaining the same or a comparable energy output, which scales with the peak flame temperature.

Relatively recently in the world of combustion research, a new technology that is referred to as "flameless combustion" has emerged. This technology as been shown to be an effective means for lowering combustion temperatures and effectively lowering pollutant concentrations, more particularly $NO_x$ production. Flameless combustion is the dominant combustion mode for a number of emerging applications in which temperature peaks associated with flames are avoided to yield lower emissions (Wünning and Wünning, 1997) or partial oxidation of the fuel. Various strategies for achieving flameless oxidation of hydrocarbon fuels have been proposed in recent years, which include flame cooling by dilution with inert species or products, staging, which involves the reburning of partially burnt products, exhaust gas recirculation, operation at very lean conditions. In its practical use, flameless oxidation is implemented under turbulent flow conditions, and the tight

coupling between chemistry and molecular and turbulent transport is very important to achieve lower emissions. However, fundamental studies of flameless combustion are relatively limited in comparison to a host of experimental and computational fluid dynamics studies, based on the Reynolds-Averaged Navier-Stokes (or RANS) equations approaches. This study will explore the effects of strain rate on the species concentrations and the temperature profile as an important contribution of turbulence to the combustion process.

## 1.2. Objectives

The objective of this thesis is to understand the effects of fuel dilution, oxidizer preheat temperature and strain rate on flameless and flame-based combustion using numerical simulations of a canonical flow, the counterflow of non-premixed fuel and preheated air streams. In particular, the study will investigate the effects of these three parameters, fuel dilutions, oxidizer preheat temperature and strain rates, on the formation of thermal $NO_x$ for a mixture of methane with nitrogen dilution. The understanding of the role of these three parameters is important towards the implementation of flameless combustion-based technologies, which is characterized in practice by the prevalence of turbulence as the primary mechanism of fuel and oxidizer mixing, and the corresponding effects of unsteadiness on the introduction of additional time scales that govern the coupling of chemistry and transport. Fuel dilution and oxidizer preheat temperatures will impact primarily the chemical kinetics associated with combustion, and secondarily the transport with the reaction zone. The strain rate contribution is relatively more complex as it impacts primarily the residence time of species in the reaction zone, and in the process alters the degree of completion of reaction. All three parameters are expected to affect the structure of the reaction zone in a flame-based or flameless combustion mode, and alter the rate of production of $NO_x$, and the dominant mechanisms responsible for its production.

## 1.3. Outline

The present study is based on parametric simulations of non-premixed streams of methane with nitrogen dilution and preheated air. Therefore, the present work is organized as follows. First, a review of the literature relevant to this study is presented in Chapter 2. Then, the numerical implementation based on Sandia's Oppdif code (1996) is described in Chapter 3.

A discussion of the various quantities and post-processing tools used is presented in Chapter 4. Then, a discussion of the results follows in Chapter 5. Since the study is equally interested in the roles of the above-mentioned three parameters on reaction zone structure and pollutants' formation in flameless combustion, which are discussed in detail for each parameter in Chapter 5, synthesis of the main results and discussion of the implications of the findings to the modeling of turbulent combustion in the flameless mode follows in Chapter 6. Finally, conclusions and future work are presented in Chapter 7. The appendix will outline the solution mechanisms and governing equations used in the Oppdif code (1996).

## CHAPTER II

## A REVIEW OF RELEVANT LITERATURES ON FLAMELESS COMBUSTION

The principal motivation for the use of flameless combustion is the associated reduction in NO emissions that is obtained through the control of product temperatures and the degree of completion of reactions. Wünning and Wünning (1997) reviewed flameless oxidation (combustion) using experimental and numerical techniques. The study reveals the ability of flameless combustion to lower $NO_x$ emissions through lowered adiabatic flame temperatures. The study, however, used lower inlet air temperatures than the study presented below and did not include a reaction flow analysis study.

Ju and Niioka (1997) studied NO formation in a non-premixed two-dimensional laminar jet flame, another canonical configuration for the understanding of the effects of turbulence on combustion. The study shows that the formation of prompt NO is observed in the flame reaction zone, while the thermal NO mechanism is the predominant path for NO formation on the high-temperature air side. The emission index of NO was shown to have a high sensitivity to the oxidizer preheat temperature, increasing drastically with an increasing preheat temperature.

Recently, Maruta et al (2000) investigated the flameless combustion of methane with nitrogen dilution and air in a laminar counterflow geometry, which is similar the geometry adopted in this study. The study revealed that when the oxidizer temperature is high (1500 K) and the fuel is at a concentration of 5%, flameless combustion can be observed. However, Maruta et al. did not investigate the effects of strain rate or preheat temperature on that same reaction zone structure along with the associated mechanism response. In many practical applications, flameless and flame-based combustion occurs in turbulent flow conditions. The burning conditions at various fuel strengths are expected to be strongly effected by strain conditions.

Sohn et al (2002) studied the effects of pressure and air-dilution on the formation of NO in a laminar counterflow geometry. Specifically, the study explored the individual reaction steps under pressure changes without diluting the fuel (methane). Their results showed that at a

pressure of 1 atm, reactions 210, 212, 213, 272, and 247 (http://www.me.berkeley.edu/gri_mech/) played an important role in both the consumption and production of thermal $NO_x$. However, this study relied on flame-based combustion using a pure (non-diluted) fuel mixture. The study presented here uses the GRI-Mech 3.0 (http://www.me.berkeley.edu/gri_mech/). This mechanism is widely used to model natural gas combustion, including the formation of $NO_x$.

# CHAPTER III

## Numerical Implementation and Diagnostics

In this chapter, the computational approach and important numerical diagnostic methods used are presented. The simulations are implemented using Sandia's Oppdif code (1996). Additional post-processing is carried out on spatial profiles of species and temperature that are generated in these simulations.

### 3.1. Computational Method (CHEMKIN Library and Application)

Oppdif is an application used to compute the solution of several parameters, i.e. temperature, species, axial (and subsequently radial or planar), and the perpendicular pressure gradients, in an opposed flow diffusion flame. Inherently, a diffusion flame must be considered in at least 2 dimensions. Oppdif, however, uses a similarity solution to reduce the problem to a one dimensional flow field. The TWOPNT software (see below) is used to solve the boundary value problem, while the CHEMKIN thermodynamic property library is employed to solve for the properties necessary for a solution. The governing equations used for the numerical solution technique are described in Appendix A.

### 3.2. Mixture Fraction and Flame Thinning

Profiles of species and temperature from the Oppdif code are further analyzed to implement reaction flow analysis. Moreover, it is found that plotting species and temperature, and reaction profiles in mixture fraction space yields a better comparison for different conditions of strain, because of flame thinning effects on spatial profiles. Here, we use a weighted mixture fraction, the Bilger mixture fraction, based on the analysis by Bilger et al. (1990). It is defined using the following expression:

$$\xi = \frac{\left[2\left(Z_C - Z_{C,\,Oxid}\right)/W_C + \left(Z_H - Z_{H,\,Oxid}\right)/2W_H - \left(Z_O - Z_{O,\,Oxid}\right)/W_O\right]}{\left[2\left(Z_{C,\,F} - Z_{C,\,Oxid}\right)/W_C + \left(Z_{H,\,F} - Z_{H,\,Oxid}\right)/2W_H - \left(Z_{O,\,F} - Z_{O,\,Oxid}\right)/W_O\right]} \qquad [1]$$

where $Z_i = \sum_{j=1}^{N} \mu_{i,j} Y_j$ for N species and $W_i$ is the atomic weight of each element.

The Bilger mixture fraction essentially removes the spatial information from the data and allows two different strain rates to be compared on an equal scale. This is seen in the case

where strain rate increases, which may result in the reaction zone becoming thinned and/or shifted in position (see Section 3.2). This makes it difficult to truly compare two profiles for different strain rates. Removing that data by using the Bilger mixture fraction allows the strain rates to be compared on an equal scale.

The stoichiometric mixture fraction is also a useful quantity. This value represents at a particular fuel concentration what mixture fraction value corresponds to stoichiometric conditions. This can be useful, since the flame in a non-premixed counterflow (or jet) diffusion flame tends to exist near or at stoichiometric conditions. The stoichiometric global reaction for methane diluted with $N_2$ in air with the fuel concentration given as $\phi$ is

$$\left(\frac{1-\phi}{\phi}N_2 + C_4\right) + 2O_2 + 7.52N_2 \rightarrow CO_2 + 2H_2O + \left(7.52 + \frac{1-\phi}{\phi}\right)N_2 \quad [2]$$

The stoichiometric mixture fraction, $\xi_{st}$, is represented in the equation as follows.

$$\xi_{st} = \frac{Z_{H,st} - Z_{H,O}}{Z_{H,F} - Z_{H,O}} \quad [3]$$

Since H is not found in the oxidizer, $Z_{H,O}$ is zero. The elemental contribution of H in $CH_4$ is $\mu_{H,CH_4} = 1/4$, while the mass fraction of $CH_4$ at stoichiometric conditions is found as follows.

$$Y_{CH_4,st} = \frac{n_{CH_4}\left(W_{CH_4}\right)}{n_{CH_4}\left(W_{CH_4}\right) + n_{O_2}\left(W_{O_2}\right) + n_{N_2}\left(W_{N_2}\right)} \quad [4]$$

Inserting the known number of moles of each species and the known molecular weights results in the following equation:

$$Y_{CH_4,st} = \frac{(1)(16)}{(1)(16) + (2)(32) + \left(7.52 + \frac{1-\phi}{\phi}\right)(28)} \quad [5]$$

The mass fraction of $CH_4$ in the fuel can be found as follows.

$$Y_{CH_4,F} = \frac{(1)(16)}{(1)(16)+\left(\frac{1-\phi}{\phi}\right)(28)} \quad [6]$$

Using the fuel concentrations as fractions, i.e. 0.15, 0.13, etc., results in six stoichiometric mixture fractions, which are given below.

| ***Fuel Concentration*** | ***Stoichiometric Mixture Fraction*** |
|---|---|
| 15% | 0.3888 |
| 13% | 0.4255 |
| 11% | 0.46904 |
| 9% | 0.5214 |
| 7% | 0.58561 |
| 5% (Flameless) | 0.666213 |

**Table 3.1** Stoichiometric Mixture Fraction vs Fuel Concentration

When a strain is applied to a diffusion flame, the flame tends to thin. This is due to an increase in the perpendicular (or radial) velocity with increasing inlet velocity caused by conservation of mass at the stagnation plane (see Fig. 4.1 repeated from Maruta et al, 2000, below). This perpendicular velocity increase tends to transport the species that diffuse across the stagnation plane further away from the origin (or axis) and therefore lowering the mass fraction of fuel that has diffused into the oxidizer. With a smaller mass fraction of fuel available as x increases due to more of the diffused fuel being transported further along the y axis, there are, therefore, less reactants available for chemistry in the x-direction. This would mean that the actual distance in x occupied by a flame is smaller and therefore, the flame is thinned.

Due to the decrease in flame thickness, the spatial profiles of the intermediate species and products should be thinned, i.e. their parabolic spatial profile in X would become thinned as well. Figure 3.2 shows this through the product $H_2O$.

Whether in flame-based or flameless mode, species and temperature profiles respond to strain by 'flame thinning' as shown in Fig. 3.2 for spatial profiles of $H_2O$ at different strain rates. Plotting profiles in terms of the Bilger mixture fraction correlates well different operating conditions (reactants, inlet velocities and preheat temperatures) as illustrated in Fig. 3.3. Figure 3.3 shows a plot of the fuel, oxidizer, and product of a 15% methane counter-flow diffusion flame at 24 $sec^{-1}$ strain rate.

It can be seen from Fig.'s 3.4 and 3.5 that the fuel and oxidizer follow a similar pattern, only reversed and that the temperature plot shows a different profile than the spatial plot presented earlier. This is due to the relative weighting of the Bilger Mixture Fraction by the Mass Fractions. The flame is located where these two go to zero and the products (in this case $H_2O$ and $CO_2$) and the products reach their peak.

## 3.3. Emission Index

The emission index for NO is a convenient way of describing the amount of NO produced per gram of fuel. It is a global quantity representing the amount of species formed (through the reaction rate of that species) to the amount of fuel. This quantity can be used to compare different fuel concentrations along with different strain rates and preheat temperatures. The relationship for the Emission Index of NO used in this study is given as follows.

$$EI_{NO} = \frac{W_{NO}\int_0^L \omega_{NO}\,dx}{W_{CH_4}\int_0^L \omega_{CH_4}\,dx} \qquad [6]$$

where, *W* refers to the molecular weight of the species associated with the index, and ω is the net production rate in mols/($cm^3$ sec). The length scale, *L*, corresponds to the length of the computational domain, and refers physically to the separation distance between the fuel and oxidizer jet inlets. The integral here is carried out by applying the trapezoid rule to the data

gathered by the Oppdif postprocessor for the Reaction Rates for each species. The index has dimensions of $\left[ gm_{NO} \middle/ kgm_{CH_4} \right]$. In addition to the global contribution from all reactions involving the production and consumption of NO, the relative contributions of thermal, prompt, reburn and $N_2O$ mechanisms are also evaluated to identify possible shifts in the dominant NO chemistry as a function of the computational parameters.

### 3.4. Reaction Rate

All chemical reactions take place at a finite rate, which of course depends on many factors such as temperature, fuel dilution, strain rate, etc. The law of mass action states that the rate of disappearance of a species is proportional to the product of the concentrations of the reacting species, where each of those concentrations is raised to a power equal to the corresponding Stoichiometric coefficient (Glassman, 1996). This means that rate of change in the concentration of a species is proportional to the concentrations of all species involved in the reaction as well as the reaction Stoichiometric coefficients, which results in an inherent dependence of species production (and consumption) on elementary reaction steps.

By exploring the individual contributions of individual reactions allows the effects of strain rate to be seen on certain reactions deeming them negligible or significant. Given any global individual reaction, there are of course numerous elementary reactions that take place, such as N+OH ↔ NO+H and NO+O+M ↔ $NO_2$+M. Investigating the effects strain rate, fuel concentration, and preheat temperature have on the contributions of these reactions to producing (or consuming) $NO_x$ may shed light on the mechanism itself and how to reduce these harmful emissions.

The reaction rates presented in this study are in units of $sec^{-1}$, which correspond to the product of the reaction rate (in moles/$cm^3$/s) by the molecular weight and its division by the mixture density. The OPPDIF post processing code uses a filter to remove the unimportant reactions as well as scale (or normalize) the overall reaction rate by $\dot{\omega}_k W_k / \rho$.

## 3.5. $NO_x$ Formation and Mechanism

Glassman (1996) identifies three mechanisms for the formation of NO in combustion: 1) The oxidation of atmospheric (from the oxidizer stream) $N_2$ via thermal NO mechanisms, 2) prompt NO mechanisms; and 3) oxidation of nitrogen-containing compounds in fossil fuels. In the present study, we are concerned with the first two mechanisms, thermal and prompt $NO_x$ formations.

The thermal mechanisms are described by the extended Zel'dovich mechanism:

$$O + N_2 \leftrightarrow NO + N,$$
$$N + O_2 \leftrightarrow NO + O,$$
$$N + OH \leftrightarrow NO + H$$

Additional considerations based on the assumption of steady state N concentrations and partial equilibrium for the reaction, $H + O_2 \leftrightarrow OH + O,$ the rate production of NO may be expressed in terms of the rate constants for the reactions above, and the concentrations of O, $O_2$, $N_2$ and NO. This overall rate increases with the temperature of the mixture along with the concentration of intermediate species such as O. This study will focus on those reactions associated with the extended Zel'dovich mechanism. Thermal NO has been seen through various studies (Glassman, 1996) to be highly temperature dependent and due to the lack of dependence on the fuel, thermal No formation has been found to be prominent outside the reaction zone.

Prompt NO mechanisms are relatively more complex and mechanisms for prompt NO formation has been developed with reasonable confidence only recently (Miller and Bowman, 1989). Prompt NO is formed when the nitrogen in the air reacts to form CN compounds, which subsequently can react and form NO. Prompt NO is usually found within the reaction zone as a reaction with the fuel is needed to produce the CN compounds necessary for the formation of prompt NO.

The two mechanism discussed above are considered within most current literature and study to be the most important forms of NO production. Therefore, these two are the focus of this study. It is imperative, however, to note that since these two mechanisms are present both outside and inside (prompt) and outside (thermal) the reaction zone. As will be seen later, it

will be therefore difficult to compare the two in mixture fraction space. However, the integral of these two over the entire mixture fraction domain will allow the relative contributions to be studied and their individual contribution to the overall reaction to be determined.

The mechanism that governs the formation of $NO_x$ has been well studied and documented, however, total agreement of a concrete mechanism that fully governs the production of nitrous oxides has not been reached. The GRI-Mech mechanism (http://www.me.berkeley.edu/gri_mech/) is used to represent the individual elementary reactions involved in the gas phase combustion of natural gases (such as methane and propane) as part of the whole global reaction (Glassman, 1996). The full GRI-Mech 3.0 mechanism for the combustion of methane is given in Appendix B.

### 3.6. Computational Configuration and Conditions

The configuration used in this study is a counterflow of fuel and oxidizer. The solution is computed using Sandia's Oppdif code along with the GRI-Mech 3.0 mechanism (Glassman, 1996) for methane and $NO_x$ chemistries. The range of fuel concentrations is 5 to 15% at intervals of 2%, while the velocity ranges from 10 to 60 cm/s at intervals of 10 cm/s. The preheat temperature ranges from 1100 to 2100 K in intervals of 200 K, while the fuel inlet temperature was taken as a constant 300 K. The separation distance between the two inlets is 5 cm. Using the definition for strain rate stated above, the resulting strain rates are 4, 8, 12, 16, 20 and 24 all in units of $sec^{-1}$.

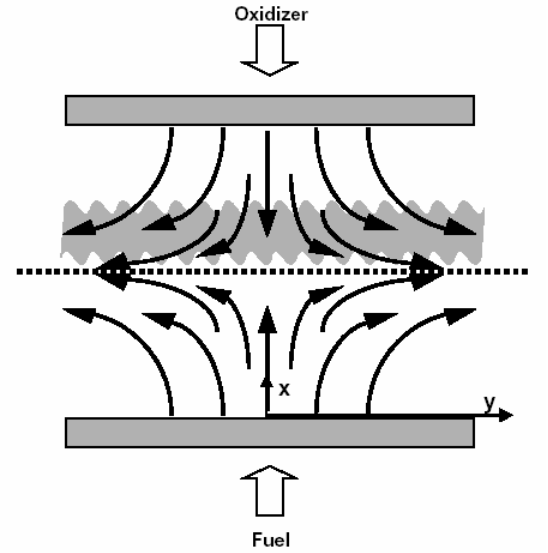


**Figure 3.1.** Planar Diffusion Flame (from Appendix I).

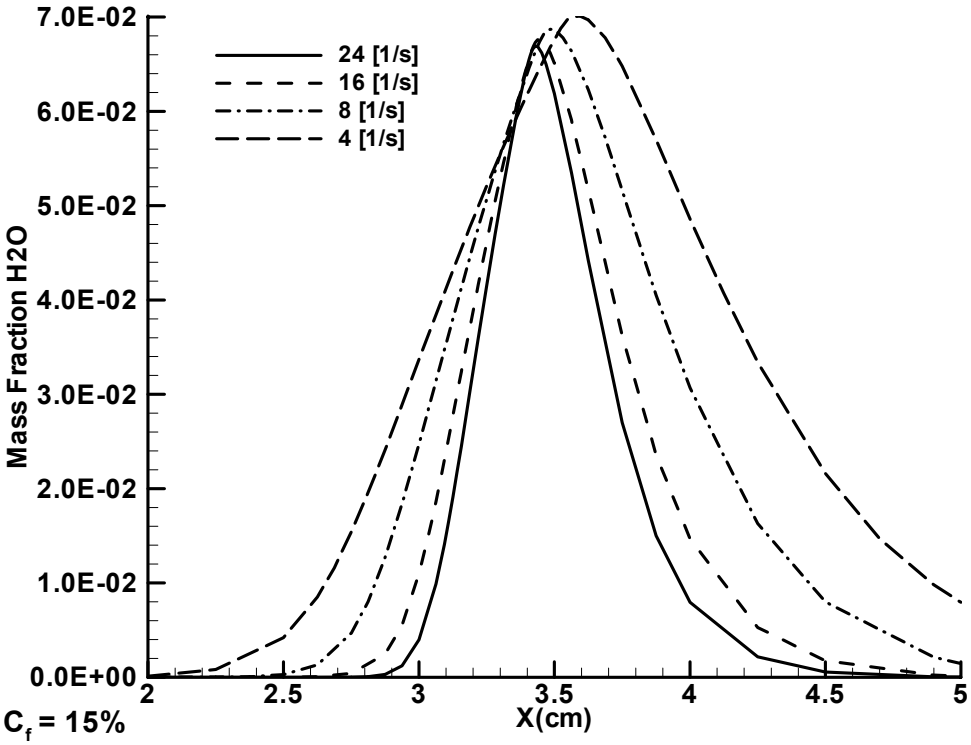


**Figure 3.2.** Spatial Profile of $H_2O$ for Varying Inlet Velocities (Strain Rates)

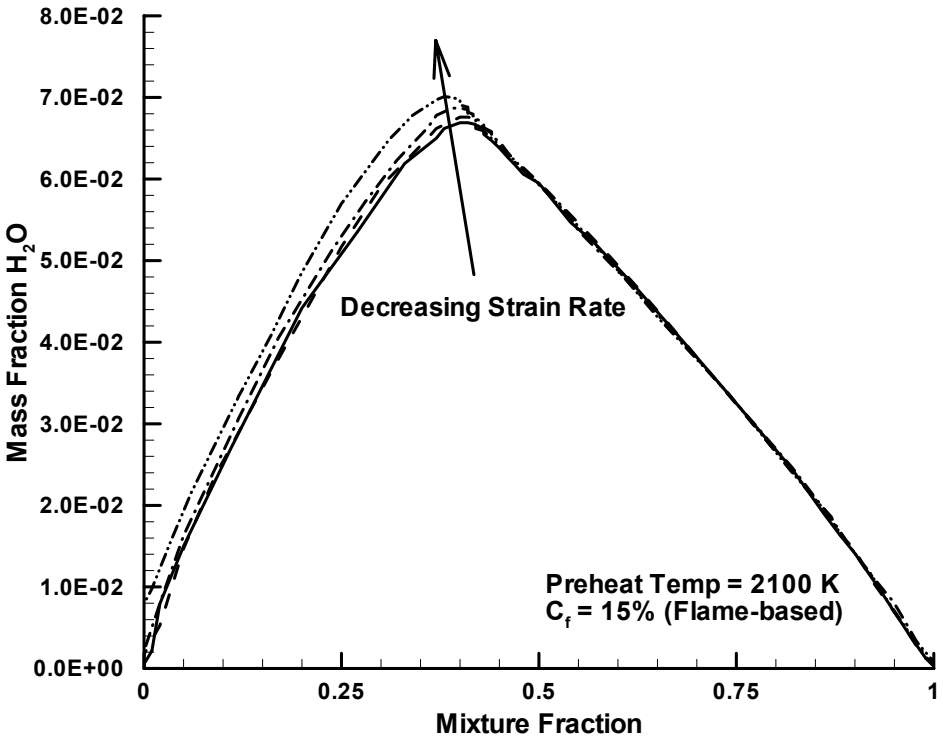


**Figure 3.3.** Profile of $H_2O$ vs Mixture Fraction for Varying Inlet Velocities (Strain Rates)

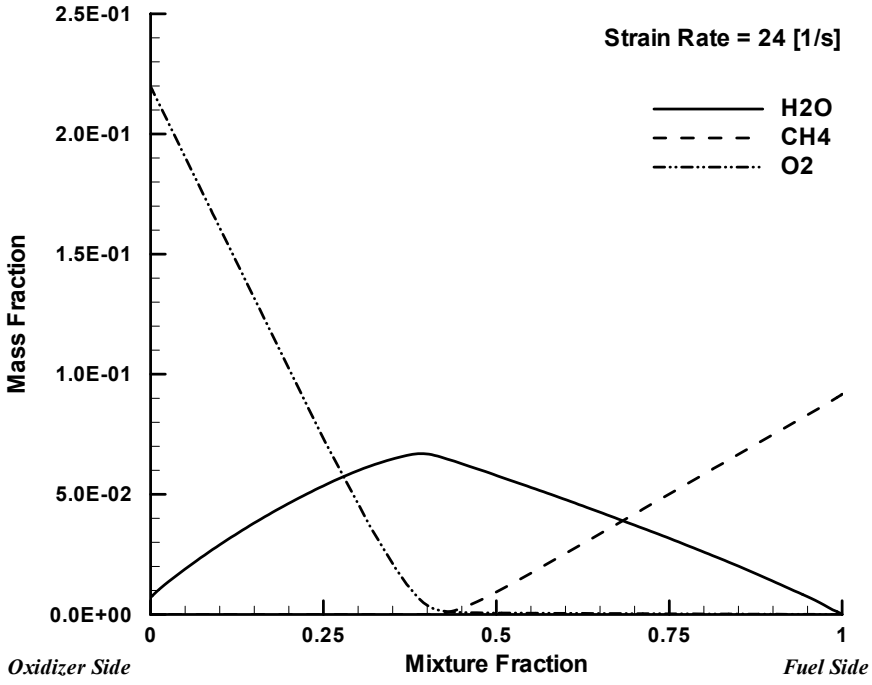


**Figure 3.4.** Reactants and Water for 15% Methane

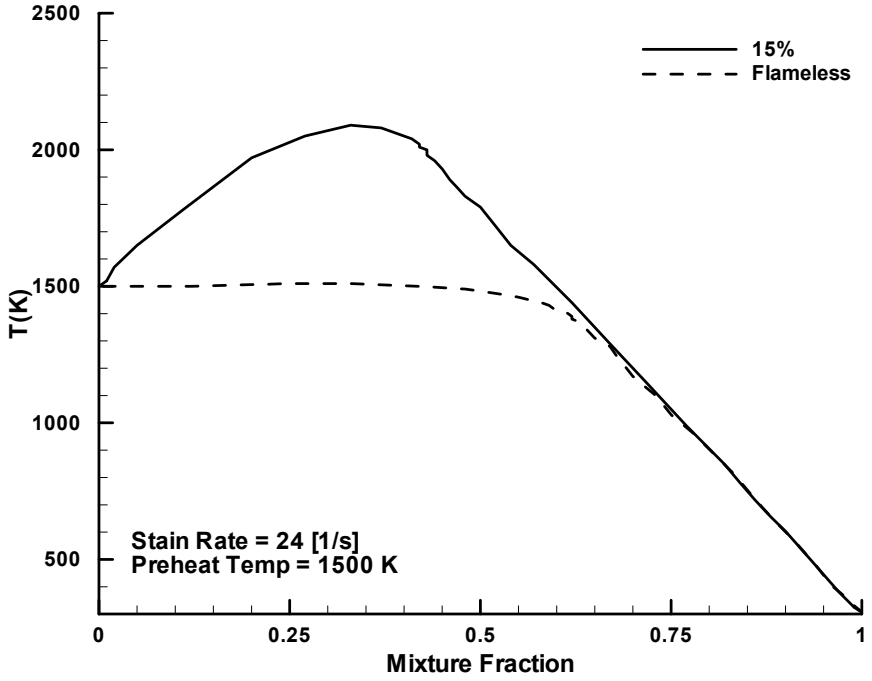


**Figure 3.5.** Temperature Profile in Mixture Fraction Space for Flame-based vs Flameless

# CHAPTER IV

# RESULTS

This chapter presents results of the parametric computations of the effects of fuel concentration, strain rate, and oxidizer preheat temperature on the reaction zone structure and $NO_x$ formation under flame-based and flameless conditions. The discussion is based on identifying the separate contributions of the above parameters, as outlined in the sections below. Chapter V provides a synthesis of the relative contributions of these parameters and implications to the modeling of these contributions in practical problems. In the following sections, the computational approach is benchmarked against the results by Maruta et al. (2000). Then, results are presented for the effects of the three different parameters considered separately. In addition to the various computational diagnostic approaches discussed in the previous chapter, the presentation will also adopt the strategy of comparison of NO profiles to another intermediate, $H_2$. The two intermediates are characterized by different dominant production and consumption mechanisms that yield different and disparate rates, with $H_2$ being the faster produced and consumed. An important consequence for the differences between the two species is that both may respond differently to changes in fuel concentration, oxidizer preheat temperature and strain rate.

## 4.1. Benchmark of Combustion Code

Maruta et al. (2000) describe the reaction zone structure of a high temperature air diffusion (non-premixed) flame ("flameless combustion"). This study showed through computation and experiment that the burning of methane and highly preheated air in a flameless combustion process produced results depicting the behavior of $NO_x$ with fuel concentration; yet do not provide a comparison to other fuels as well as other more typical combustion processes.

The Maruta study employed a one dimensional numerical solution technique, which allowed the study to be expanded to a wider air temperature range than the experimental work. The computational work was done using a complex chemistry code based on work developed by Giovangigli and Smooke (1987). This code uses the CHEMKIN library with an appropriate application code (Oppdif was used to reproduce the Maruta results).

In Figure 4.1 (Maruta et al., 2000), it is evident that at a fuel concentration below approximately 5% (or possibly between 5 and 7%), the peak reaction zone temperature is less than the oxidizer temperature. The study describes "a moderate chemical reaction" occurring when the point of equal reaction zone temperature and oxidizer temperature. This is evident through non-published data regarding the species concentrations of a few intermediate species. These high inlet air temperature reactions with no reaction zone temperature peak are identified as *flameless combustion*.

Figure 4.2 was formed from data gathered using the Oppdif software for 5%, 7%, 11%, and 15% fuel concentrations. It can be seen that the same absence of a temperature peak at 5% methane is present in this data. This fuel concentration is referred to throughout the rest of this study as Flameless combustion. However, it also can be seen that the peak temperature for 15% methane is approximately 400 K higher than the data in the Maruta paper (Maruta et al., 2000). This is possibly due to the difference in computation of strain rate. This study uses an average strain rate given as:

$$\text{Strain} = 2\frac{\text{Velocity}}{\text{Separation Distance}} = \frac{2u}{d}.$$

The separation distance is constant for all configurations at 5 cm, while the velocity is varied to produce varying strain rates. For the data below, a strain rate of 11 $sec^{-1}$ is used, which results in a velocity of 27.5 cm/s for each of the oxidizer and the fuel.

Seeing this temperature peak similarity, however, shows that the computational approach is valid for comparing sensitivities of profiles and characteristics; although, relative magnitudes may vary due to differences in solution techniques. The Oppdif combustion code solution technique is discussed in the following section.

## 4.2. Effects of Fuel Concentration

Fuel concentration affects directly the strength of the reacting mixture. The additional dilution of nitrogen on the fuel stream results in an important reduction in flame temperature, which affects the dominant mechanisms for $NO_x$ formation, especially the thermal NO production mechanism.

As fuel concentration is increased, it is evident that for given conditions, the amount of fuel available for use in the elementary reactions involving $CH_4$ is increased. This would tend to increase the overall rate of chemistry as well as the overall adiabatic flame temperature as seen above in the Benchmark section. This section explores the effects that changing fuel concentration has given certain computational parameters on the species $H_2$ and NO.

Figure 4.3 demonstrates this overall increase in both NO and $H_2$ as a function of fuel concentraion ($C_f$) for the two bounding strain rates 24 and 4 $sec^{-1}$. It can be seen here that, the hydrogen molecule has little to no sensitivity to strain rate, while NO has an overall increase in peak mass fraction with decreasing strain rate. Both of these peaks, however, retain a high sensitivity to fuel concentration.

Figure 4.4 indicates that the trend of increasing peak NO mass fraction with increasing fuel concentration is seen when the preheat temperature is taken as 1100 K. At this preheat, however, the sensitivity of both species is lower than observed at the higher preheat temperature explored above. Yet, even as the fuel concentration is lowered, the sensitivity of NO is shown to be much greater than that of $H_2$ as indicated by the changes in peak $H_2$ from a strain rate of 24 to 4 $sec^{-1}$ being a factor of 10, whereas the changes in peak NO over the same strain rates is nearly a factor of 100.

It can also be seen that there is a higher sensitivity of peak NO to strain rate at higher fuel concentrations. This is possibly due to the reduction in the anount of fuel available to be used, which places a limit on the amount of NO production, and thereby limits the effects of strain rate on this same parameter.

As discussed earlier, the emission index is a global quantity that can be used to measure the overall increase of NO production, in kilograms, per gram of fuel consumed. Figures 4.5 and 4.6 indicate an expected overall increase in the emission index of NO as fuel concentration increases. The dependence of emission index on fuel concentration follows a steadily increasing path with increasing fuel concentration at low strain rates, however when the strain rate is increased (See below for discussion), the dependence is lessened.

When considering the preheat temperature, an expected overall decrease for the emission index of NO at both strain rates decreases when preheat temperature is decreased. A decrease in preheat temperature lessens the incoming enthalpy to the reaction, which is what has been proposed to be the driving force behind the flameless reaction mechanism (Maruta et al., 2000). This is discussed more in depth in the Effects of Preheat Temperature section.

After studying the global quantities such as peak mass fractions and emission index for NO and $H_2$, it is worthwhile to explore the specific profiles of these two species to show whether the trends found through the study of the global quantities can be applied to the specific profiles.

Figure 4.7 shows the mass fraction profile of $H_2$ as a function of mixture fraction. The contours represent a specific fuel concentration increasing as depicted by the arrow, while the preheat temperature and strain rate are taken as 2100 K and 24 $sec^{-1}$, respectively. Here, the overall trend of decreasing NO mass fraction with decreasing fuel concentration can be observed.

Figure 4.7 shows profiles of the $H_2$ mass fraction as a function of the mixture fraction for different conditions of fuel concentrations at a preheat temperature of 2100 K and a strain rate of 24 $sec^{-1}$. A similar plot is shown for the lower preheat temperature of 1100 K in Fig. 12. It can also be seen that there is a shift in the value of the mixture fraction at which the peak $H_2$ mass fraction occurs. In this case, the shift is toward fuel rich conditions. Overlayed on the plot is a line depicting the stoichimetric mixture fraction for each fuel concentration corresponding to the peak mass fraction of $H_2$. The peak shift is due to the shift of the stoichiometric conditions (the flame location) towards zero as the fuel concentration is increased. The same shift is again seen in Fig. 4.8. In contrast to the higher preheat temperature profiles, the shift toward the stoichiometric mixture fraction is more prevalent in the lower preheat temperature case.

Figure 4.9 shows NO mass fraction profiles as a function of the mixture fraction for different values of the fuel concentration and at a preheat temperature of 2100 K and a strain rate of 24 $sec^{-1}$. Figure 4.10 shows the same corresponding figure for a preheat temperature of 1100 K. The two figures show essentially similar trends for NO and $H_2$, which are associated mainly

with an increase in the peak values as the fuel concentration is increased and when the preheat temperature is increased. The shifts in peaks NO mass fraction are less pronounced for the higher temperature conditions with fuel concentration than with preheat temperature. This shift will be discussed in Sec. 4.4.

At 1100 K, however, the peaks are shifted towards the flame or stoichimetric mixture fraction. Note also that the profile of NO at flameless conditions, i.e. 5% fuel concentration, is negligible compared to the flame-based cases. Yet, at higher preheat temperatures, as shown in Fig. 4.9, the excess enthalpy brought into the reaction zone by the higher temperature oxidizer allows for a more energetic reaction and a higher profile is seen.

The same trends are observed here in that NO mass fractions decrease, not only with decreasing fuel concentration, but also with decreasing strain rate as shown in Figs. 4.11 and 4.12. Figure 4.11 shows NO mass fraction profiles as a function of the mixture fraction for different fuel concentrations and a preheat temperature of 2100 K, and a lower strain rate of 4 $sec^{-1}$ than in Fig. 4.9. An equivalent plot to Fig. 4.10 is shown in Fig. 4.12 for the lower strain rate case of 4 $sec^{-1}$ and a preheat temperature of 1100 K.

Just as in Fig. 4.11, the same trend is present with a similar shift in NO mass fraction peak when the same preheat temperature is used with a decreasing strain rate. The increasing magnitude with decreasing strain rate is also observed in Fig 4.12.

The trend of an increase in peak NO and $H_2$ mass fractions is reinforced with the review of NO and $H_2$ profiles at the limiting preheat temperatures of 1100 and 2100 K and the limiting strain rates of 4 and 24 $sec^{-1}$. However, as demonstrated above, there is a shift with increasing fuel concentration of the location of the peak value for each species in mixture fraction space. This is due to the relocation of the stoichiometric mixture fraction corresponding to each fuel concentration.

Looking at the contributions of individual reactions as a function of mixture fraction allows the effects of strain rate to be seen on certain reactions deeming them negligible or significant. For an individual species, there are elementary reactions that take place. For this

reason, reaction flow analysis for $NO_x$ may shed light on the mechanism itself and how to reduce $NO_x$ emissions.

A general trend is observed that shows a decreasing reaction rate with decreasing fuel concentration. The trend is present in Figs. 4.13 to 4.16, which show the net reaction rate of NO as a function of the mixture fraction for the limiting conditions of the ranges of parameters considered in this study and the various fuel concentrations considered from flameless to flame-based. The dependence, however, is lessened or increased when either the strain rate or preheat temperature are varied. The trend of consumption, i.e. a negative reaction rate, is consistent for all cases as decreasing with increasing fuel concentration. The production rate, however, show a greater sensitivity to strain rate and preheat temperature. The presence of a local peak on the oxidizer side at the higher preheat temperatures and higher fuel concentrations may be attributed primarily to the role of air dissociation, which may play a role in the production of thermal NO. The remaining production and consumption peaks coincide approximately with chemical activity within the reaction zone.

Figure 4.17 shows the peak reaction rate for NO as a function of fuel concentration for the bounding preheat temperatures and a strain rate of 24 $sec^{-1}$. It can be seen that as fuel concentration increases, the peak reaction rate increases, i.e. the rates of production of NO increase. It is also apparent that there is an increased dependence of peak reaction rate on fuel concentration at lower preheat temperatures, while at lower strain rates, there is an increase in magnitude, but the similar trend remains.

From Figs. 4.19 and 4.20, it can be seen that indeed the thermal NO contributions are more prominent outside the reaction zone, however, as fuel concentration is reduced, the thermal NO peak outside the reaction zone is shifted towards the oxidizer side, where the high temperature oxidizer is providing excess enthalpy to sustain the weak chemical reaction found in flameless combustion.

Figures 4.21 through 4.24 show the emission index of both thermal and prompt NO mechanisms. The results show that both mechanisms follow similar trends of increasing with increasing fuel concentration. This trend is consistent with that of increasing overall emission index with increasing fuel concentration. However, at higher preheat temperatures,

the highly temperature dependent thermal mechanism has a larger contribution than the prompt mechanism; while at lower preheat temperatures, prompt NO becomes the more dominant mechanism. This is discussed in more detail in Sec. 4.4. As fuel concentration increases, the dominance of either thermal (at high preheat temperatures) or prompt (at low preheat temperatures) increases, i.e. the gap between the two mechanisms becomes larger.

Figure 4.25 shows the dependence of the radicals O and OH along with the peak temperature, which are all heavily involved in the mechanism that produces thermal NO. All three increase with an increasing fuel concentration, however, the radicals increase by over 75%, while the temperature increases approximately 12%. This seems to indicate that the sensitivity of thermal NO production lies more with the radical formation than the peak temperature.

## 4.3. Effects of Strain Rate

In contrast with fuel concentration, strain rate affects the residence time of species in the reaction zone and contributes to the further thinning of the flame structure, thereby altering the balances of transport by convection and diffusion within the flame. Changes in residence time will affect primarily relatively slow reactions, such as the ones associated with the thermal NO production mechanism. Further increases in strain may result in incomplete combustion, leading eventually to the extinction of the flame. However, strain rate (when based solely on inlet velocity as in this study) affects the transport of fuel and oxidizer to the flame. It is important to note that a diffusion flame exists at the mercy of the incoming fuel and oxidizer velocities. A diffusion flame cannot move or react as a premixed flame can; it is reliant on the transport and diffusion of the two species into one another to "feed' it. Therefore, while the residence time is lessened as strain rate is increased; the transport of fuel and oxidizer into the flame is increased, providing more "food" for the flame. Residence time will have an increased effect on slower reaction mechanisms. NO and $H_2$ differ in their relative reaction speeds. $H_2$ is a fast reaction in comparison with NO and will therefore have a lessened sensitivity to a decrease in residence time, while NO would have a much greater sensitivity to this parameter.

As strain rate increases, the residence time for chemistry decreases, and accordingly the Damkohler number, which measures the ratio of chemical time scales to transport time scales, also decreases. In flames, increased strain may result in their local extinction, and prior to that an important reduction in the heat release rate and the rate of chemistry. In flameless combustion, increased strain also results in tangible reductions in the rate of heat release and chemistry. Figure 4.26, which shows peaks of NO and $H_2$ mass fractions as functions of strain rate at a preheat temperature of 2100 K, depicts this decrease in peak $H_2$ and peak NO concentraion due to a decrease in residence time for 15% methane dilution, i.e. flame-based combustion. It can be seen that NO and $H_2$ follow similar trends. The dependence of peak of NO and $H_2$ is monotonic as a function of strain rate. Both initially increase with strain rate, but then decrease at higher strain rate values; this is due to the initial increase in transport of both fuel and oxidizer to the flame, i.e. a higher supply of fuel and oxidizer is brought to the flame, while at even higher strain rates, residence time is decreased and the progress of teh NO reaction is slowed and due to it's relatively slow reaction, the mass fractions decrease. Similarly, $H_2$ follows the same trend; however, it is also important to note that the magnitude of the peak $H_2$ mass fractions are of the same order, yet the net change from the lowest strain rate to the highest is much smaller for the hydrogen molecule, indicating that $H_2$ is less sensitive to increases in strain rate than NO due to the faster $H_2$ mechanism.

Figure 4.26 is a good example of the balance between residence time and transport. When strain rate is decreased, residence time is increased, while a lower supply of fuel and oxidizer is brought into the flame. This results in an initial increase in both mass fractions as more fuel and oxidizer is supplied to the flame, however, as strain is lowered further, the flame begins to feel the effects of less fuel and oxidizer transport and there is then a decrease in both.

Figure 4.27 shows that the $H_2$ dependence on strain rate is not the same for all oxidizer preheat temperatures. When fuel dilution is held constant and preheat temperature is changed to 1100 K, $H_2$ increases monotonically with strain rate. However, the difference between the maximum of the hydrogen peak values and the minimum is again very small, reinforcing the

conclusion that the hydrogen molecule mass fraction is much less sensitive to strain rate than NO. NO, however, does follow the same trend as observed when the preheat temperature is 2100 K. The magnitude, however, is diminished by a factor of 10.

In the flameless combustion case, i.e. fuel concentration of 5%, the data indicates that $H_2$ is much less sensitive to strain rate than NO. However, in Figure 4.28, which shows the peaks of NO and $H_2$ mass fractions for the flameless condition, the trends for peak $H_2$ mass fraction have reversed from decreasing with strain rate at a preheat temperature of 2100 K and increasing with strain rate at a preheat temperature of 1100 K to the exact opposite.

The trend of increasing hydrogen has been reversed as can be seen in Figure 4.29. The changes, however between the peak $H_2$ mass fraction corresponding to the highest and lowest strain rates is increased when the preheat temperature is lowered to 1100 K. Figure 4.29 sees the peak mass fraction of NO begin to decrease and then at higher strain rates, begin to increase again. This is possibly due to the overall weak chemical reaction.

As discussed before, the emission index of NO is a good way of describing the global effects of varying one parameter over another. In Figures 4.30 and 4.30, a trend of decreasing emission index of NO is seen with increasing strain rate for both flameless and flame-based combustion. This is to be expected based on the peak decrease in NO discussed earlier. The emission index decreases overall as preheat temperature decreases. However, here it can be seen that in the case of flameless combustion with a lower preheat temperature, i.e. much less enthalpy carried with the oxidizer, the emission index of NO drops to nearly zero, indicating a strong reliance on preheat temperature for that case. The balance between transport (providing enough fuel and oxidizer) and residence time (lessening the time frame the fuel and oxidizer have to react) can be seen again at high temperatures in the flame-based case. Figure 4.30 depicts as sharp increase in emission index of NO at a strain rate of 12 $sec^{-1}$. The magnitudes of these indexes are much less than the flameless case; however, the rise in emission index could be caused again by the balance found between transport and residence time that take place with the weak chemical reaction that occurs in flameless combustion.

Fig 4.31 shows the peak NO and $H_2$ mass fractions as a function of strain rate for a flame-based condition corresponding to $C_f$ = 15% and a preheat temperature of 2100 K. The NO

mass fraction displays a much stronger dependence on strain rate than hydrogen, which has little to no dependence holds on strain rate. The behavior of the two species is primarily determined by the rates of their production in comparison with the residence times associated with each strain rate. The rate production of $H_2$ is relatively fast; and, therefore, this rate is not affected by the shorter residence times associated with increasing strain rates.

Figure 4.32 shows that the trend observed in Fig. 4.31 for the flame-based conditions are found in the flameless case; however, hydrogen does seem to have a slightly stronger dependence on strain rate in flameless combustion rather than flame-based combustion. Here, the lower temperatures at flameless conditions reduce the rates of the primary reactions that produce intermediates in the reaction zone.

The general trend of increasing reaction rate with increasing strain rate is observed for both flameless and flame-based combustion as seen in Figs. 4.34 through 4.37 which show the reaction rate profiles of NO as a function of the mixture fraction for the various limiting parameters of preheat temperature and fuel concentration and for all values of strain rates considered. Yet, the difference between the highest and lowest strain rates becomes smaller as fuel concentration is decreased, i.e. there is an increased sensitivity to strain rate as fuel concentration is increased. In the flame-based case, as strain rate is decreased, there is an overall decrease in reaction rate for NO. This again is due to the decrease in residence time and the response of the reaction mechanism for NO to those decreased values. With flameless combustion, however, we see an increase in reaction rate as strain rate is increased, yet the magnitudes of these profiles are much, much lower than the flame-based case, where there is a stronger chemical reaction taking place. Figure 4.37 shows that at low preheat temperature less enthalpy is brought into the reaction to sustain the flameless reaction. At higher temperatures, it is important to note the presence of the thermal NO contribution (or "hump") outside the reaction zone. This is diminished when preheat temperature is lowered due to the mechanism's high dependence on temperature. This 'hump' is associated primarily with the dissociation of air, which may occur outside the primary reaction zone that consumes the fuel.

Exploring the global quantities of peak reaction rates again is useful to further reinforce the trend of increasing reaction rate for NO with increasing strain rate. In these plots, it can be seen that the production rate of NO increases with strain rate for the flame-based case of 15% fuel concentration, but decreases with the increasing strain rate in the flameless case.

Figures 4.38 through 4.41 depict the individual contributions to overall reaction rate from both thermal and prompt NO. These plots show that as fuel concentration is decreased, the overall contribution from thermal NO is decreased. There can also be seen a shift in thermal reaction rate contribution towards the oxidizer side in mixture fraction space. Figure 4.38 shows that the contribution of thermal NO inside the reaction zone is negligible compared to outside, which means there is less thermal NO contributing to the formation of NO within the reaction zone, yet outside the reaction zone, the contribution is only changed in magnitude.

Figures 4.42 through 4.45 depict the emission index of NO resulting from the individual thermal and prompt NO mechanisms along with the overall emission index of NO. An overall decrease can be seen in both indices as strain rate increases, however, the balance between transport and residence time can be seen in the thermal NO emission index suggesting that the thermal mechanism is perhaps the slower progressing mechanism. It can again be seen that when preheat temperature is decreased, the dominant NO production mechanism shifts from thermal to prompt due to the high dependence of the thermal mechanism on temperature. Strain rate is seen to have no appreciable role in either the flame-based or the flameless cases in shifting the dominating contribution of thermal to prompt NO. The emission index for NO shows similar magnitudes at higher preheat temperatures. This is due to the normalization by the amount of fuel consumed. However, as preheat is lowered, the sensitivity of flameless combustion to oxidizer temperature and subsequently excess enthalpy is seen as the emission index drops drastically.

## 4.4. Effects of Oxidizer Preheat Temperature

It has been established through many studies that NO mass fraction increases with increasing temperature. Increasing the preheat temperature increases the amount of enthalpy brought into the reaction, which tends to fuel the emergence of thermal NO according to the Zel'dovich mechanism. Figure 4.46 shows peak $H_2$ and NO mass fractions as functions of

preheat temperatures for both flame-based and flameless conditions and at the two limiting strain rate conditions of 4 and 24 $sec^{-1}$. In the configuration studied, the peak mass fraction of NO increases with the increase of preheat temperature. Hydrogen also shows a dependence on preheat temperature, while again showing little or no sensitivity to strain. The trend of increasing NO with increasing preheat temperature follows for $H_2$, though NO shows a highly non-linear dependence, while the dependence of $H_2$ is nearly linear.

Figures 4.47 and 4.48 reinforce the conclusion that with increasing preheat temperature increases the production of NO. The emission index of NO increases almost exponentially with the preheat temperatures, at temperatures above 1300 K, below which at low strain rates, the emission index drops more rapidly. Flameless combustion, however, continues to display strong dependence on the excess enthalpy brought into the mixture by the higher temperature oxidizer by showing a dramatic drop in the emission index of NO at low preheat temperatures.

Examining the specific profiles for the limiting fuel concentrations and strain rates reveals an increase in both hydrogen and NO with increasing preheat temperature. The trend of NO mass fraction increasing with decreasing strain rate is also observed here. The relative ineffectiveness of varying strain rates has on the peak mass fraction of $H_2$ can also be seen here. It is also apparent that hydrogen is not as sensitive to changes in preheat temperatures as NO. This can be also seen in Fig 4.49.

Figures 4.49 and 4.50 reveal that the magnitude of the mass fraction of hydrogen is much less sensitive than NO to the same parameter. Figures 4.50 and 4.51 also suggest that within the flameless case at both limiting strain rates, the dependence of NO is much more sensitive to preheat temperature. This is again due to the dependence of flameless combustion on the excess enthalpy brought into the mixture by the oxidizer, meaning a lower preheat temperature will bring a lower enthalpy into the mixture and hence lower the amount of NO formed.

To understand the specific trends of the various elementary reactions or sub-mechanisms, a reaction a reaction flow analysis is implemented. Figures 4.53 through 4.56 show the profiles of the contributions from thermal and prompt mechanisms to the production of NO for the

various limiting conditions considered for strain rate and fuel concentrations, and at varying preheat temperatures. As would be expected, the reaction rate decreases with decreasing preheat temperature, though the dependence is lessened at lower strain rates. A decreasing reaction rate for NO can be seen with a decreasing oxidizer preheat temperature. However, as strain rate is decreased the sensitivity of the reaction rate to preheat temperature is diminished within the reaction zone. The role of thermal NO outside the reaction zone is still, however, highly dependent upon temperature and therefore responds to a change in preheat temperature at all strain rates. When considering flameless, however, the contribution of thermal NO outside the reaction zone disappears. There is still an overall decrease in reaction rate as preheat temperature is lowered. This value is much more sensitive to this parameter when considering flameless combustion due to the high dependence flameless combustion has on the excess enthalpy brought into the reaction by the high temperature oxidizer.

Figures 4.57 through 4.60 depict the contribution of both thermal and prompt NO for different preheat temperatures in both the flame-based and flameless cases. For the flame-based case, it can be seen through Figs. 4.57 and 4.58 that the role of thermal NO outside the reaction zone is nearly eliminated at lower preheat temperatures leaving the production of NO by both mechanisms solely inside the reaction zone. With this reduction comes a shift from a much more dominant thermal NO mechanism to more of a balance between the two mechanisms. Figures 4.59 and 4.60 also show a similar trend with the flameless case, however, as temperature is decreased to 1100 K, the flameless reaction becomes much weaker and the reaction rates become much, much smaller and shift towards the oxidizer side and the higher temperature air, which the flameless phenomenon is so dependent upon.

Figures 4.61 to 4.64 show the emission index for the individual contributions as a function of preheat temperature. Both indices increase with an increasing preheat temperature along with the overall emission index of NO, however, as seen in earlier sections, as oxidizer preheat temperature increases, there is a shift from dominance of prompt NO to a dominant thermal NO mechanism. This is again due to the high dependence the thermal NO mechanism has on temperature. As seen in Figs. 4.61 through 4.62, the contribution of

thermal NO outside the reaction zone nearly disappears as preheat temperature is lowered. This leaves the contribution within the reaction zone, which is small in comparison to that of prompt NO. Figures 4.63 and 4.64 illustrate the high dependence on temperature of flameless combustion. At low preheat temperatures, not enough energy is introduced into the reaction by the oxidizer to sustain a stronger reaction; while at higher temperatures, reaction rates increase (though still relatively weak) and the emission indices increase almost exponentially.

## 4.5. General Observations

In flameless combustion, the temperature of the 5% methane flame does not increase far above the inlet oxidizer temperature of 1500 K, while a stronger reaction in the 15% methane is observed and a much higher temperature is reached. Emissions in the flameless regime are reduced due to the apparent lack of a strong chemical reaction. It is evident in the data above that the emissions are greatly reduced; however, as seen above, the energy produced from this type of reaction is minimal. This would seem to suggest this type of flame would only find an application in processing the fuel into products without a temperature increase. The absence of a temperature peak is the likely cause of much lower NO and CO emissions in the flameless combustion regime. The absence of enough energy and enough reactants to produce a strong reaction lead to the reactants coexisting within the reaction, where with a higher fuel concentration, the two react and drive the mass fractions to zero within the reaction zone.

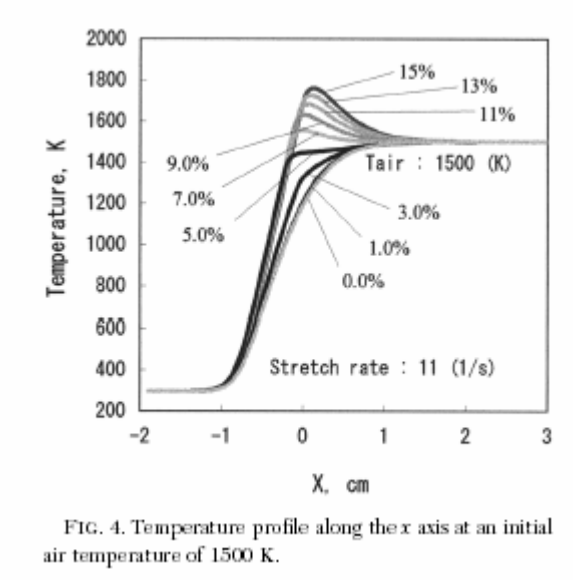


FIG. 4. Temperature profile along the $x$ axis at an initial air temperature of 1500 K.

**Figure 4.1.** Maruta Temperature Profiles for Varying Fuel Concentrations

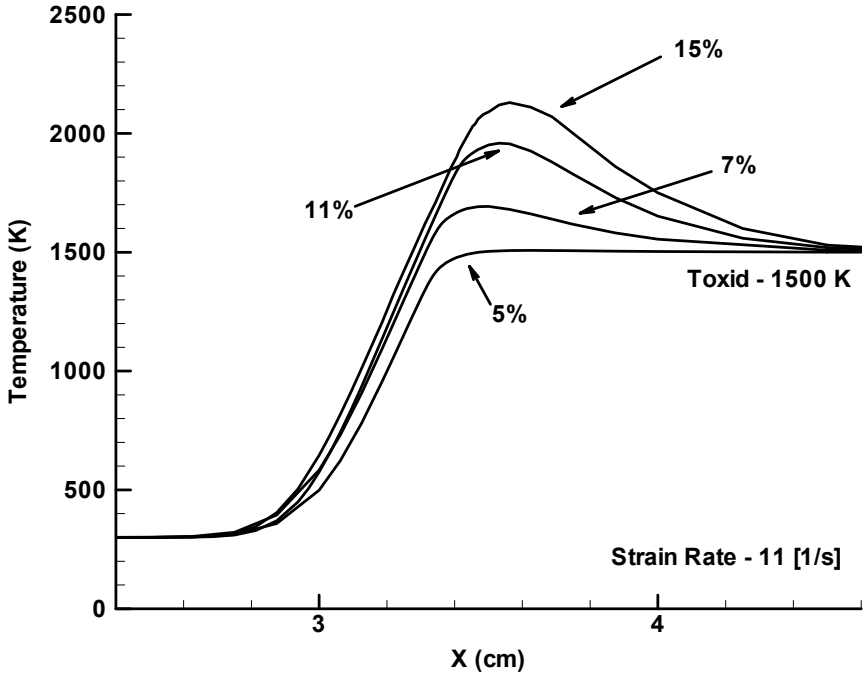


**Figure 4.2.** Spatial Temperature Profiles for Varying Fuel Concentrations

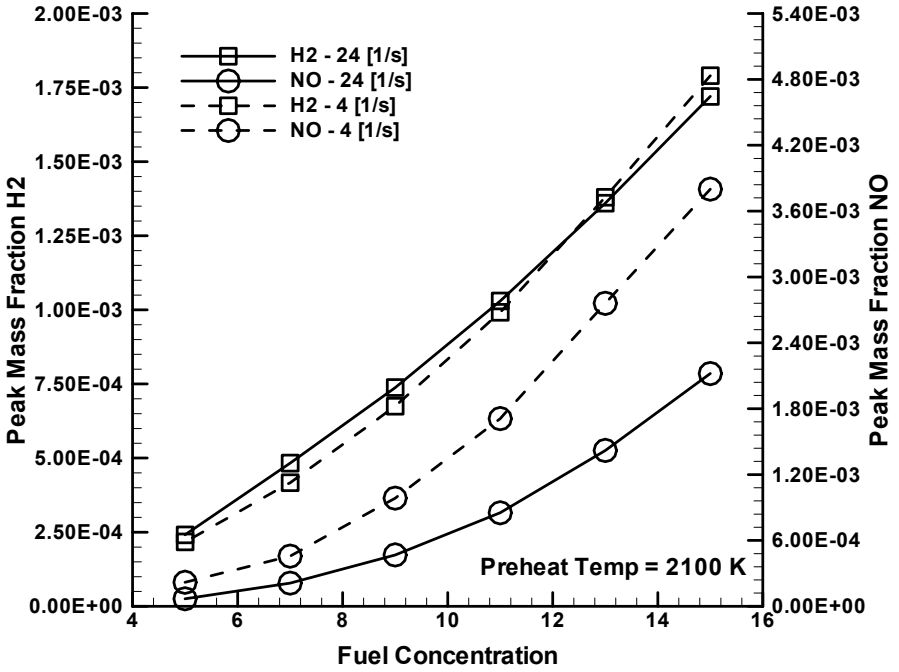


**Figure 4.3.** Peak $H_2$ and NO Mass Fraction vs $C_f$ for 2100 K

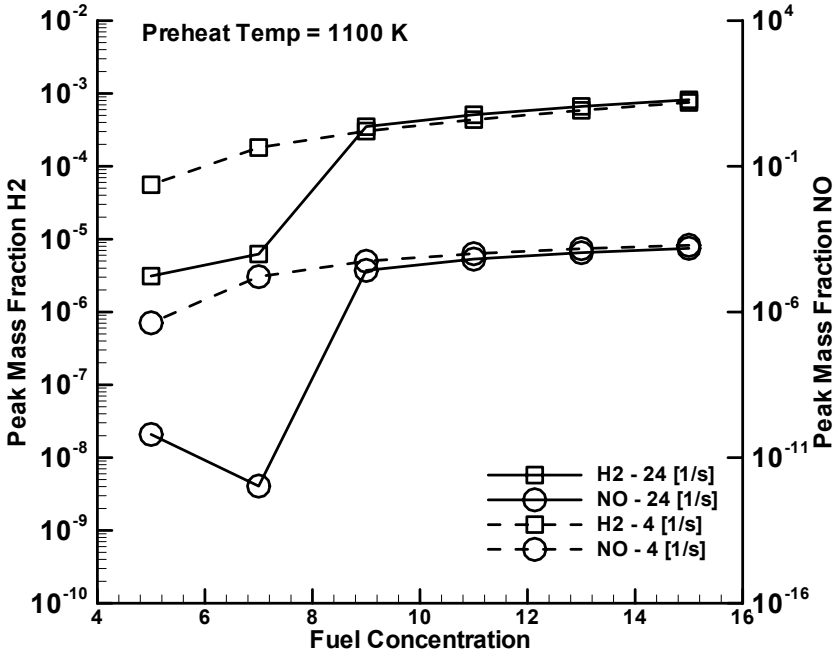


**Figure 4.4.** Peak $H_2$ and NO Mass Fraction vs $C_f$ for 1100 K

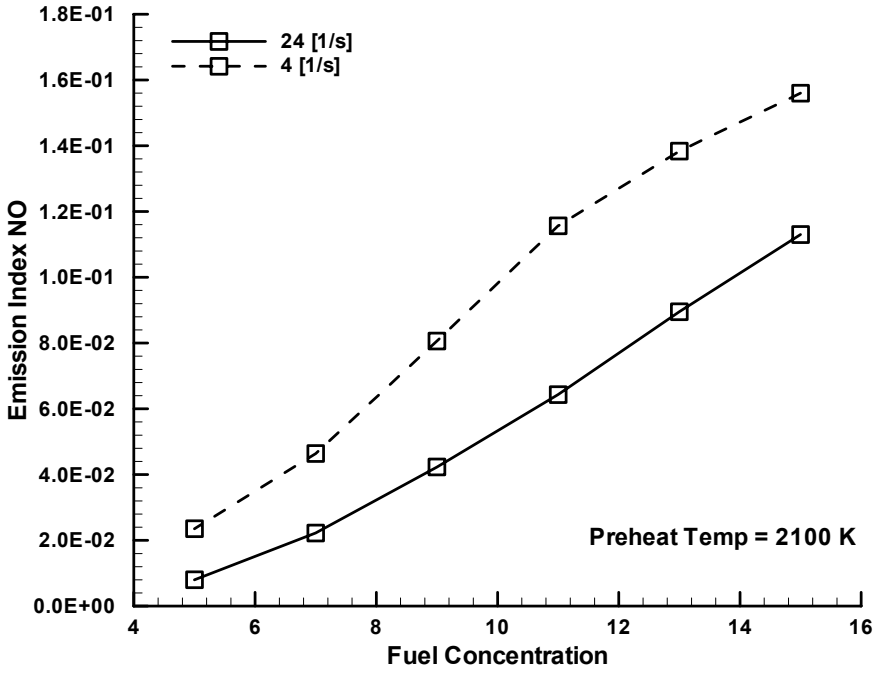


**Figure 4.5.** Emission Index for NO vs $C_f$ for 2100 K

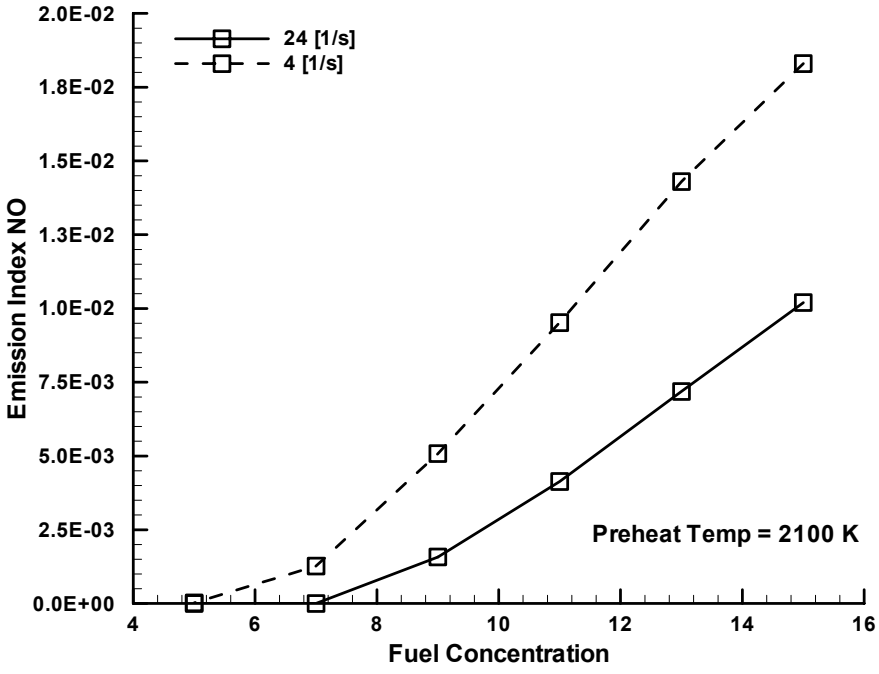


**Figure 4.6.** Emission Index for NO vs $C_f$ for 1100 K

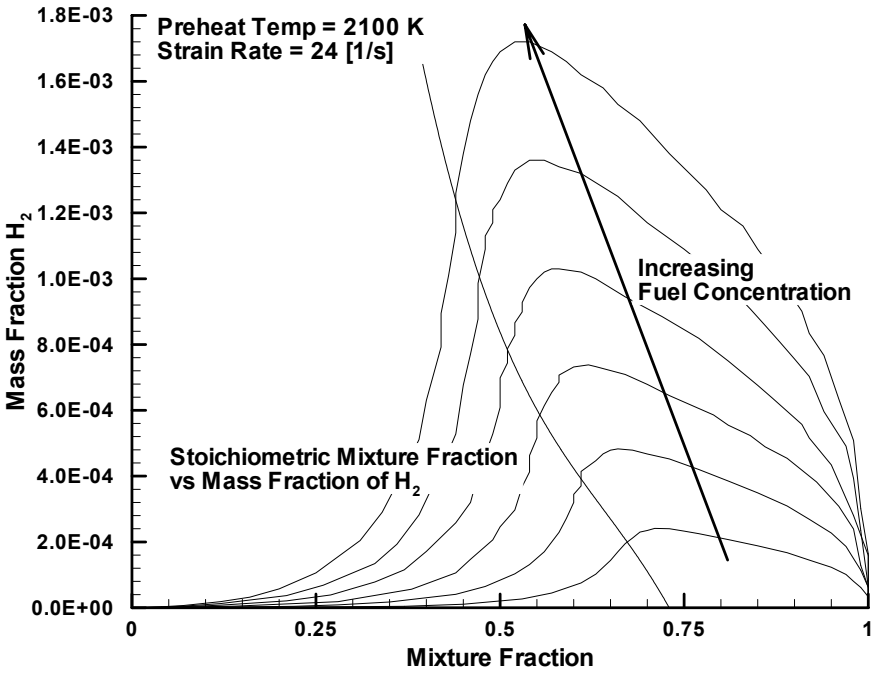


**Figure 4.7.** $H_2$ Profile vs $C_f$ for 2100 K & 24 $sec^{-1}$

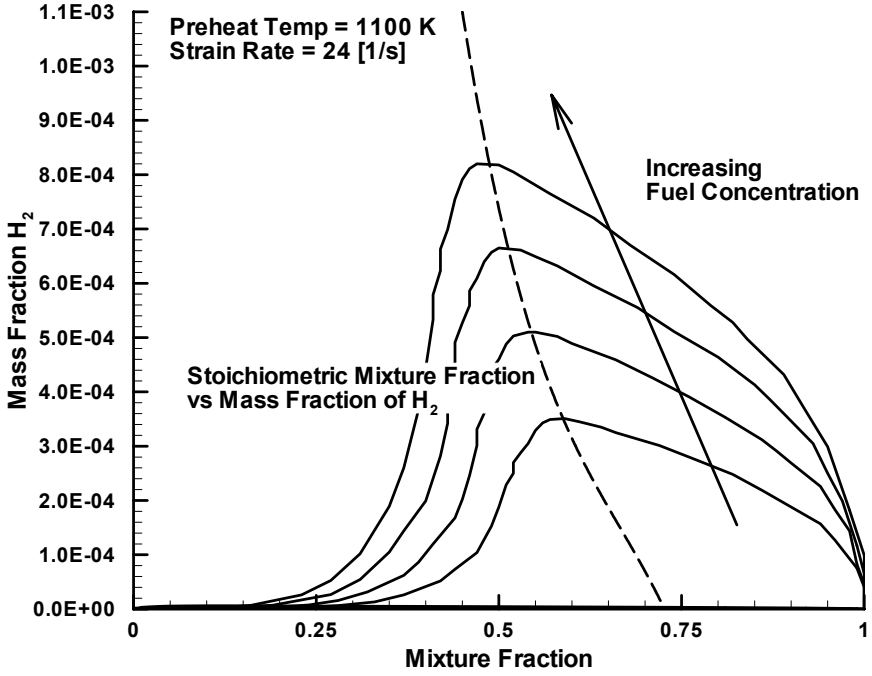


**Figure 4.8.** $H_2$ Profile vs $C_f$ for 1100 K & 24 $sec^{-1}$

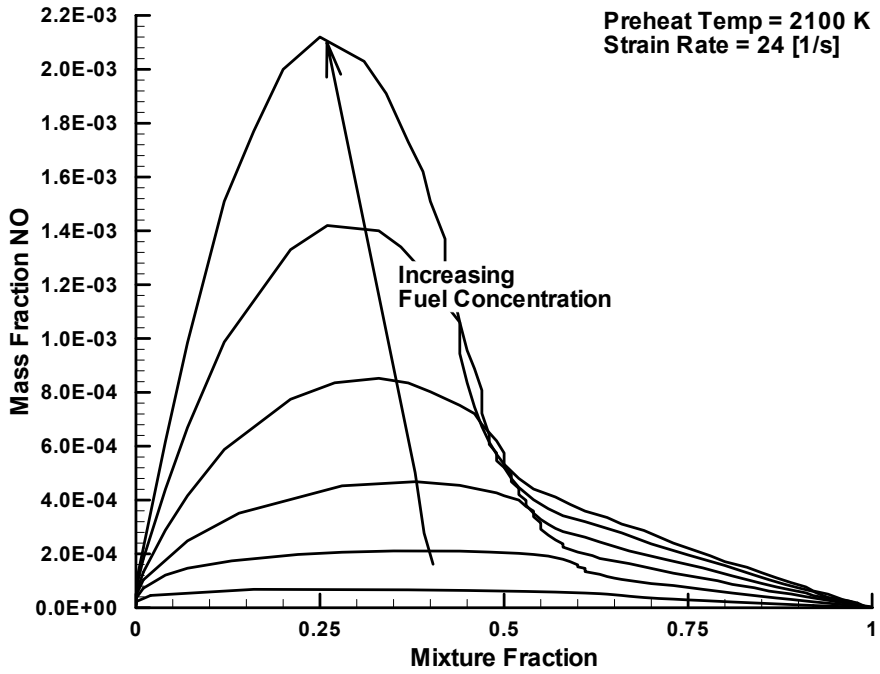


**Figure 4.9.** NO Profile vs $C_f$ for 2100 K & 24 $sec^{-1}$

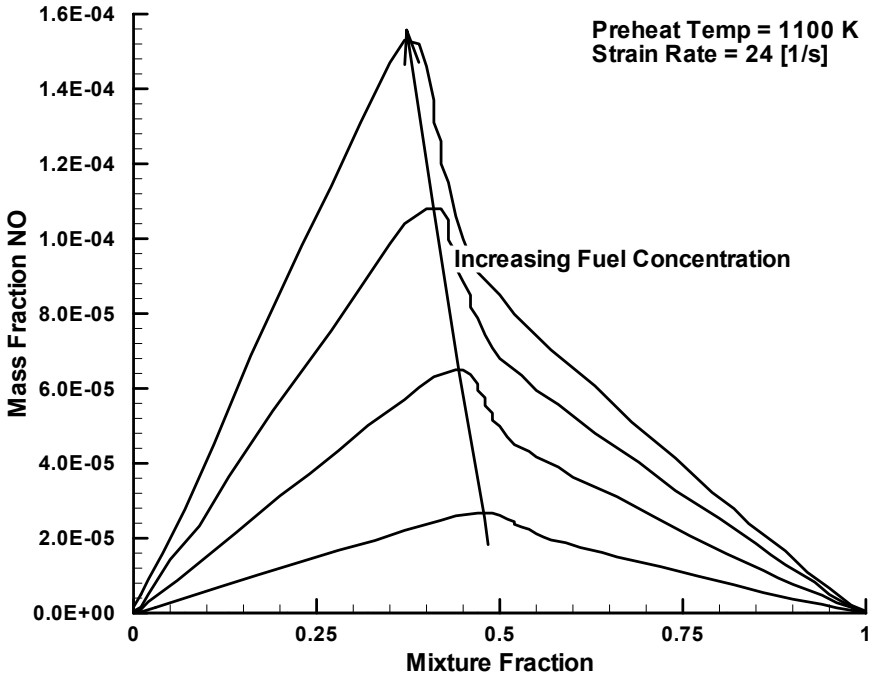


**Figure 4.10.** NO Profile vs $C_f$ for 1100 K & 24 $sec^{-1}$

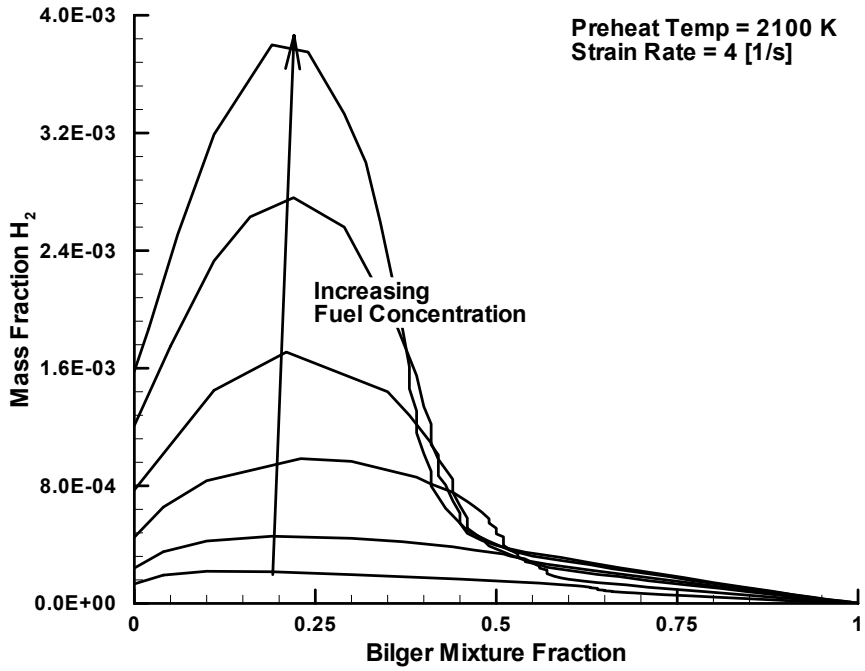


**Figure 4.11.** NO Profile vs $C_f$ for 2100 K & 4 $sec^{-1}$

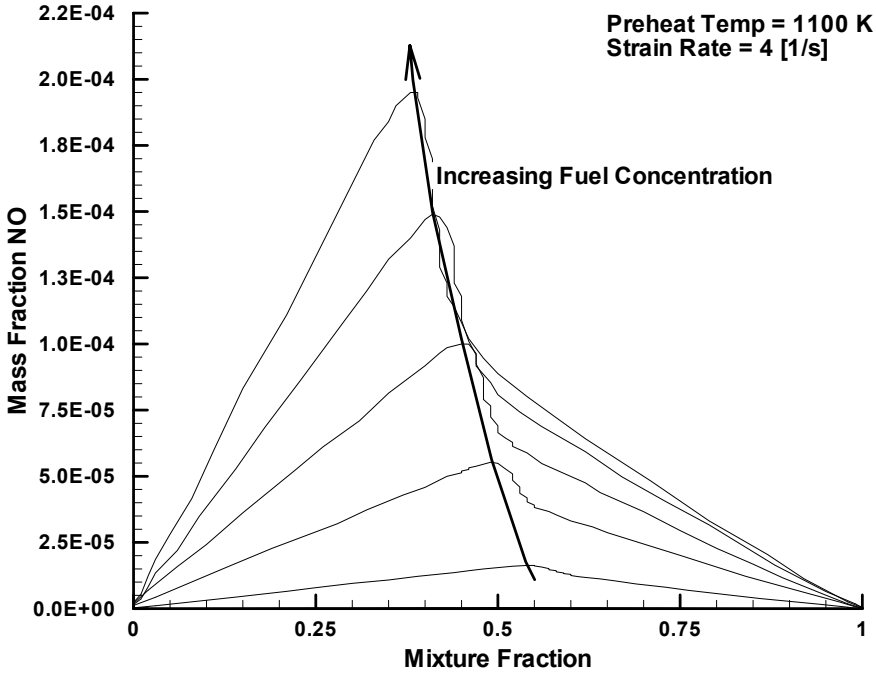


**Figure 4.12.** NO Profile vs $C_f$ for 1100 K & 4 $sec^{-1}$

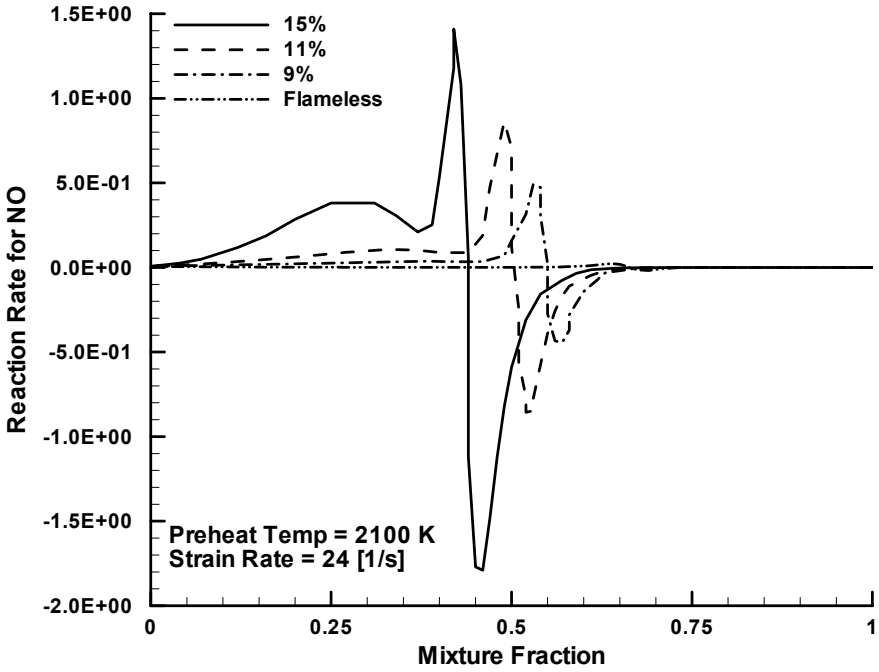


**Figure 4.13.** Overall Reaction Rate for NO vs $C_f$ for 2100 K & 24 $sec^{-1}$

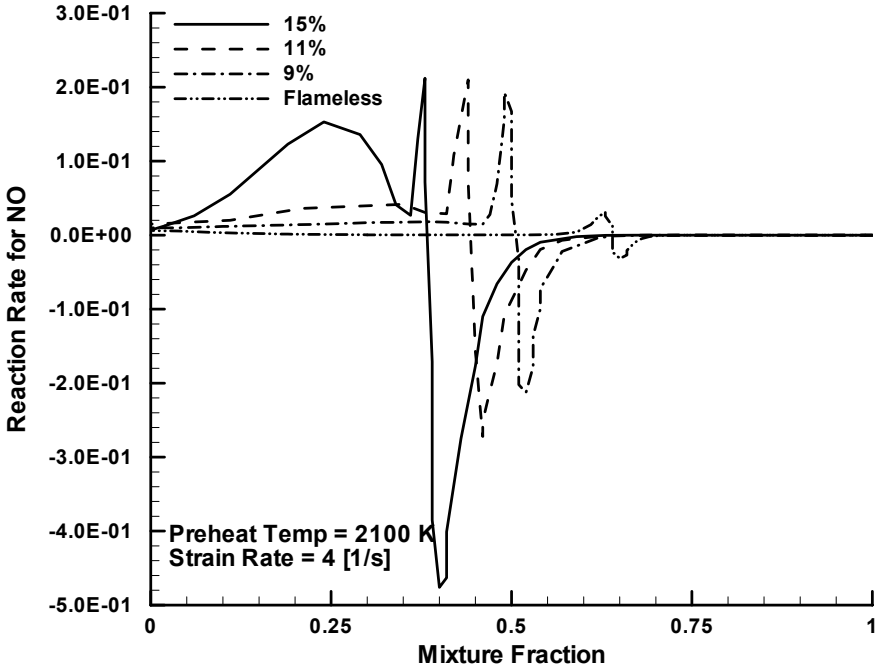


**Figure 4.14.** Overall Reaction Rate for NO vs $C_f$ for 2100 K & 4 $sec^{-1}$

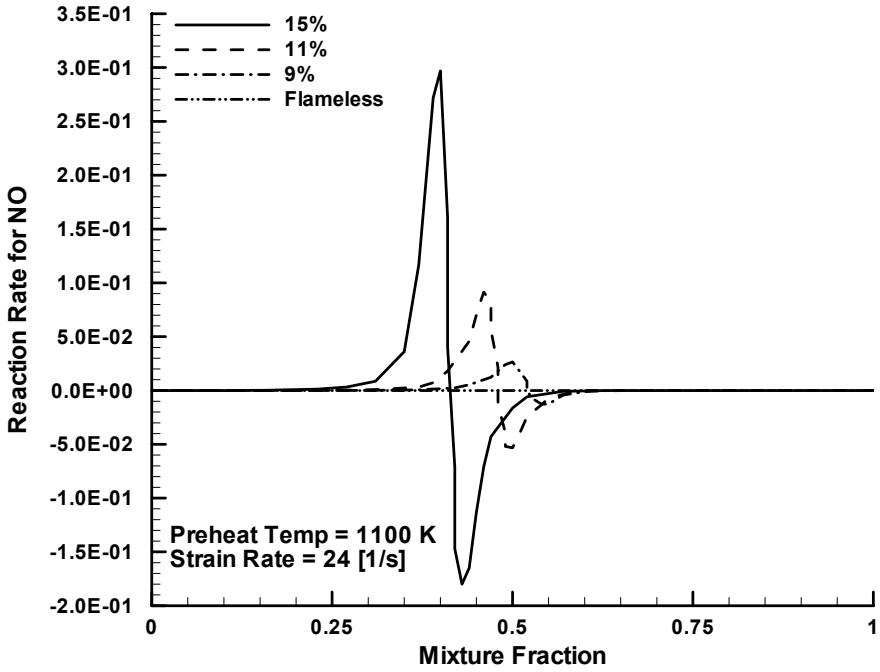


**Figure 4.15.** Overall Reaction Rate for NO vs $C_f$ for 1100 K & 24 $sec^{-1}$

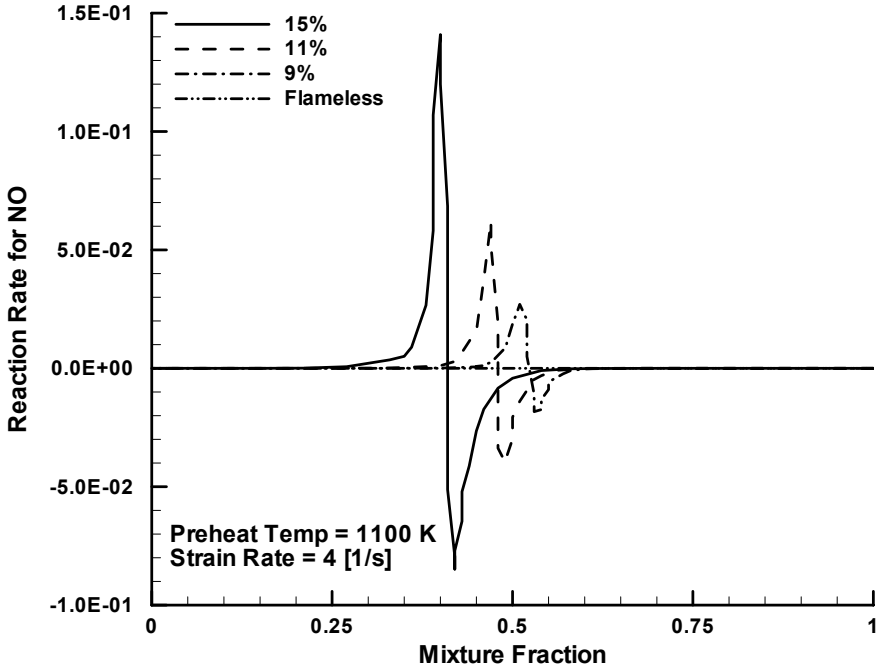


**Figure 4.16.** Overall Reaction Rate for NO vs $C_f$ for 1100 K & 4 $sec^{-1}$

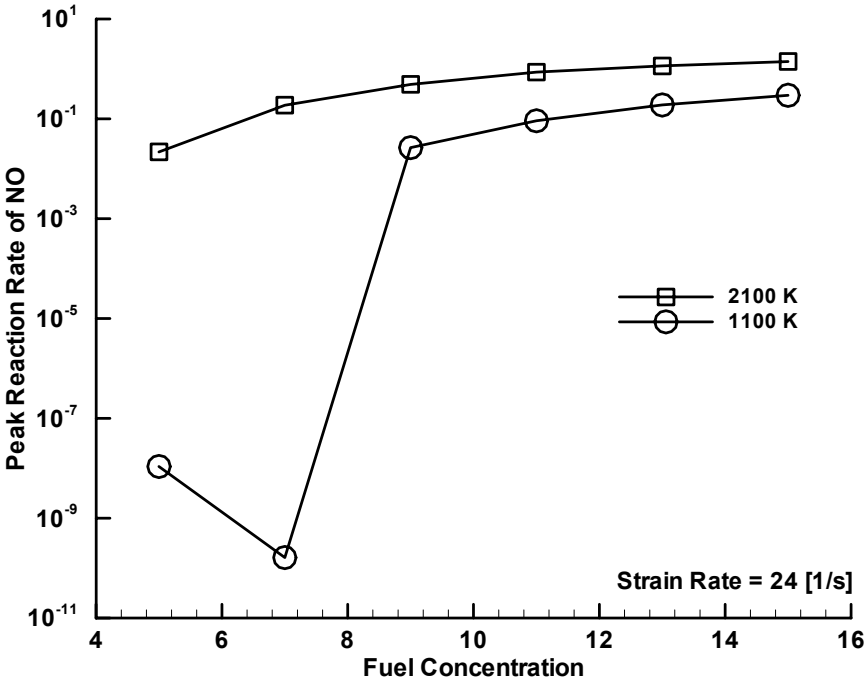


**Figure 4.17.** Peak Reaction Rate for NO vs $C_f$ for 24 $sec^{-1}$

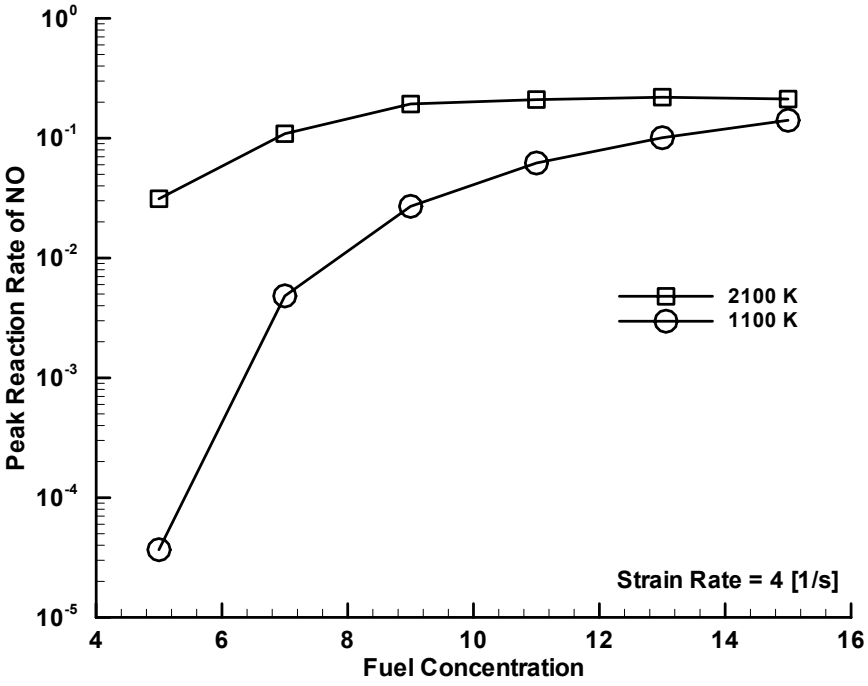


**Figure 4.18.** Peak Reaction Rate for NO vs $C_f$ for 4 $sec^{-1}$

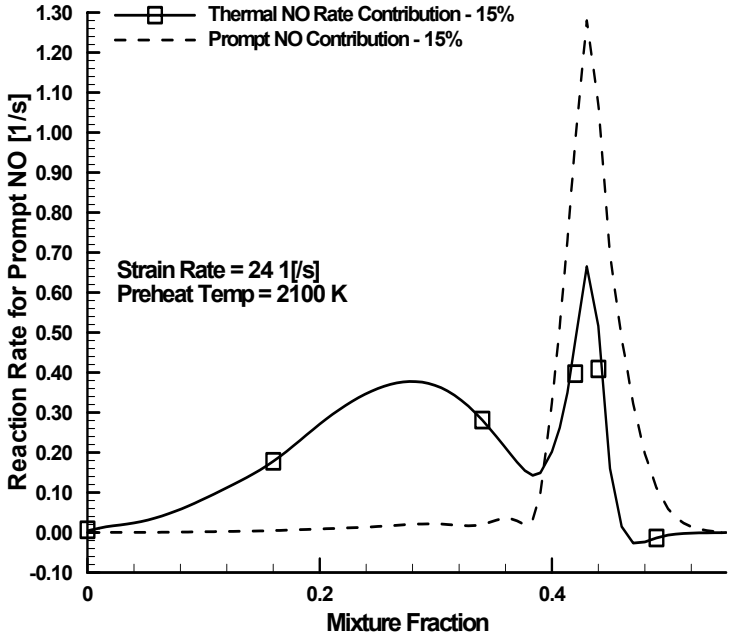


**Figure 4.19.** Thermal vs Prompt NO for 15% at 2100 K, and 24 $sec^{-1}$

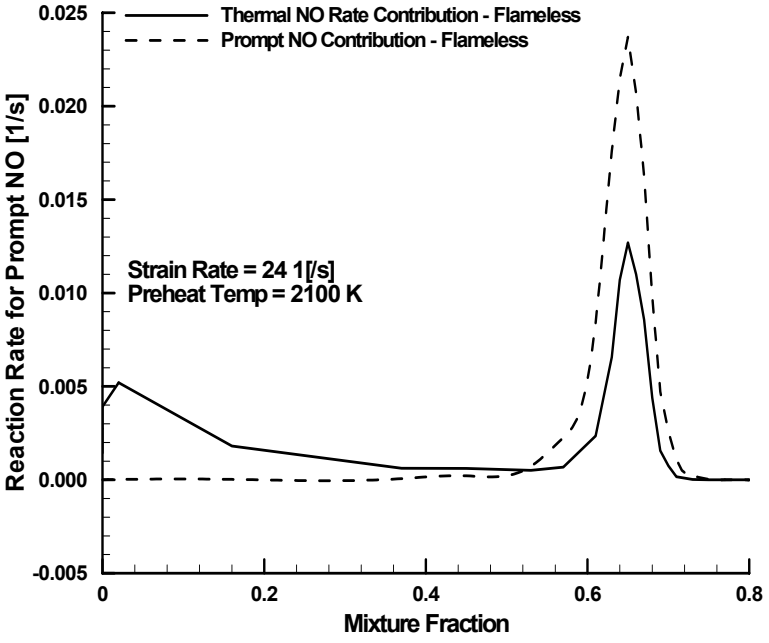


**Figure 4.20.** Thermal vs Prompt NO for Flameless at 2100 K, and 24 $sec^{-1}$

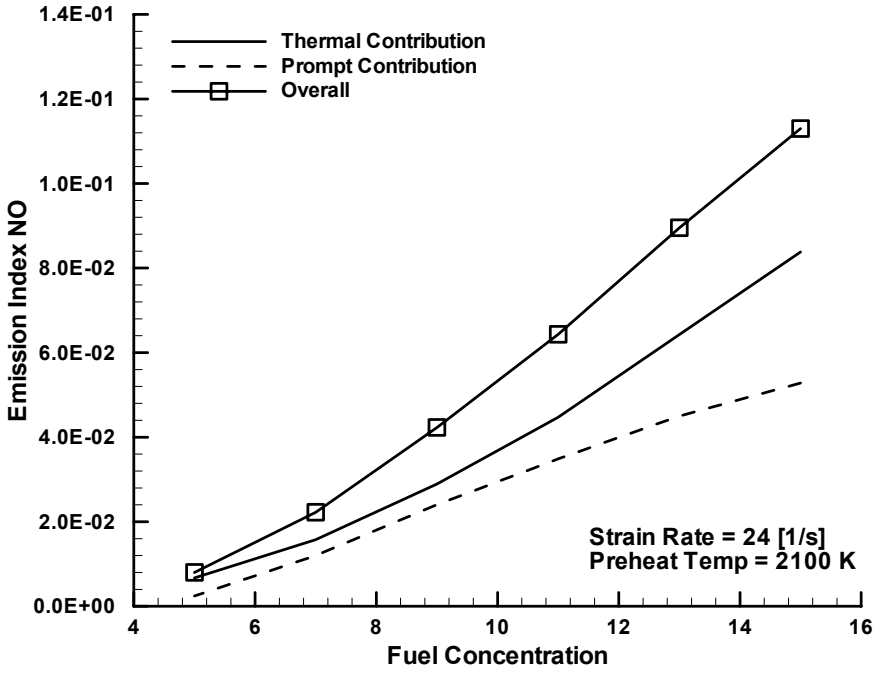


**Figure 4.21.** Emission Index for Thermal and Prompt NO vs $C_f$ at 2100 K, and 24 $sec^{-1}$

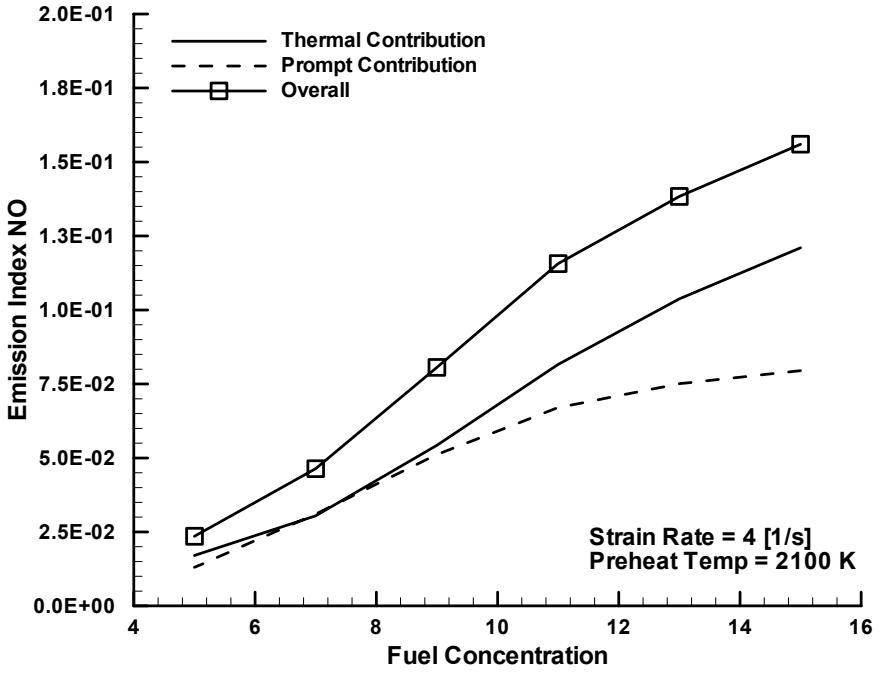


**Figure 4.22.** Emission Index for Thermal and Prompt NO vs $C_f$ at 2100 K and 4 $sec^{-1}$

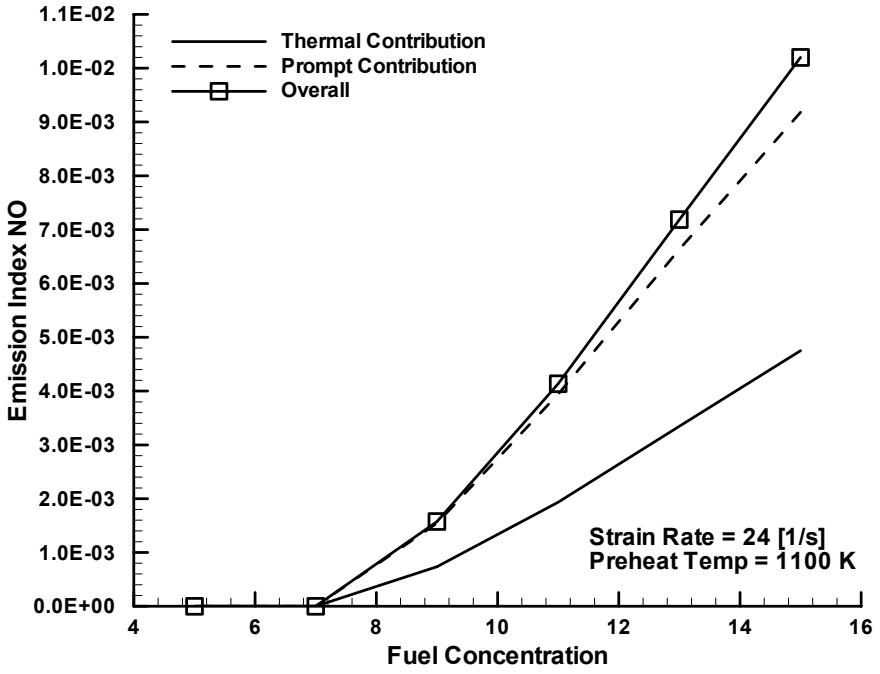


**Figure 4.23.** Emission Index for Thermal and Prompt NO vs $C_f$ at 1100 K and 24 [1/s]

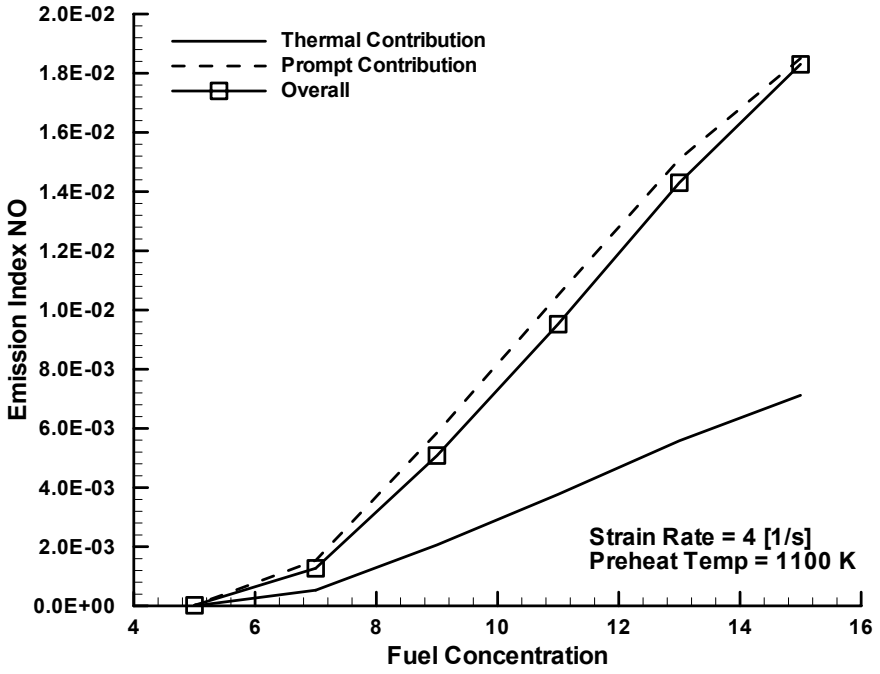


**Figure 4.24.** Emission Index for Thermal and Prompt NO vs $C_f$ at 1100 K and 4 $sec^{-1}$

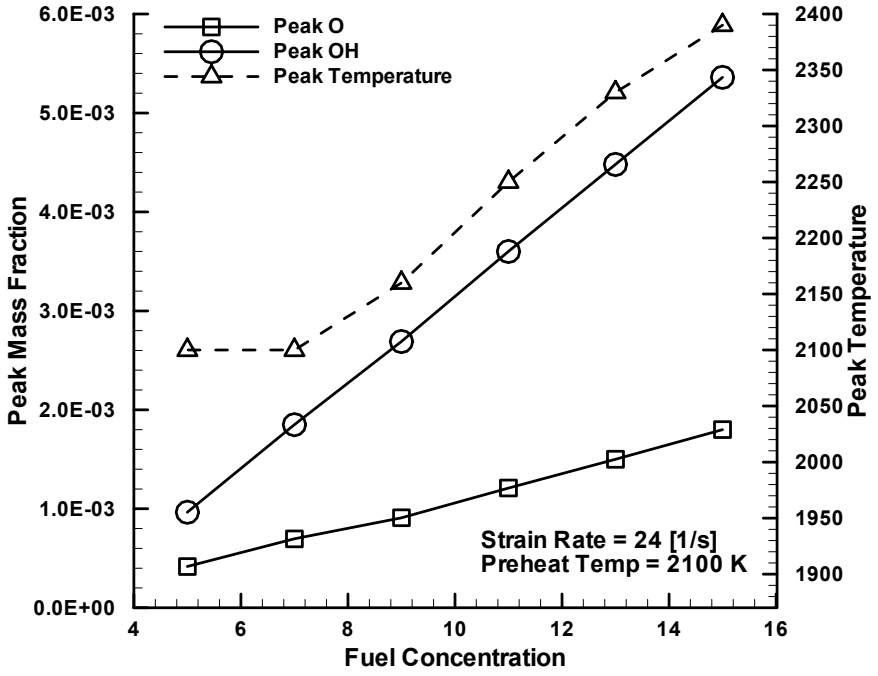


**Figure 4.25.** Peak Radical Mass Fractions vs Fuel Concentration for 2100 K and 24 $sec^{-1}$

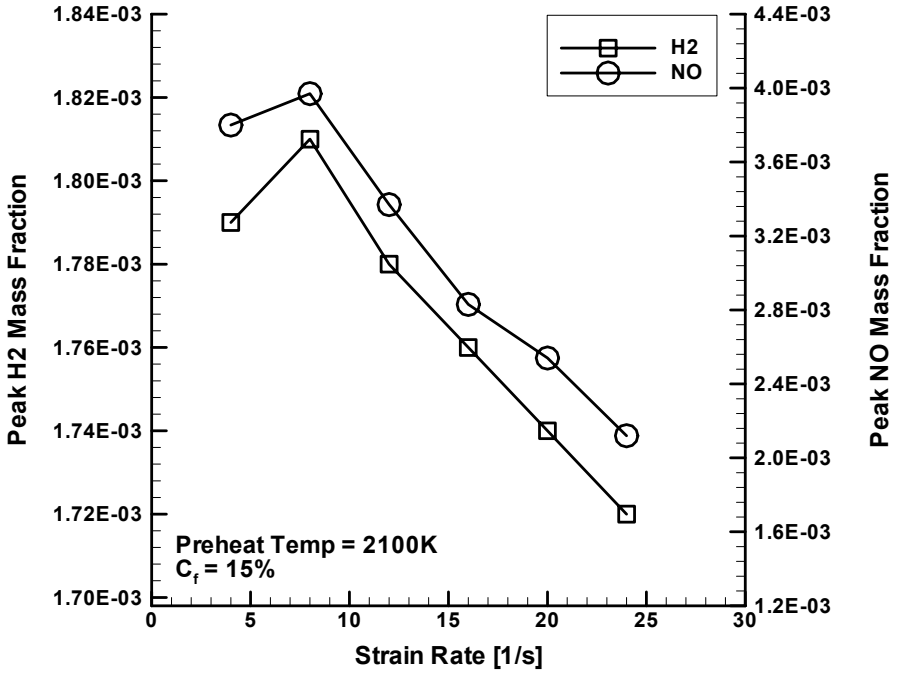


**Figure 4.26.** Peak $H_2$ and NO Mass Fractions vs Strain for 2100 K

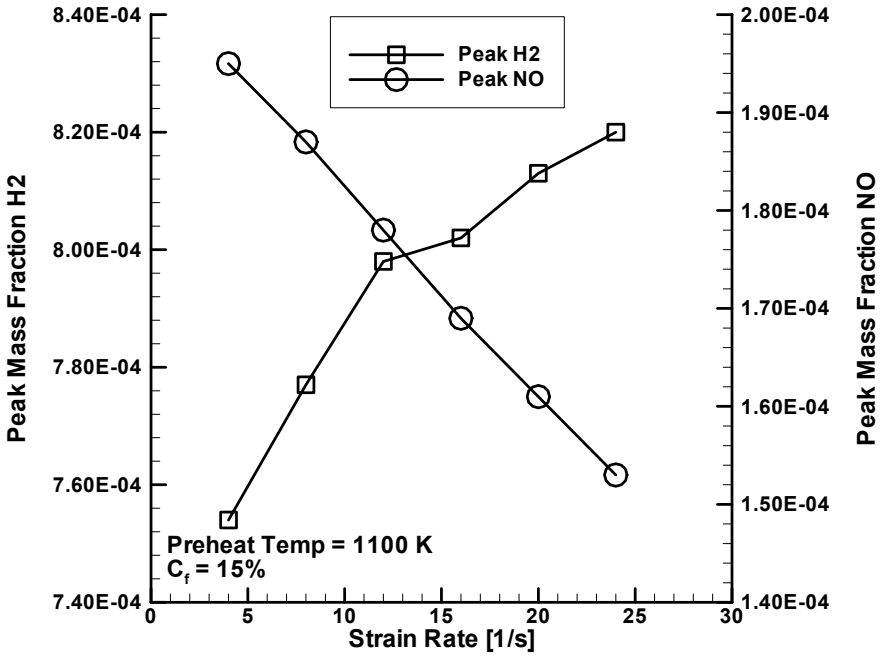


**Figure 4.27.** Peak $H_2$ and NO Mass Fractions vs Strain for 1100 K

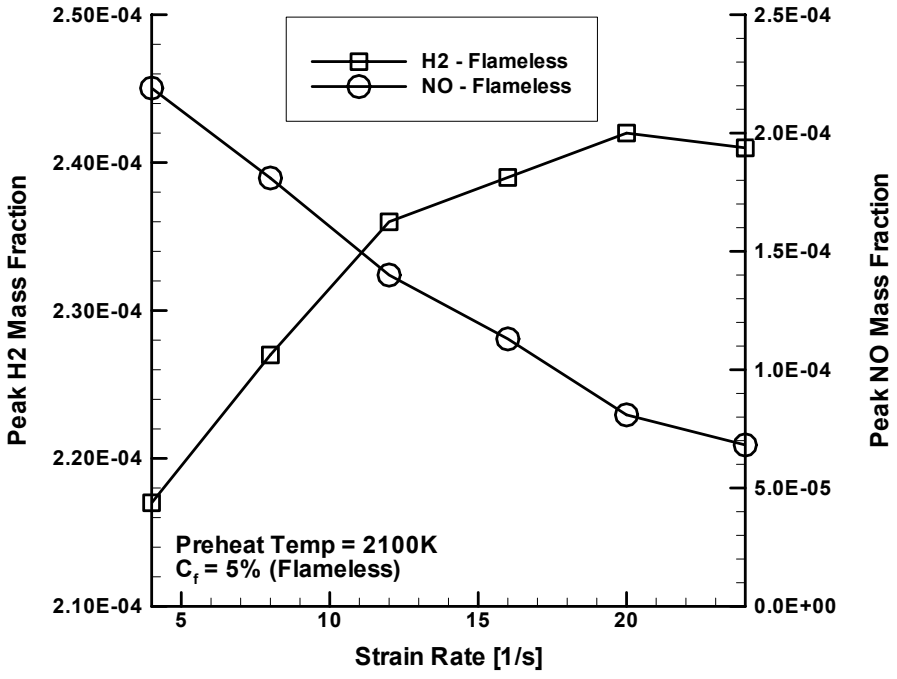


**Figure 4.28.** Peak $H_2$ and NO Mass FractionsVs Strain for 2100 K Flameless

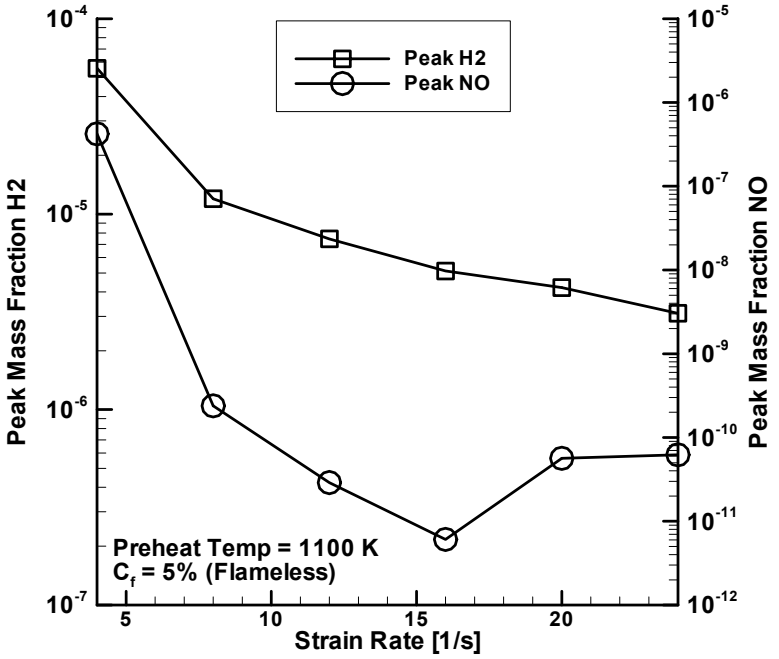


**Figure 4.29.** Peak $H_2$ and NO Mass FractionsVs Strain for 1100 K Flameless

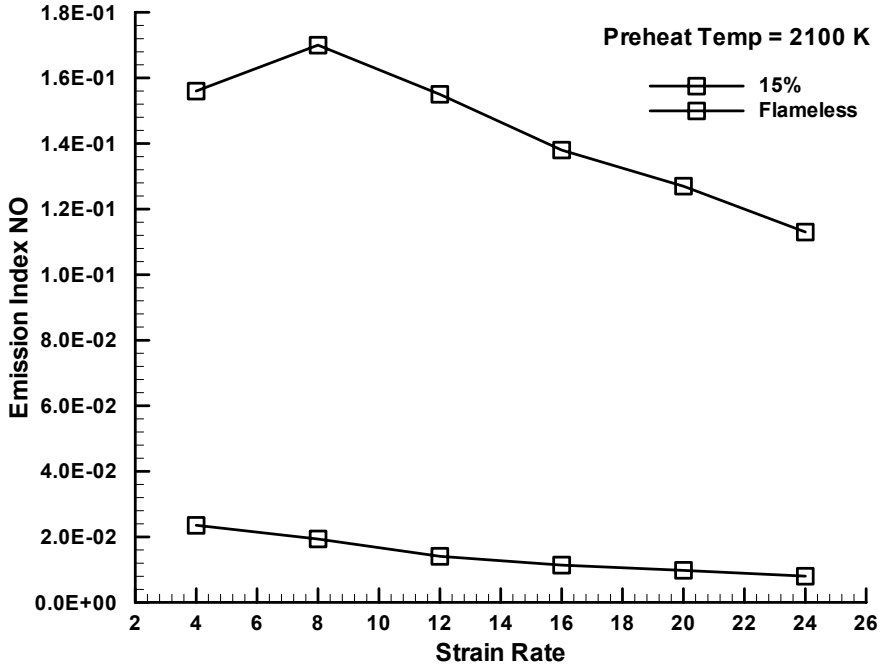


**Figure 4.30.** Emission Index for NO vs Strain for Flame-based and Flameless at 2100 K

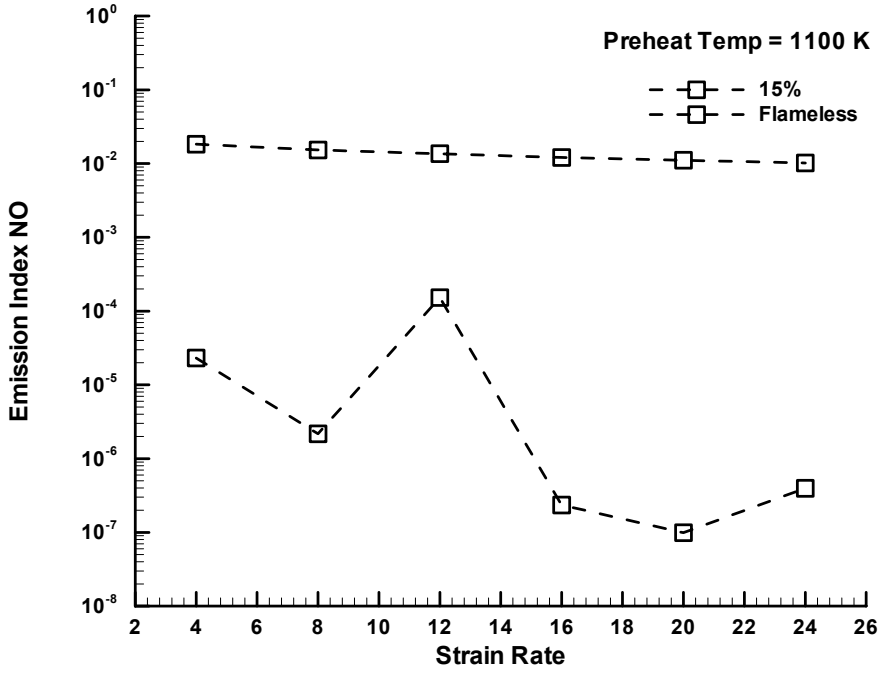


**Figure 4.31.** Emission Index for NO vs Strain for Flame-based and Flameless at 1100 K

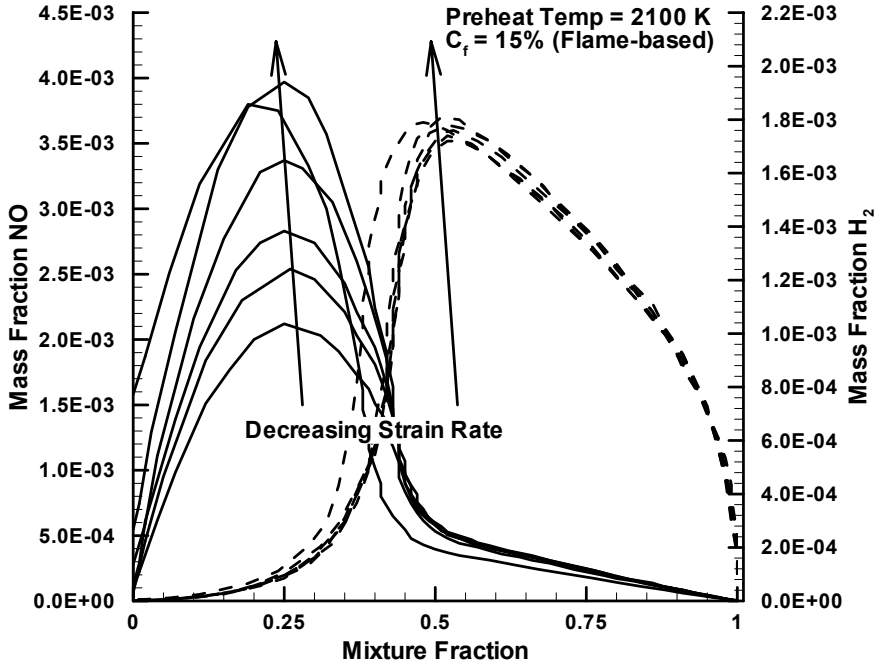


**Figure 4.32.** $H_2$ and NO Profiles vs Strain for Flame-based

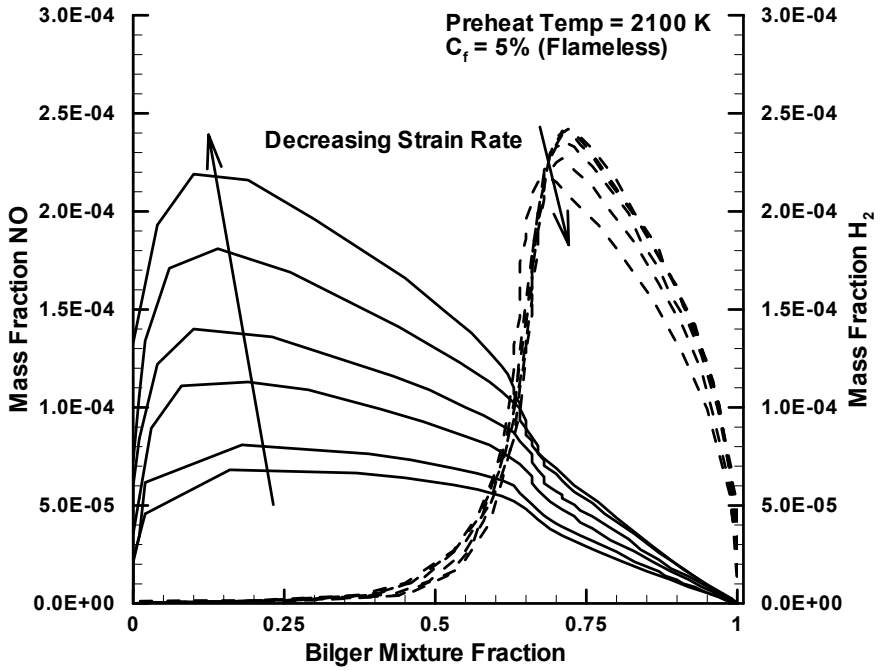


**Figure 4.33.** $H_2$ and NO Profiles Vs Strain for Flameless

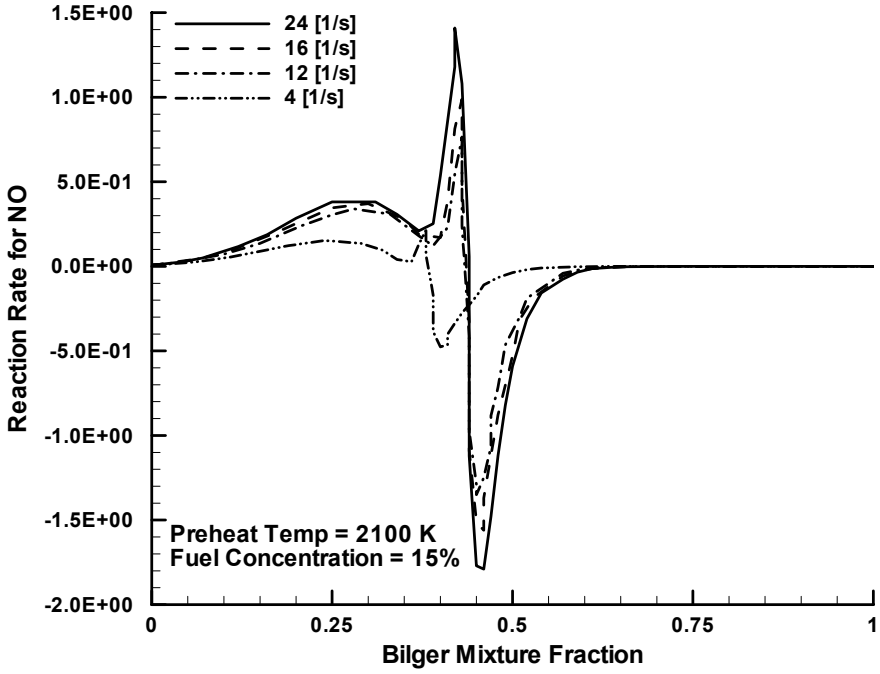


**Figure 4.34.** Overall Reaction Rate for NO vs Strain for 2100 K & 15%

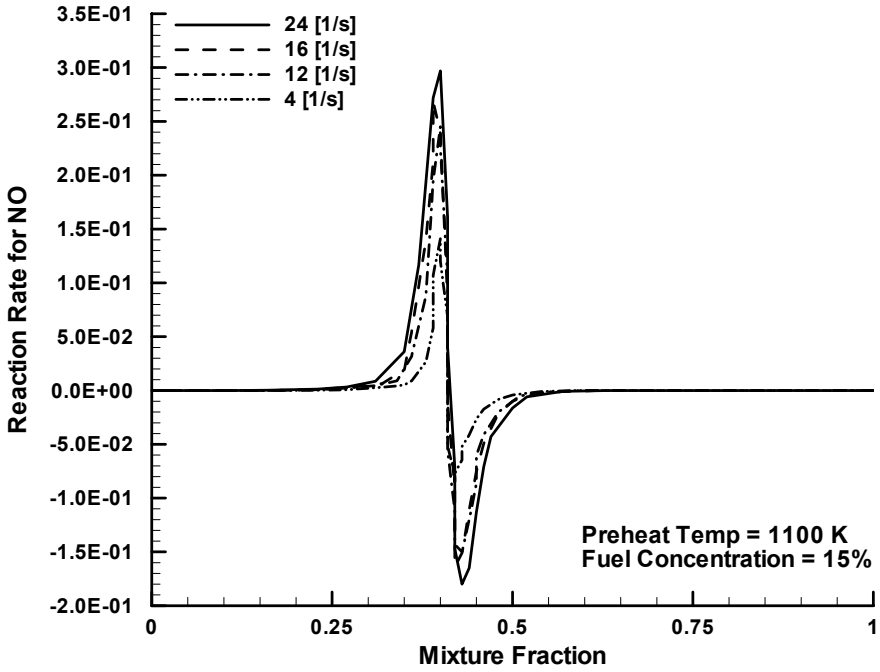


**Figure 4.35.** Overall Reaction Rate for NO vs Strain for 1100 K & 15%

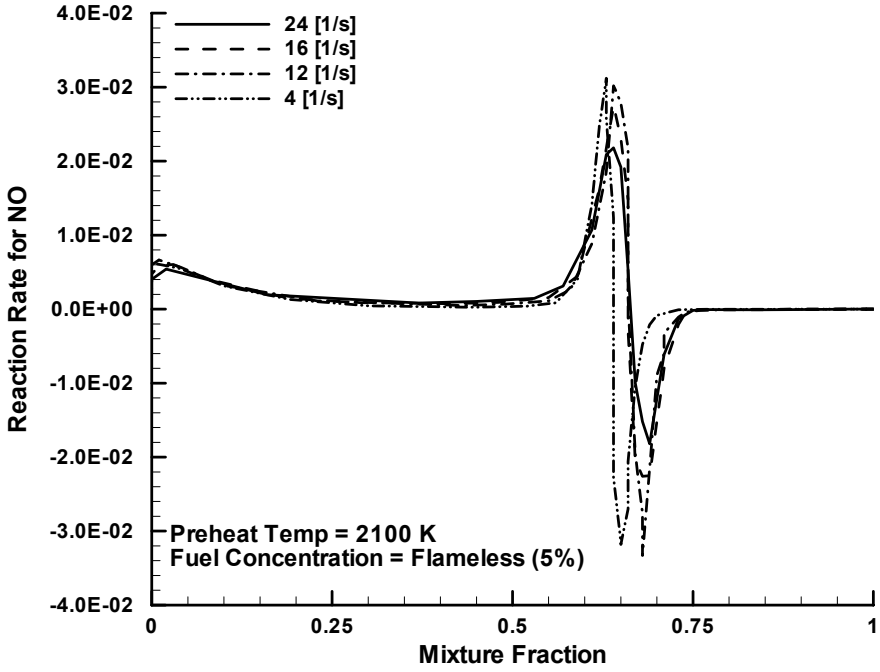


**Figure 4.36.** Overall Reaction Rate for NO vs Strain for 2100 K & Flameless

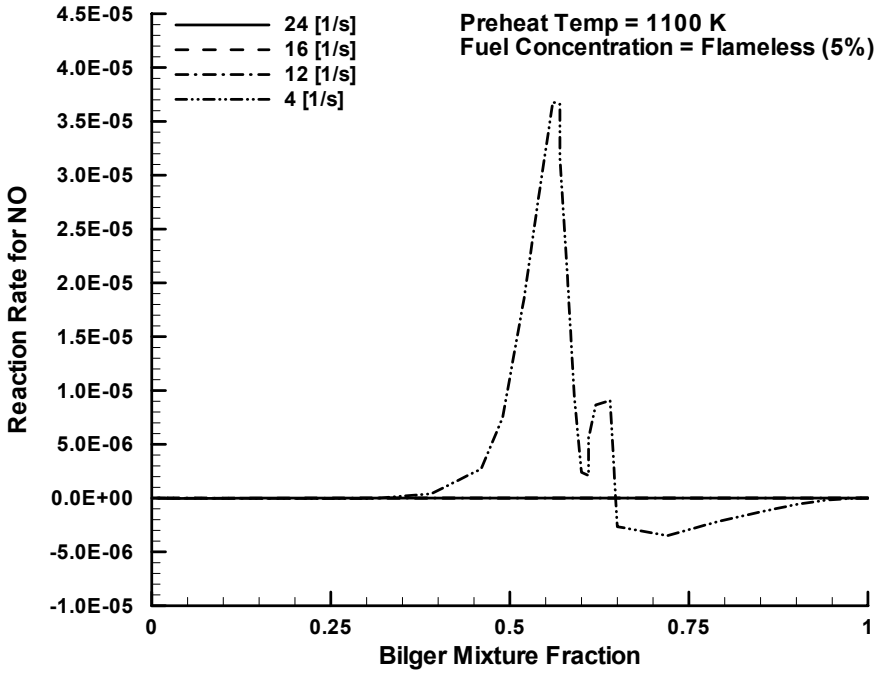


**Figure 4.37.** Overall Reaction Rate for NO vs Strain for 1100 K & Flameless

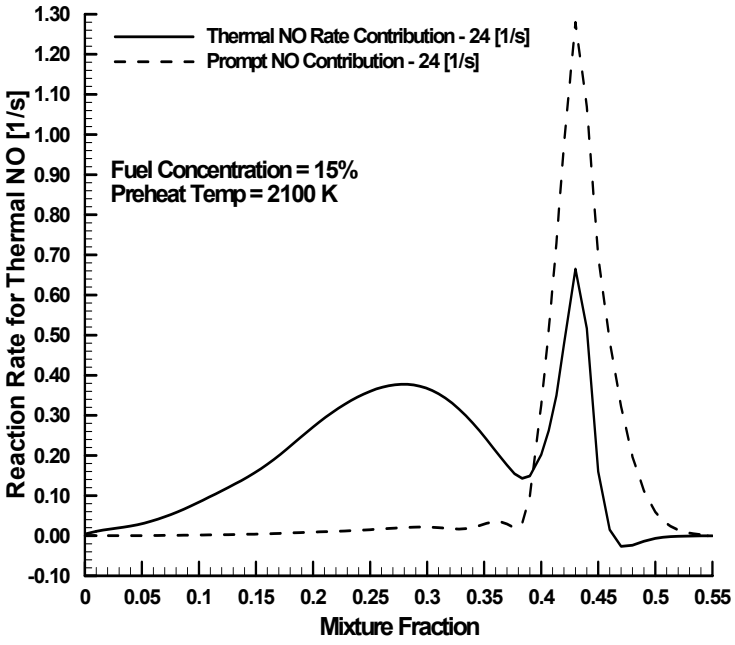


**Figure 4.38.** Thermal and Prompt NO for15% at 2100 and 24 $sec^{-1}$

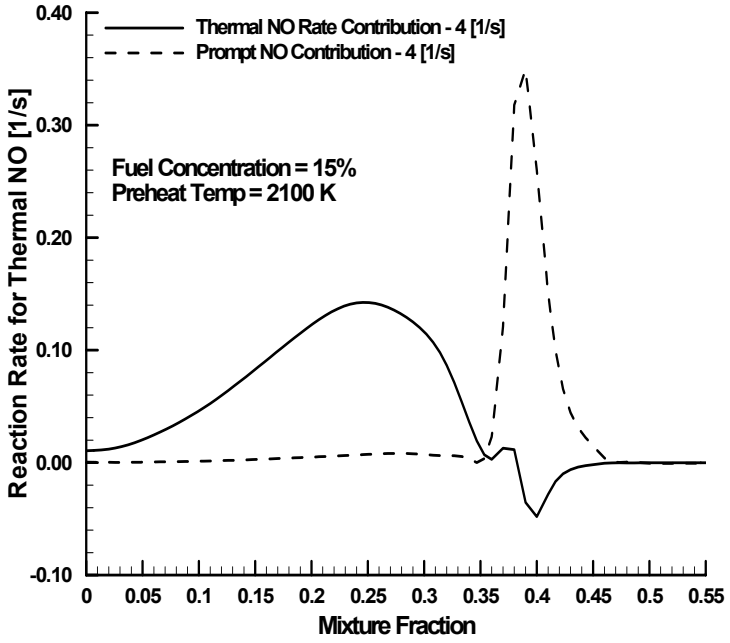


**Figure 4.39.** Thermal and Prompt NO vs Strain Rate for15% at 2100 and 4 $sec^{-1}$

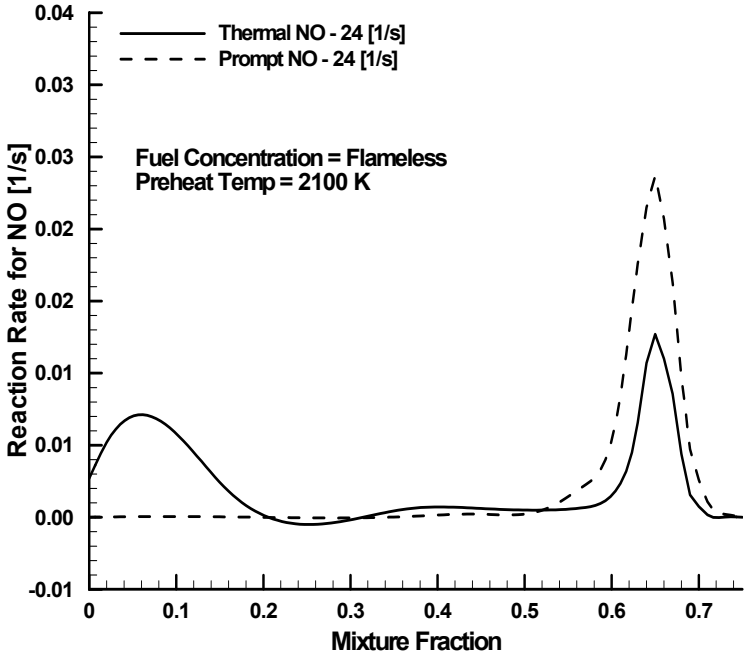


**Figure 4.40.** Thermal and Prompt NO for Flameless at 2100 K at 24 $sec^{-1}$

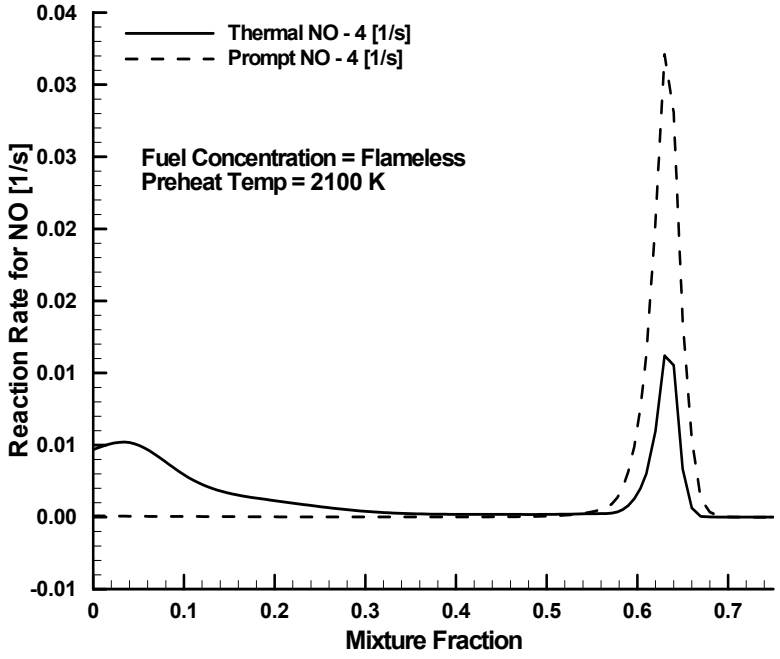


**Figure 4.41.** Thermal and Prompt NO for Flameless at 2100 and 4 $sec^{-1}$

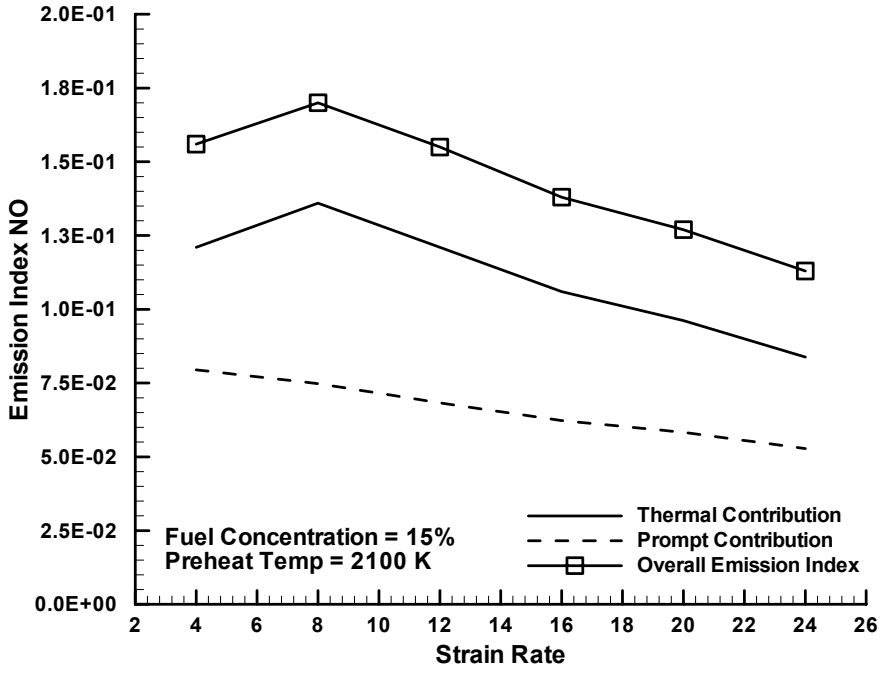


**Figure 4.42.** Emission Index for Thermal and Prompt NO vs Strain for 15% at 2100 K

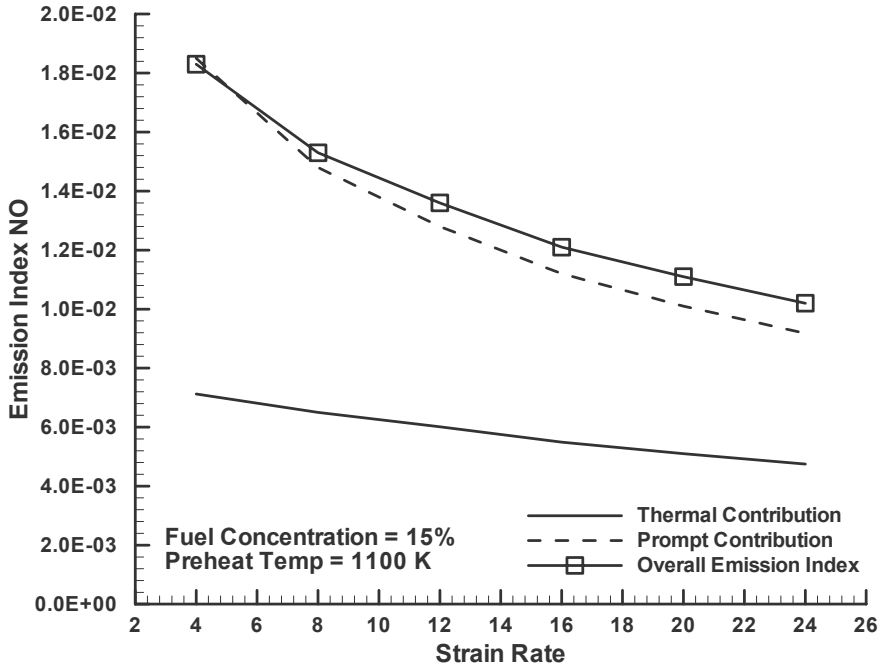


**Figure 4.43.** Emission Index for Thermal and Prompt NO vs Strain for 15% at 1100 K

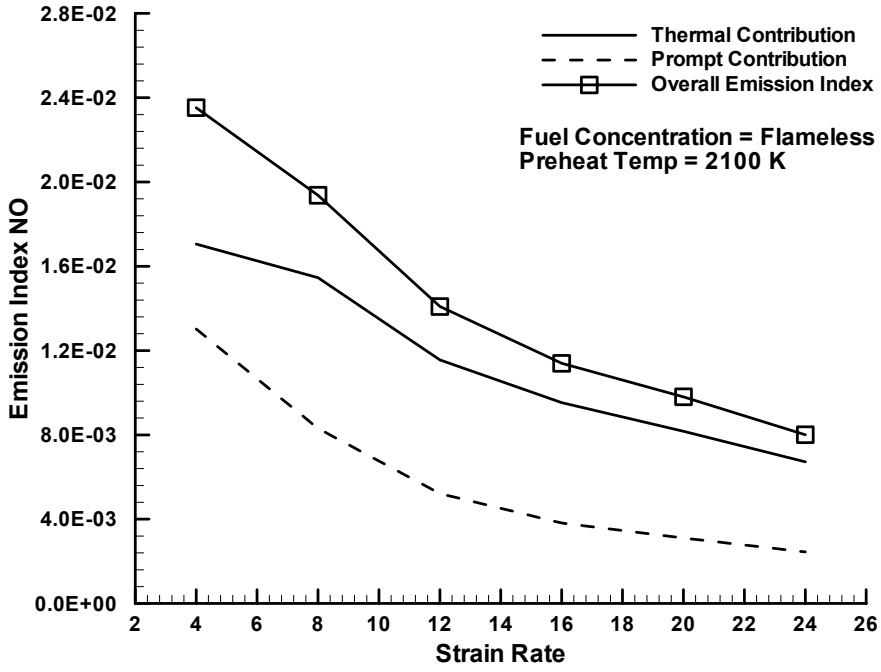


**Figure 4.44.** Emission Index for Thermal and Prompt NO vs Strain for Flameless at 1100 K

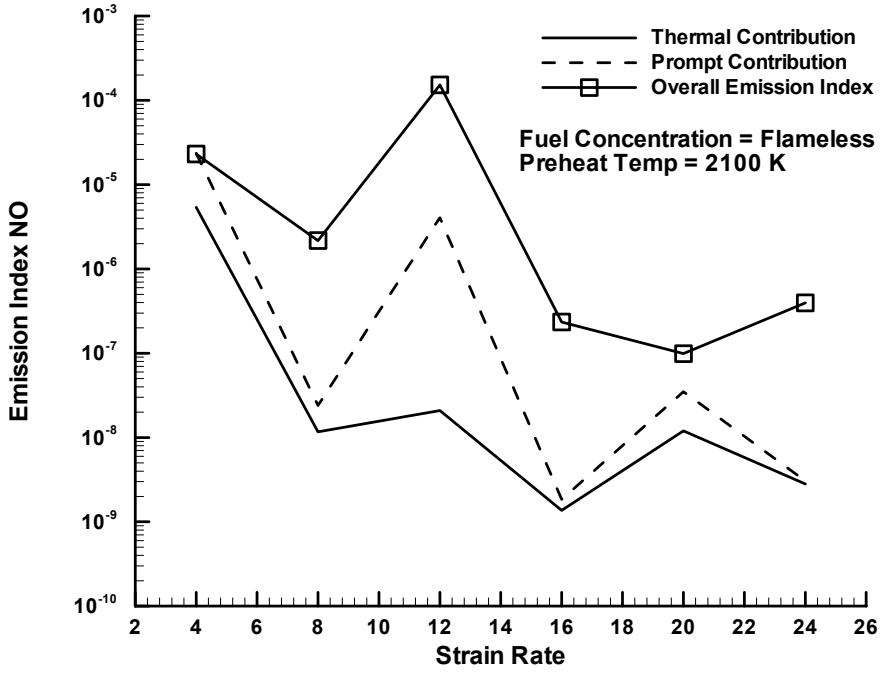


**Figure 4.45.** Emission Index for Thermal and Prompt NO vs Strain for Flameless at 1100 K

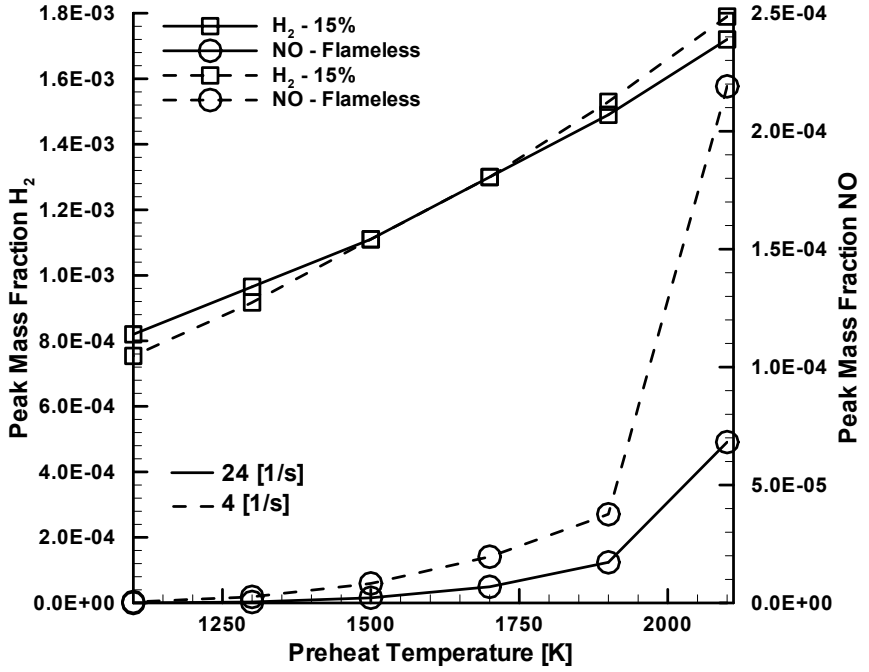


**Figure 4.46.** $H_2$ and NO Profiles Vs Preheat for Flame-based and Flameless

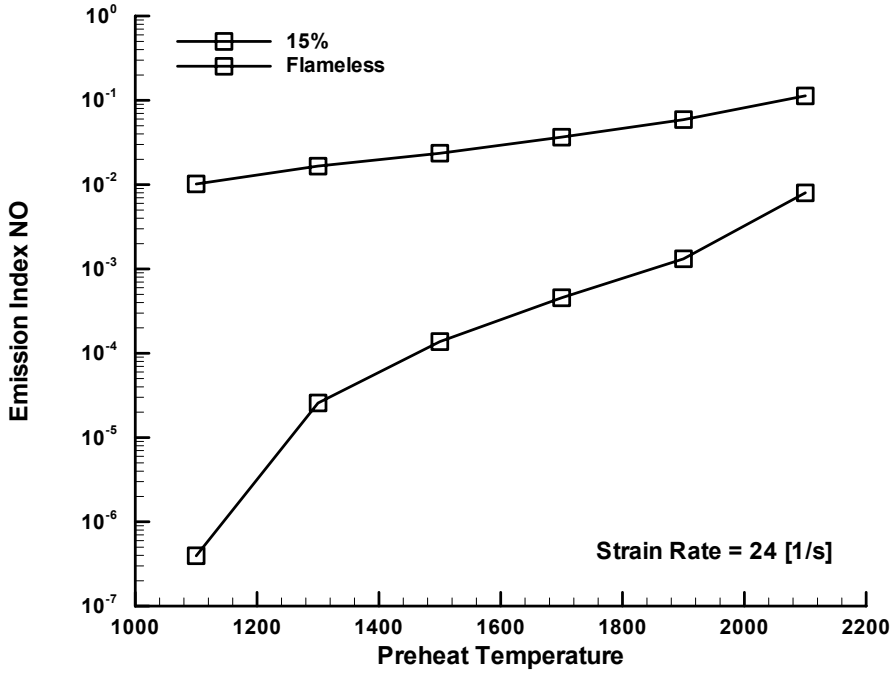


**Figure 4.47.** Emission Index NO vs Preheat for Flame-based and Flameless at 24 $sec^{-1}$

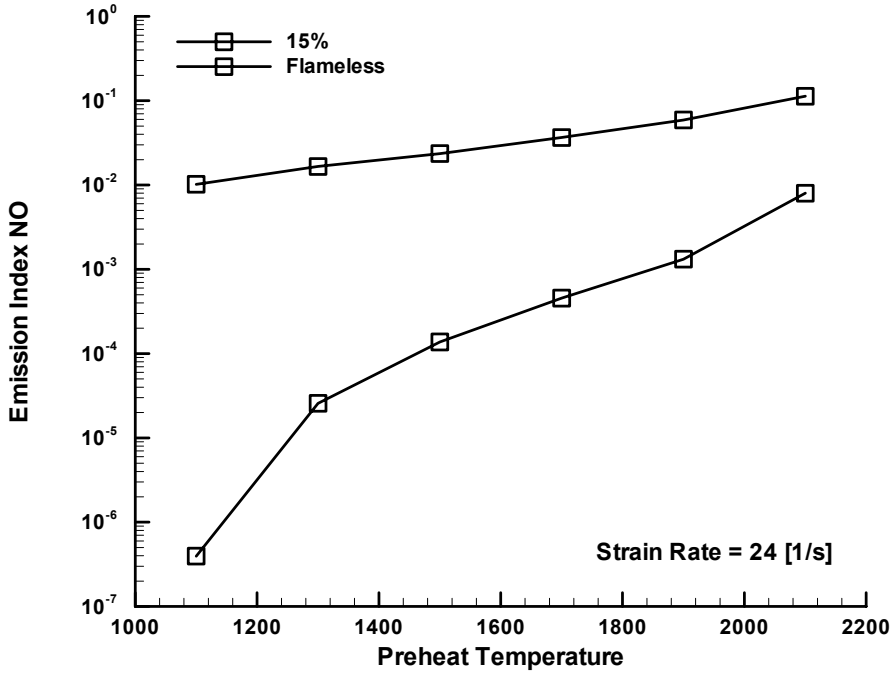


**Figure 4.48.** Emission Index NO vs Preheat for Flame-based and Flameless at 4 $sec^{-1}$

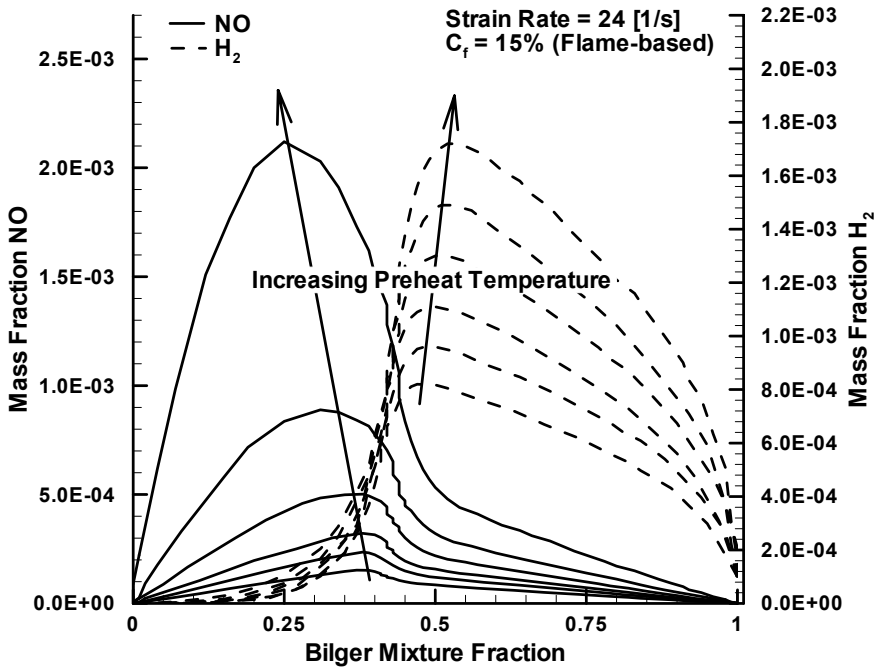


**Figure 4.49.** $H_2$ and NO Profiles vs Preheat for Flame-based with 24 $sec^{-1}$

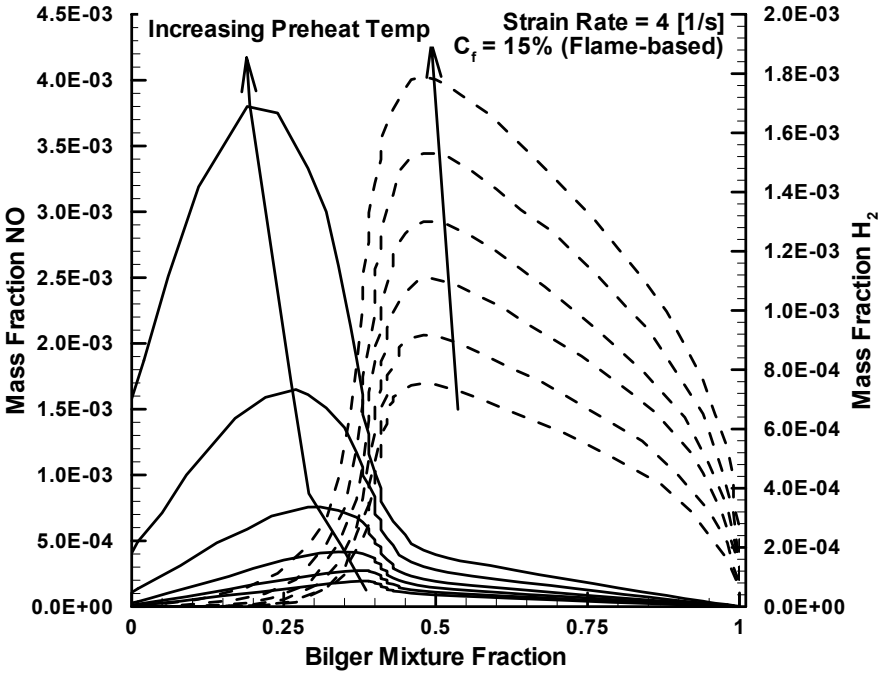


**Figure 4.50.** $H_2$ and NO Profiles vs Preheat for Flame-based with 4 $sec^{-1}$

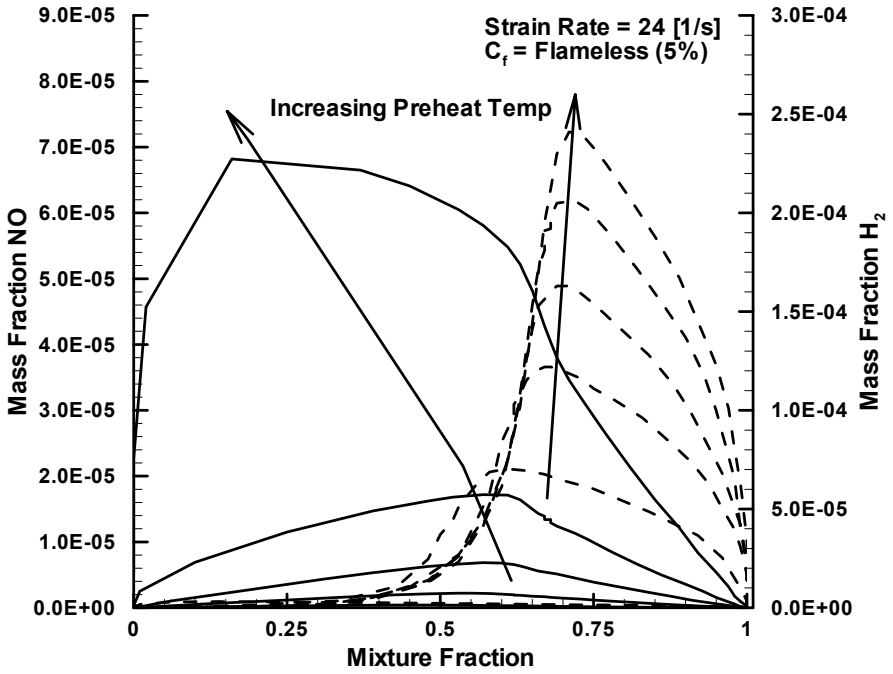


**Figure 4.51.** $H_2$ and NO Profiles vs Preheat for Flameless with 24 $sec^{-1}$

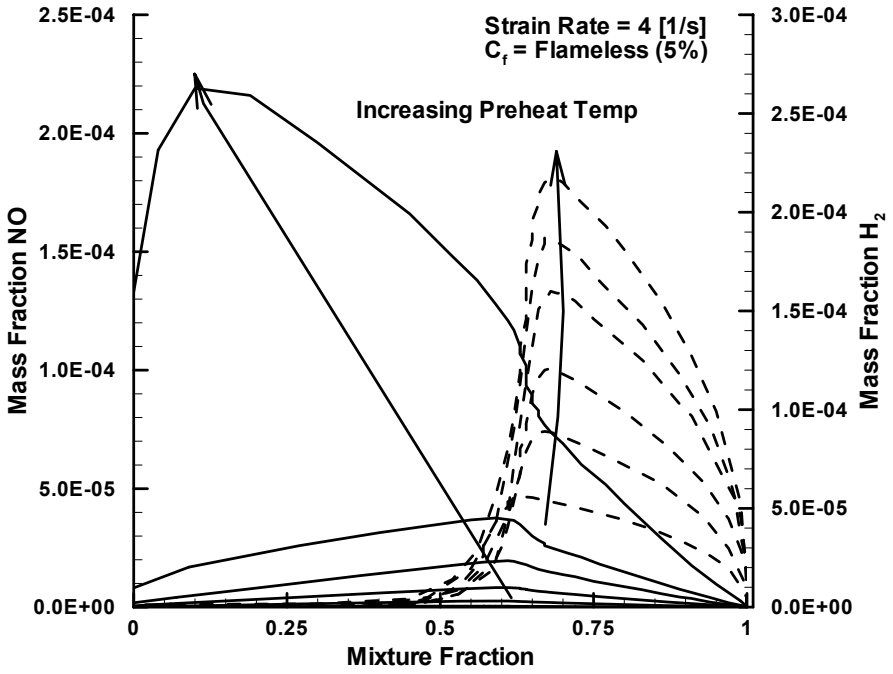


**Figure 4.52.** $H_2$ and NO Profiles vs Preheat for Flameless with 4 $sec^{-1}$

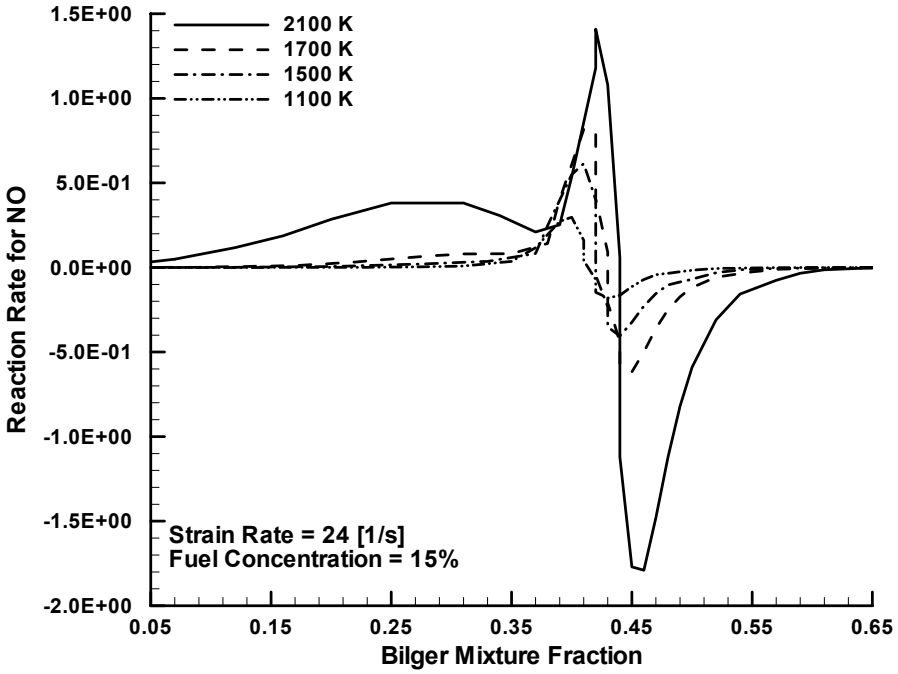


**Figure 4.53.** Overall Reaction Rate for NO vs Preheat Temp for 24 $sec^{-1}$ & 15%

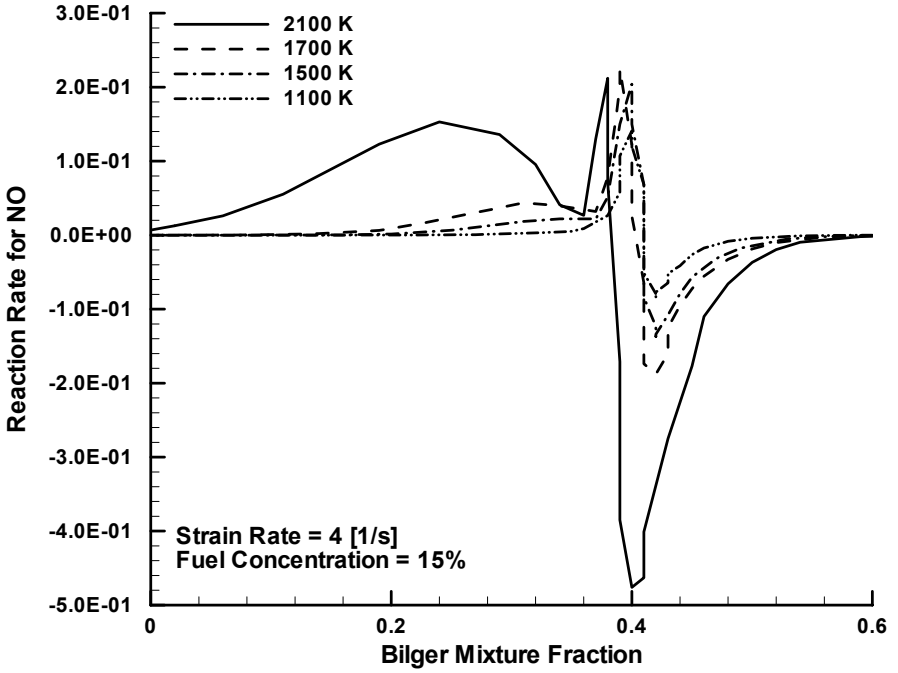


**Figure 4.54.** Overall Reaction Rate for NO vs Preheat Temp for 4 $sec^{-1}$ & 15%

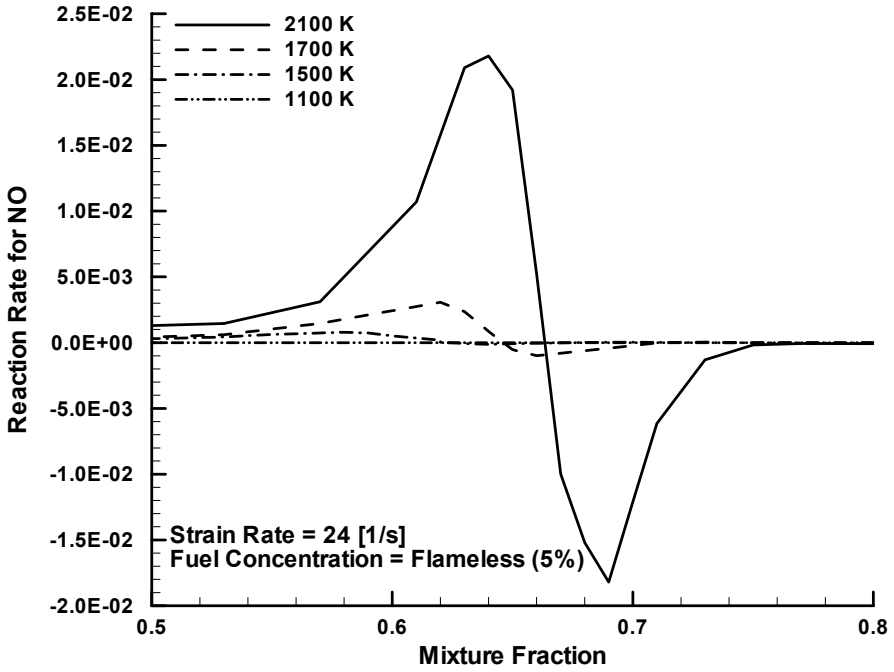


**Figure 4.55.** Overall Reaction Rate for NO vs Preheat Temp for 24 $sec^{-1}$ & Flameless

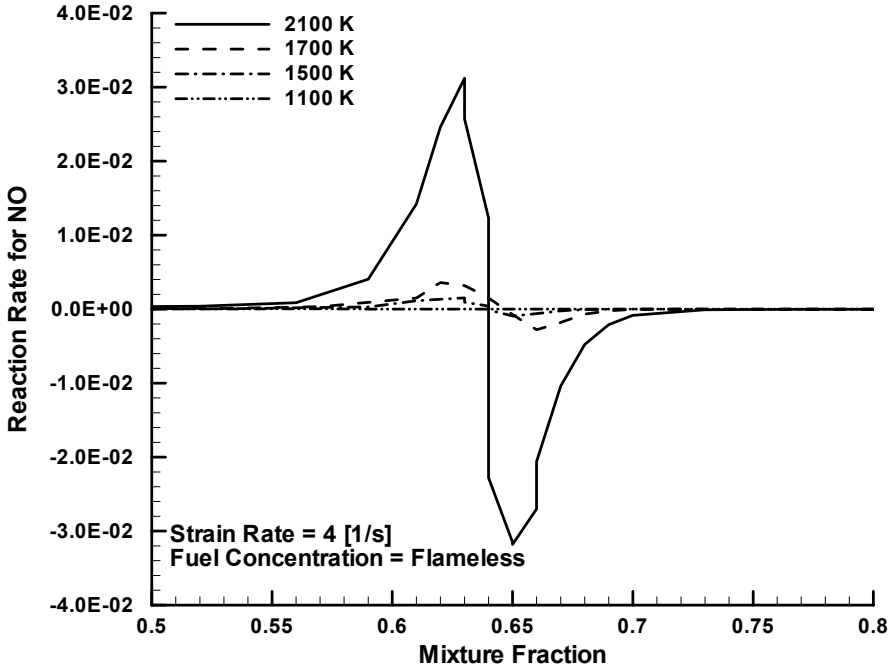


**Figure 4.56.** Overall Reaction Rate for NO vs Preheat Temp for 4 $sec^{-1}$ & Flameless

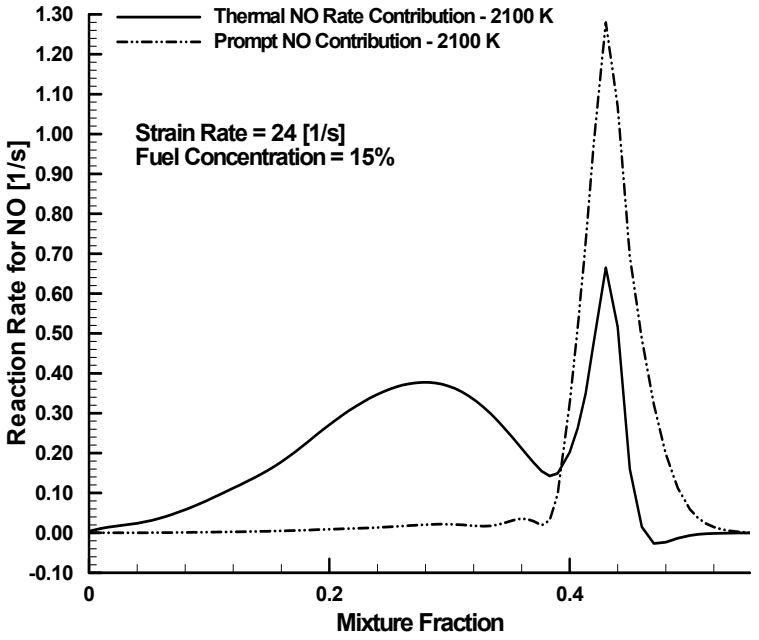


**Figure 4.57.** Thermal and Prompt NO vs Preheat for15% at 2100 and 24 $sec^{-1}$

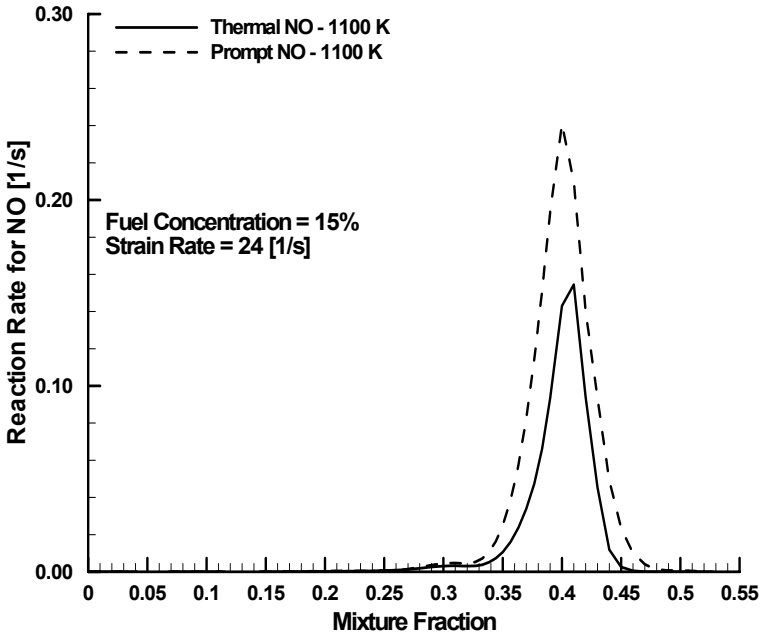


**Figure 4.58.** Thermal and Prompt NO vs Preheat for15% at 2100 and 4 $sec^{-1}$

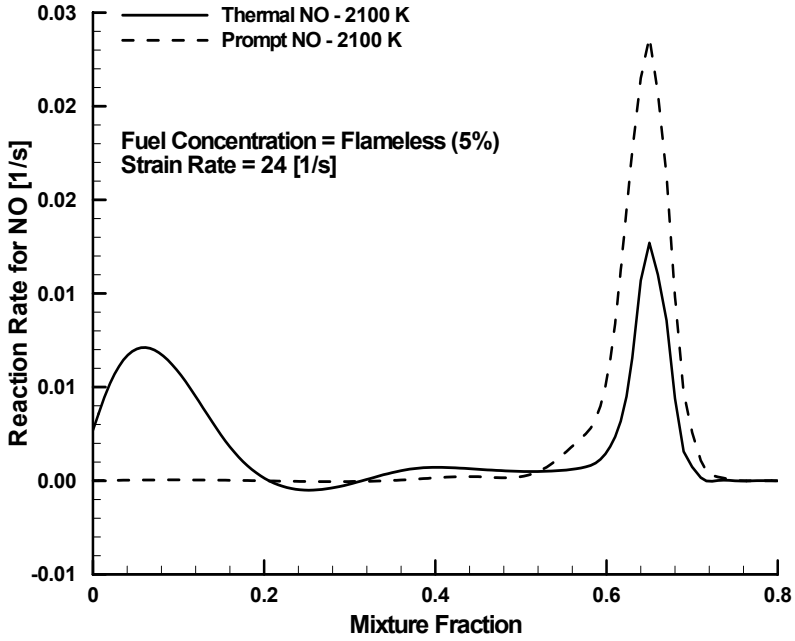


**Figure 4.59.** Thermal and Prompt NO vs Preheat for Flameless at 2100 and 4 $sec^{-1}$

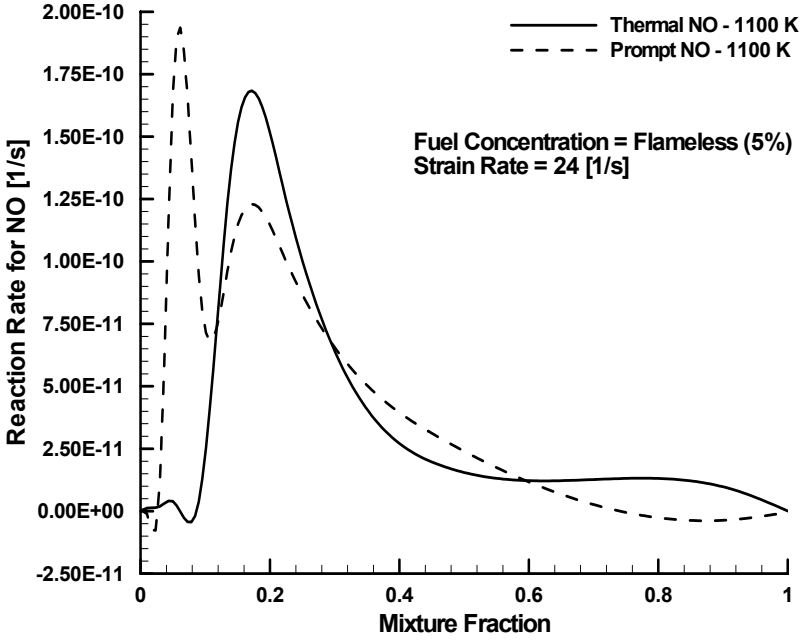


**Figure 4.60.** Thermal and Prompt NO vs Preheat for Flameless at 2100 and 4 $sec^{-1}$

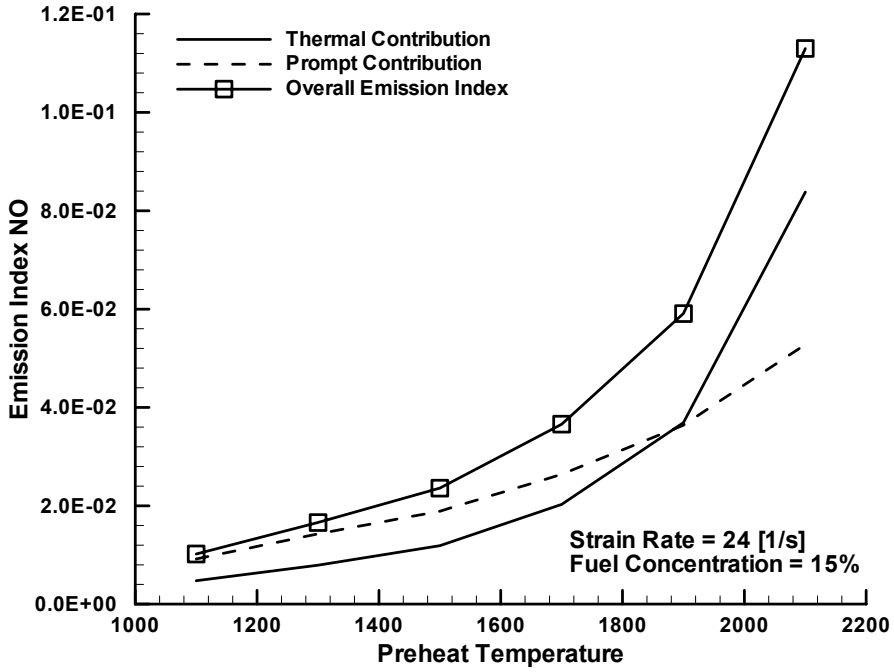


**Figure 4.61.** Emission Index for Thermal and Prompt NO vs Preheat for 15% at 24 $sec^{-1}$

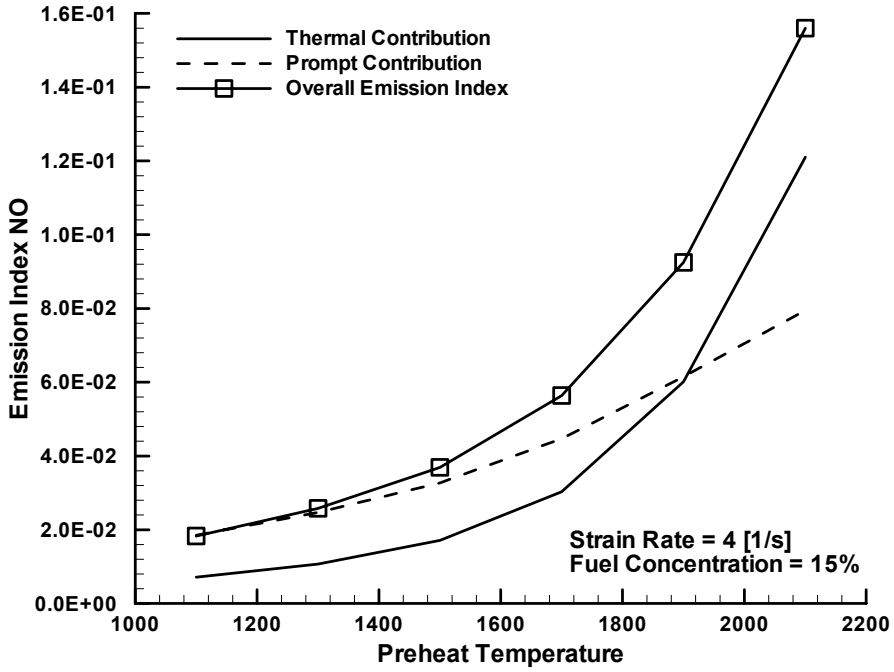


**Figure 4.62.** Emission Index for Thermal and Prompt NO vs Preheat for 15% at 4 $sec^{-1}$

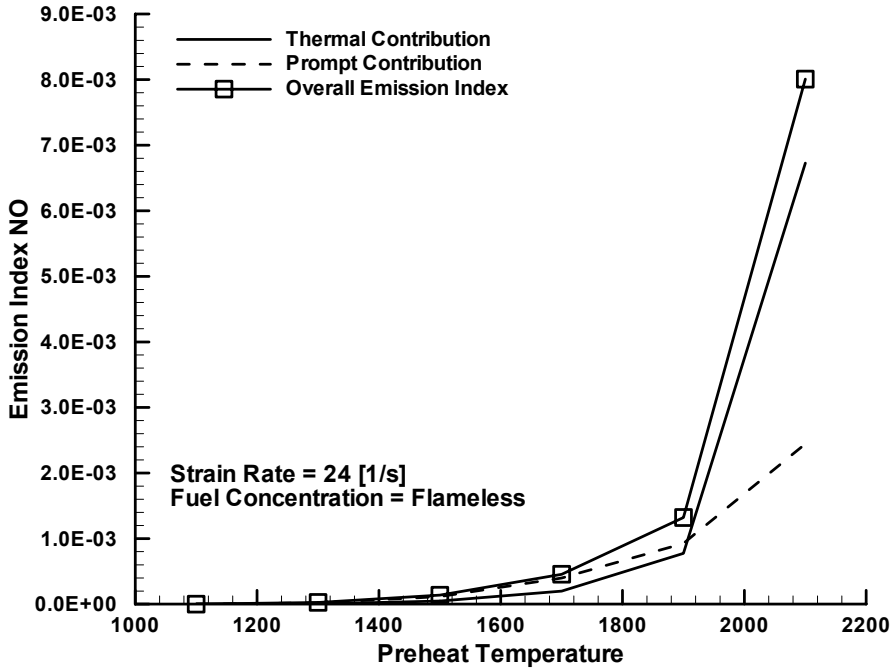


**Figure 4.63.** Emission Index for Thermal and Prompt NO vs Preheat for Flameless at 24 $sec^{-1}$

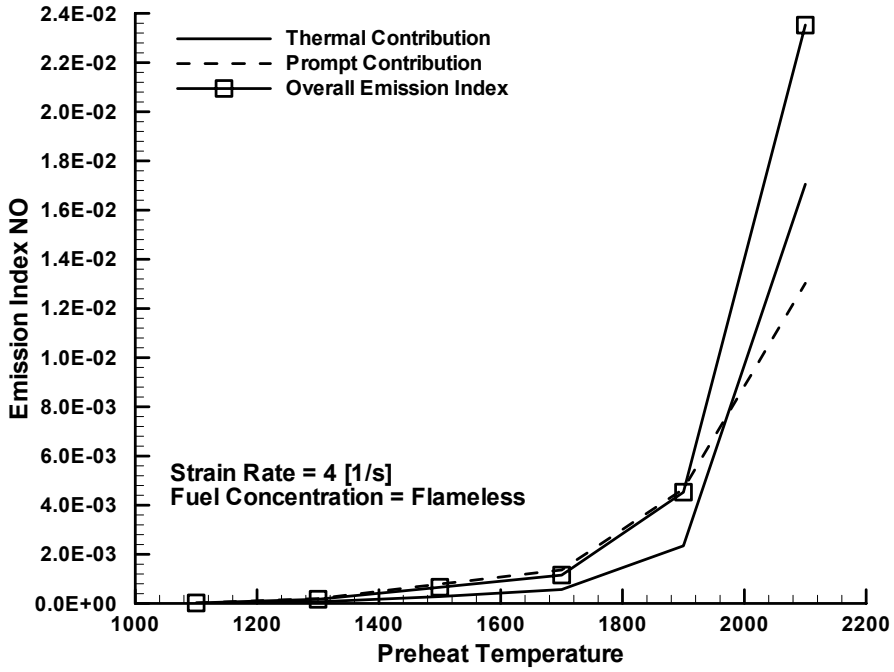


**Figure 4.64.** Emission Index for Thermal and Prompt NO vs Preheat for Flameless at 4 $sec^{-1}$

# CHAPTER V

# SYNTHESIS

## 5.1. NO and $H_2$ Emissions and Damkohler Number

As discussed above, when considering combustion as a power source on any scale, an aspect that deserves much consideration is that of emissions. Figures 8 and 9 depict the mass fraction of NO versus Bilger mixture fraction and the peak $NO_x$ as a function of strain rate. NO is the largest contributor to $NO_x$ and is therefore the only species considered here. NO profiles in mixture fraction space yield differing peaks for the various fuel dilutions and strain rates. The peak NO concentration decreases with increased strain. As in steady flames, the correlation of NO with strain rate is closely associated with residence time, and the reduction of residence time associated with increased strain. The Damkohler number is a dimensionless number used to show the relativistic scales of mixing and chemistry, i.e. $\mathrm{Da} = \tau_m / \tau_{ch}$ , where $\tau_m$ is the mixing time and $\tau_{ch}$ is the characteristic time of the chemical reaction. The mixing time is generally regarded as $\tau_{fl} = \tau_m = L/(V_F + V_O) = L/2V$ (Sohn et al., 2002) when the oxidizer and fuel are at the same inlet velocity. The chemical reaction characteristic time is not so simple, however, since there are several methods of determining this parameter. Williams (2000) proposes the use of $S_L = \sqrt{D_g / \tau_{ch}}$ , where $S_L$ (the laminar flame speed) and $D_g$ (a characteristic thermal diffusivity) are applied to a Stoichiometric mixture (premixed) of the fuel and oxidizer, while Golovitchev and Jarnicki (2001) suggest $c/c_1 = \tau_c / \tau_m + \tau_{ch}$ for a partially stirred reactor, where c is the concentration (in mean molar density) in the reaction zone and $c_1$ is the concentration at the reactor exit (or a post-combustion position). Though there exist several ways of finding the Damkohler number, it is used to give a representative relationship between the fluid flow regime time scales and the chemical reaction time scales. When the Damkohler Number is large, the reaction is proceeding quickly, i.e. $\tau_{ch}$ is small, while the opposite is true for small *Da*, where the reaction time and the mixing time scales are closer, meaning either a slower flow regime for a constant reaction time scale or a slower reaction given a constant mixing time scale. Given a constant fuel, as in this study, the reaction time scale is more or less constant,

which leaves the mixing time scale the controlling variable. Therefore, when this scale is lessened as in a slower velocity regime, the *Da* number is smaller. In this case, that means that the overall amount of chemistry is larger, which means greater NO concentration peaks as seen in Figure 8. Figure 9 depicts a similar trend for $NO_2$ to that of NO that is shown and described above. Though the trend is present, the relative magnitudes for $NO_2$ mass fraction is negligible compared to NO and are therefore omitted from any further discussion.

## 5.2. Summary of the Effects of Fuel Concentration

Through the data presented above, it can be seen that there is a general decrease in the production of NO and $H_2$ with a decrease in fuel concentration. This is due to the reduced fuel present to transport to the flame, i.e. to supply the chemical reaction. There is also a shift present in the location of the peak mass fraction for both species. This shift represents a shift in flame position in mixture fraction space towards stoichiometric conditions. The emission index of NO was found to decrease as fuel concentration is lowered due in part to the weakening reaction as fuel concentration is decreased. A decrease in reaction rate is observed with a decrease in fuel concentration. This is also due to the relative weakening chemical reaction caused by a decrease in fuel concentration. While there is a decrease in the overall contribution of both thermal and prompt NO as fuel concentration is decreased, there is also a decrease in the individual contributions of thermal and prompt NO. The contributions do not shift between a much more dominant thermal NO mechanism to more of a balance between thermal and prompt NO as fuel concentration is varied, however, at lower fuel concentrations, the contributions become much more balanced. Due to the high dependence on temperature seen in the thermal NO mechanism, the thermal NO mechanism is dominant at higher preheat temperatures, while the prompt is dominant at lower preheat temperatures.

## 5.3. Summary of the Effects of Strain Rate

With an increase in strain rate, a decrease in residence time is observed by the flame, which results in lower mass fractions of the two species studied. Initially, however, there can be seen an increase in mass fraction due to the increase in transport of fuel and oxidizer to the flame to support the chemistry. As strain rate is increased further, the residence time is

diminished to the point that it begins to effect the formation of both species and there is a subsequent decrease in both species mass fractions. Hydrogen is formed through a much faster mechanism than NO and therefore does not respond as readily to the decrease in residence time, i.e. the mechanism is forming $H_2$ on a time scale much smaller than the residence time. NO, however, is formed through a relatively slow mechanism and is more susceptible to changes in residence time, resulting in a greater sensitivity to strain rate. The emission index follows a similar pattern to that of the mass fraction of NO and increases with a decrease in strain rate due to an increase in residence time. At a fuel concentration of 15% and 2100 K preheat, the balance between transport and residence time is seen. An overall decrease in reaction rate for NO is observed with a decrease in strain rate. This is again due to the decrease in residence time and the response of the NO mechanism to that change. The contributions of the two reactions considered here follow the same trend as the overall reaction rate. Strain rate appears to have little effect on the individual contributions of these mechanisms. However, as strain rate increases, the difference between the two contributions lessens.

## 5.4. Summary of the Effects of Preheat Temperature

An increase in both species mass fractions is seen with an increase in preheat temperature for both flame-based and flameless cases. This is due to the higher enthalpy brought into the reaction by the high temperature oxidizer. This provides the driving force for flameless combustion and the weak chemical reaction becomes weaker as preheat temperature is decreased. NO, however, through the production by thermal NO, is more sensitive to preheat temperature than $H_2$. The emission index for NO is seen to be highly temperature dependent for both the flame-based and flameless cases. The flameless case, however, shows a much higher dependence on preheat temperature than the flame-based case due to the high dependence on excess enthalpy by the flameless case. The overall reaction rate increases with an increasing preheat temperature due to the increased energy brought into the reaction at higher preheat temperatures. The thermal NO mechanism is highly temperature dependent and becomes more dominant at higher preheat temperatures. At lower preheat temperatures; however, there is a shift between thermal and prompt as the role of thermal NO outside the reaction zone is diminished.

# CHAPTER V

## CONCLUSIONS

Fuel Concentration, Strain Rate, and Oxidizer Preheat Temperature play a major role in the formation of NO and H2 in counter-flow diffusion flames. It was seen that fuel concentration can play a major role in weakening (lowering fuel concentration) or strengthening (raising fuel concentration) the chemical reaction and subsequently, increasing or decreasing the productions of both NO and $H_2$. Strain rate has been seen to have a large effect on the slower mechanisms, but not the fast ones due to a balance between decreased residence times and higher transport and vice versa. For this reason, it may be useful to employ strain rate effects to simulate the conditions that exist in a finite length of a turbulent flame and shed light on the parameters that govern the flame characteristics. Preheat temperatures were seen to force the flame to respond to more or less excess enthalpy brought into the reaction zone by the high temperature oxidizer. This plays a vital role in sustaining the weak chemical reaction taking place in flameless combustion.

This study shows that flameless combustion can find a possible application in fuel reforming to produce hydrogen, however the three parameters discussed here play major roles in the balance between the desired product (hydrogen) and the undesired by-product (NO).

## REFERENCES


Bilger, R. W., Stårner, S. H., and Kee, R. J.. *On reduced mechanisms for methane air combustion in non-premixed flames*, Combust. & Flame, **80**: 135-149 (1990).

Golovitchev, V. I. and Jarnicki, R., *Numerical Modeling of High Temperature Air "Flameless" Combustion*, The 4th International Symposium on High Temperature Air Combustion and Gasification, 26-30 November, 2001, Rome – Italy.

Ju, Y., Guo, H., Maruta, K., and Liu, F., *On the Extinction Limit and Flammability Limit of Non-Adiabatic Stretched Methane-Air Premixed Flames*, J. Fluid Mech., **342**: 315-334 (1997).

Giovangigli, V., and Smooke, M. D., *Combust. Sci.Technol,.* **53**:23–49 (1987).

Glassman, I., *Combustion,* Third Edition, Academic Press, New York, 1996.

Gregory P. Smith, David M. Golden, Michael Frenklach, Nigel W. Moriarty, Boris Eiteneer, Mikhail Goldenberg, C. Thomas Bowman, Ronald K. Hanson, Soonho Song, William C. Gardiner, Jr., Vitali V. Lissianski, and Zhiwei Qin, http://www.me.berkeley.edu/gri_mech/.

Guo, H., Ju, Y., Maruta, K., Niioka, T., and Liu, F., *Radiation Extinction Limit of Counterflow Premixed Lean Methane-Air Flames*, Combust. & Flame, **109**: 639-646 (1997).

Ju, Y. and Niioka, T., *Computation of NOx emission of a methane–air diffusion flame in a two-dimensional laminar jet with detailed chemistry*, Combust. Theo. Model., **1**: 243-258 (1997).

Lutz, A.E., Kee, R.J., Grcar, J.F., Rupley, F.M., *OPPDIF: A Fortarn Program for Computing Opposed-Flow Diffusion Flames*, Sandia National Laboratories Report, SAND96-8243, 1996.

Maruta, K, Muso, K., Takeda, K. and Niioka, T., *Reaction Zone Structure In Flameless Combustion*, Proc. of the Combust. Instit. **28**: 2117–2123 (2000).

Miller, J.A., and Bowman, C.T., *Mechanism and Modeling of Nitrogen Chemistry in Combustion*, Prog. Energy Combust. Sci., 15(4): 287-338 (1989).

Orsino, S., Weber, R., and Bollettini, U., *Numerical Simulation of Combustion of Natural Gas with High-Temperature Air*, Combust. Sci. & Tech., **170**: 1-34 (2001).

Plessing, T. Peters, N., and Wünning J. G., *Laseroptical Investigation of Highly Preheated Combustion with Strong Exhaust Gas Recirculation*, Proc. of the Combust. Instit., 27: 3197–3204 (1998).

Sohn, C.H., Jeong, I.M., and Chung S.H., *Numerical Study of the Effects Of Pressure and Air-Dilution on NO Formation in Laminar Counterflow Diffusion Flames of Methane in High Temperature Air,* Combust. Flame, 130:83-93 (2002).

Williams, F. A., *Progress in Knowledge of Flamelet Structure and Extinction*. Prog. Energy & Combust. Sci., **26**: 657-682 (2000).

Wünning, J. A. and Wünning, J. G., *Flameless Oxidation to Reduce Thermal NO-Formation*, Prog. Energy and Combust. Sci., **23**: 81-94 (1997).

## APPENDIX A

## THE OPPDIF FORMULATION AND SOLUTION METHOD

Oppdif is a combustion application that utilizes the CHEMKIN Thermodynamic Library to solve an opposed flow diffusion flame. The code utilizes a similarity solution to transform either a 3 dimensional axisymmetric (see Figure 1-A) configuration or a 2 dimensional planar (see Figure 2-A) into a 1 dimensional problem. The code solves for temperature, species, and velocity profiles and returns these into a binary data file. A postprocessor allows this data to be separated and configured to a particular case. The solution technique used is TWOPNT, which solves "the two-point boundary value problem for the steady-state form of the discretized equations", while the CHEMKIN Thermodynamic Property Library is used to determine the necessary thermodynamic properties for that solution.

For the two dimensional case,

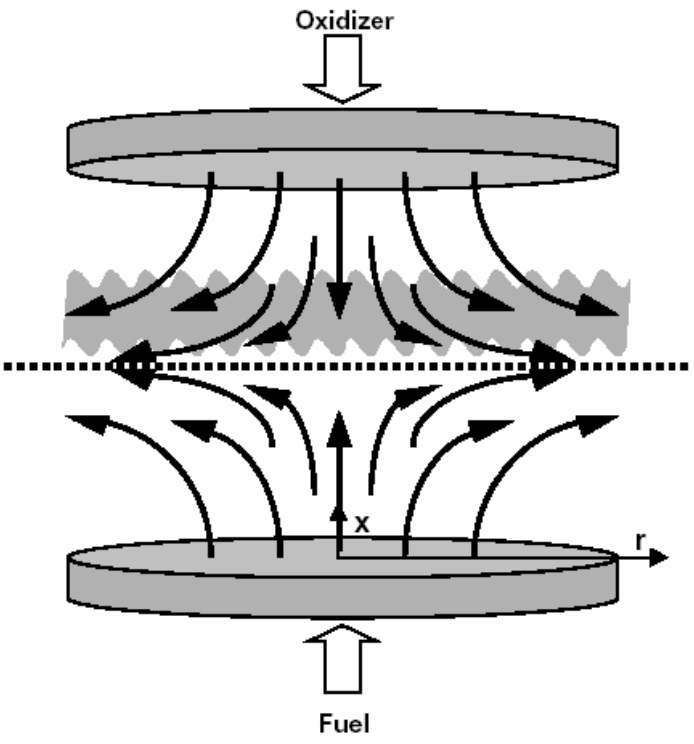


**Figure 4.65.** Figure 1-A: Axi-symmetric Opposed Flow Diffusion Flame

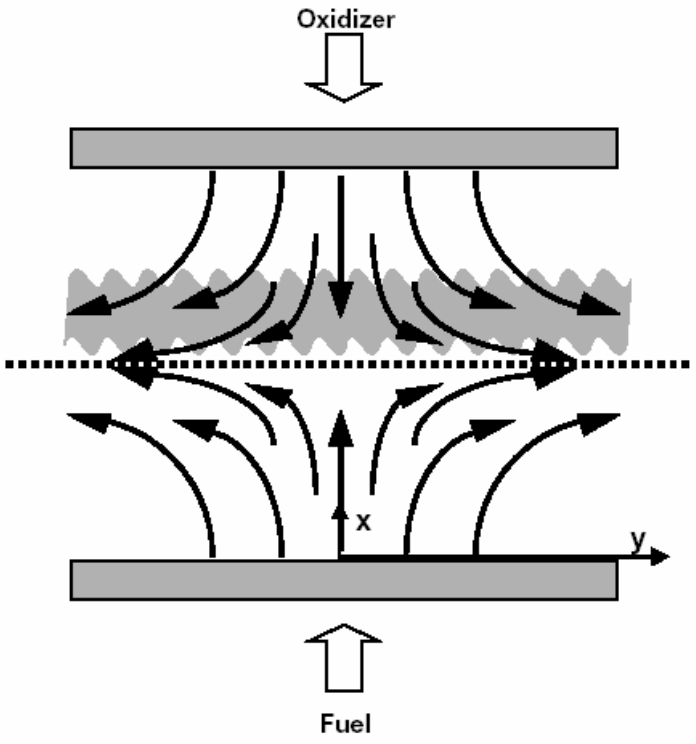


**Figure 4.66.** Figure 2-A: Planar Opposed Flow Diffusion Flame

At steady-state, the continuity equation becomes $\frac{\partial}{\partial x_j}\left(\rho u_j\right) = 0$. Oppdif breaks this down into a single equation for both the 3D and the 2D cases:

$$\frac{\partial}{\partial x}(\rho u) + \frac{1}{\xi^{n-2}}\frac{\partial}{\partial \xi}\left(\rho v \xi^{n-2}\right) = 0$$

In this case, $\xi$ represents either the radial direction for the 3D case or the y direction for the 2D case and n assumes the value of 3 for the 3D case and 2 for the planar case. Using the substitutions $G(x) = -\frac{\rho u}{\xi}$ and $F(x) = \frac{\rho u}{(n-1)}$ reduces the continuity equation to:

$$G(x) = \frac{dF(x)}{dx}$$

This means that since F and G are functions of x only, and then pressure, temperature, velocity, and species concentrations are all also functions of x. The perpendicular case can now be assumed to follow:

$$H-(n-1)\frac{d}{dx}\left(\frac{FG}{\rho}\right)+\frac{nG^2}{\rho}+\frac{d}{dx}\left[\mu\frac{d}{dx}\left(\frac{G}{\rho}\right)\right]=0$$

The Energy equation is given as:

$$\rho u\frac{dT}{dx}-\frac{1}{c_p}\frac{d}{dx}\left(\lambda\frac{dT}{dx}\right)+\frac{\rho}{c_p}\sum_k c_{p,k}Y_k V_k\frac{dT}{dx}+\frac{1}{c_p}\sum_k h_k\dot{\omega}_k=0$$

The species equation is:

$$\rho u\frac{dY_k}{dx}+\frac{d}{dx}(\rho Y_k V_k)-\dot{\omega}_k W_k=0$$

Here, $V_k$ is either given by the multi-component formulation (when the keyword MULT is used):

$$V_k=\frac{1}{X_k\overline{W}}\sum_{j\neq k}^{K}W_j D_{k,j}\frac{dXLj}{dx}-\frac{D_k^T}{\rho Y_k}\frac{1}{T}\frac{dT}{dx}$$

or, when the mixture-averaged formulation is used (when the keyword MIX is used):

$$V_k=-\frac{1}{X_k}D_{km}\frac{dX_k}{dx}-\frac{D_k^T}{\rho Y_k}\frac{1}{T}\frac{dT}{dx}$$

where $D_{km}=\dfrac{1-Y_k}{\sum_{j\neq k}^{K}\dfrac{X_j}{D_{jk}}}$ and $D_{k,,j}$ , $D_{km}$, $D_{jk}$ and $D_k^T$ are the multi-component, mixture averaged, binary, and thermal diffusion coefficients, respectively.

The boundary conditions for these equations are as follows:

At x = 0 (Fuel Side):

$$F=\frac{\rho_F u_F}{(n-1)};\quad G=0;\quad T=T_F;\quad \rho u Y_k+\rho Y_k V_k=(\rho u Y_k)_F$$

At x = Final Length, L (Oxidizer Side):

$$F=\frac{\rho_O u_O}{(n-1)};\quad G=0;\quad T=T_O;\quad \rho u Y_k+\rho Y_k V_k=(\rho u Y_k)_O$$

## APPENDIX B

## THE GRI-MECH CHEMICAL MECHANISM

The GRI-Mech chemical mechanism used in this study is presented below (http://www.me.berkeley.edu/gri_mech/). The numbers given represent the variables in the Arrhenius Rate Expression (Glassman, 1996) of the reaction rate constants represented as $k = AT^n \exp(-E/RT)$, where the first through third columns are A, n, and E, respectively.

```
! GRI-Mech Version 3.0 7/30/99  CHEMKIN-II format
! See README30 file at anonymous FTP site unix.sri.com, directory gri;
! WorldWideWeb home page http://www.me.berkeley.edu/gri_mech/ or
! through http://www.gri.org , under 'Basic  Research',
! for additional information, contacts, and disclaimer
ELEMENTS
O  H  C  N  AR
END
SPECIES
H2      H       O       O2      OH      H2O     HO2     H2O2
C       CH      CH2     CH2(S)  CH3     CH4     CO      CO2
HCO     CH2O    CH2OH   CH3O    CH3OH   C2H     C2H2    C2H3
C2H4    C2H5    C2H6    HCCO    CH2CO   HCCOH   N       NH
NH2     NH3     NNH     NO      NO2     N2O     HNO     CN
HCN     H2CN    HCNN    HCNO    HOCN    HNCO    NCO     N2
AR      C3H7    C3H8    CH2CHO  CH3CHO
END
!THERMO
! Insert GRI-Mech thermodynamics here or use in default file
!END
REACTIONS
2O+M<=>O2+M                               1.200E+17   -1.000        .00
H2/ 2.40/ H2O/15.40/ CH4/ 2.00/ CO/ 1.75/ CO2/ 3.60/ C2H6/ 3.00/ AR/  .83/
O+H+M<=>OH+M                              5.000E+17   -1.000        .00
H2/2.00/ H2O/6.00/ CH4/2.00/ CO/1.50/ CO2/2.00/ C2H6/3.00/ AR/ .70/
O+H2<=>H+OH                               3.870E+04    2.700    6260.00
O+HO2<=>OH+O2                             2.000E+13     .000        .00
O+H2O2<=>OH+HO2                           9.630E+06    2.000    4000.00
O+CH<=>H+CO                               5.700E+13     .000        .00
O+CH2<=>H+HCO                             8.000E+13     .000        .00
O+CH2(S)<=>H2+CO                          1.500E+13     .000        .00
O+CH2(S)<=>H+HCO                          1.500E+13     .000        .00
O+CH3<=>H+CH2O                            5.060E+13     .000        .00
O+CH4<=>OH+CH3                            1.020E+09    1.500    8600.00
O+CO(+M)<=>CO2(+M)                        1.800E+10     .000    2385.00
   LOW/ 6.020E+14     .000    3000.00/
H2/2.00/ O2/6.00/ H2O/6.00/ CH4/2.00/ CO/1.50/ CO2/3.50/ C2H6/3.00/ AR/
.50/
O+HCO<=>OH+CO                             3.000E+13     .000        .00
O+HCO<=>H+CO2                             3.000E+13     .000        .00
O+CH2O<=>OH+HCO                           3.900E+13     .000    3540.00
```

```
O+CH2OH<=>OH+CH2O                         1.000E+13     .000        .00
O+CH3O<=>OH+CH2O                          1.000E+13     .000        .00
O+CH3OH<=>OH+CH2OH                        3.880E+05    2.500    3100.00
O+CH3OH<=>OH+CH3O                         1.300E+05    2.500    5000.00
O+C2H<=>CH+CO                             5.000E+13     .000        .00
O+C2H2<=>H+HCCO                           1.350E+07    2.000    1900.00
O+C2H2<=>OH+C2H                           4.600E+19   -1.410   28950.00
O+C2H2<=>CO+CH2                           6.940E+06    2.000    1900.00
O+C2H3<=>H+CH2CO                          3.000E+13     .000        .00
O+C2H4<=>CH3+HCO                          1.250E+07    1.830     220.00
O+C2H5<=>CH3+CH2O                         2.240E+13     .000        .00
O+C2H6<=>OH+C2H5                          8.980E+07    1.920    5690.00
O+HCCO<=>H+2CO                            1.000E+14     .000        .00
O+CH2CO<=>OH+HCCO                         1.000E+13     .000    8000.00
O+CH2CO<=>CH2+CO2                         1.750E+12     .000    1350.00
O2+CO<=>O+CO2                             2.500E+12     .000   47800.00
O2+CH2O<=>HO2+HCO                         1.000E+14     .000   40000.00
H+O2+M<=>HO2+M                            2.800E+18    -.860        .00
O2/ .00/ H2O/ .00/ CO/ .75/ CO2/1.50/ C2H6/1.50/ N2/ .00/ AR/ .00/
H+2O2<=>HO2+O2                            2.080E+19   -1.240        .00
H+O2+H2O<=>HO2+H2O                        11.26E+18    -.760        .00
H+O2+N2<=>HO2+N2                          2.600E+19   -1.240        .00
H+O2+AR<=>HO2+AR                          7.000E+17    -.800        .00
H+O2<=>O+OH                               2.650E+16    -.6707  17041.00
2H+M<=>H2+M                               1.000E+18   -1.000        .00
H2/ .00/ H2O/ .00/ CH4/2.00/ CO2/ .00/ C2H6/3.00/ AR/ .63/
2H+H2<=>2H2                               9.000E+16    -.600        .00
2H+H2O<=>H2+H2O                           6.000E+19   -1.250        .00
2H+CO2<=>H2+CO2                           5.500E+20   -2.000        .00
H+OH+M<=>H2O+M                            2.200E+22   -2.000        .00
H2/ .73/ H2O/3.65/ CH4/2.00/ C2H6/3.00/ AR/ .38/
H+HO2<=>O+H2O                             3.970E+12     .000     671.00
H+HO2<=>O2+H2                             4.480E+13     .000    1068.00
H+HO2<=>2OH                               0.840E+14     .000     635.00
H+H2O2<=>HO2+H2                           1.210E+07    2.000    5200.00
H+H2O2<=>OH+H2O                           1.000E+13     .000    3600.00
H+CH<=>C+H2                               1.650E+14     .000        .00
H+CH2(+M)<=>CH3(+M)                       6.000E+14     .000        .00
     LOW  /  1.040E+26   -2.760   1600.00/
     TROE/   .5620  91.00  5836.00  8552.00/
H2/2.00/ H2O/6.00/ CH4/2.00/ CO/1.50/ CO2/2.00/ C2H6/3.00/ AR/ .70/
H+CH2(S)<=>CH+H2                          3.000E+13     .000        .00
H+CH3(+M)<=>CH4(+M)                       13.90E+15    -.534     536.00
     LOW  /  2.620E+33   -4.760   2440.00/
     TROE/   .7830   74.00  2941.00  6964.00 /
H2/2.00/ H2O/6.00/ CH4/3.00/ CO/1.50/ CO2/2.00/ C2H6/3.00/ AR/ .70/
H+CH4<=>CH3+H2                            6.600E+08    1.620   10840.00
H+HCO(+M)<=>CH2O(+M)                      1.090E+12     .480    -260.00
     LOW  /  2.470E+24   -2.570    425.00/
     TROE/   .7824  271.00  2755.00  6570.00 /
H2/2.00/ H2O/6.00/ CH4/2.00/ CO/1.50/ CO2/2.00/ C2H6/3.00/ AR/ .70/
H+HCO<=>H2+CO                             7.340E+13     .000        .00
H+CH2O(+M)<=>CH2OH(+M)                    5.400E+11     .454    3600.00
     LOW  /  1.270E+32   -4.820   6530.00/
```

```
     TROE/   .7187  103.00  1291.00  4160.00 /
H2/2.00/ H2O/6.00/ CH4/2.00/ CO/1.50/ CO2/2.00/ C2H6/3.00/
H+CH2O(+M)<=>CH3O(+M)                    5.400E+11     .454    2600.00
     LOW  /  2.200E+30   -4.800   5560.00/
     TROE/   .7580   94.00  1555.00  4200.00 /
H2/2.00/ H2O/6.00/ CH4/2.00/ CO/1.50/ CO2/2.00/ C2H6/3.00/
H+CH2O<=>HCO+H2                          5.740E+07    1.900    2742.00
H+CH2OH(+M)<=>CH3OH(+M)                  1.055E+12     .500      86.00
     LOW  /  4.360E+31   -4.650   5080.00/
     TROE/   .600  100.00  90000.0  10000.0 /
H2/2.00/ H2O/6.00/ CH4/2.00/ CO/1.50/ CO2/2.00/ C2H6/3.00/
H+CH2OH<=>H2+CH2O                        2.000E+13     .000        .00
H+CH2OH<=>OH+CH3                         1.650E+11     .650    -284.00
H+CH2OH<=>CH2(S)+H2O                     3.280E+13    -.090     610.00
H+CH3O(+M)<=>CH3OH(+M)                   2.430E+12     .515      50.00
     LOW  /  4.660E+41   -7.440   14080.0/
     TROE/   .700  100.00  90000.0 10000.00 /
H2/2.00/ H2O/6.00/ CH4/2.00/ CO/1.50/ CO2/2.00/ C2H6/3.00/
H+CH3O<=>H+CH2OH                         4.150E+07    1.630    1924.00
H+CH3O<=>H2+CH2O                         2.000E+13     .000        .00
H+CH3O<=>OH+CH3                          1.500E+12     .500    -110.00
H+CH3O<=>CH2(S)+H2O                      2.620E+14    -.230    1070.00
H+CH3OH<=>CH2OH+H2                       1.700E+07    2.100    4870.00
H+CH3OH<=>CH3O+H2                        4.200E+06    2.100    4870.00
H+C2H(+M)<=>C2H2(+M)                     1.000E+17   -1.000        .00
     LOW  /  3.750E+33   -4.800   1900.00/
     TROE/   .6464  132.00  1315.00  5566.00 /
H2/2.00/ H2O/6.00/ CH4/2.00/ CO/1.50/ CO2/2.00/ C2H6/3.00/ AR/ .70/
H+C2H2(+M)<=>C2H3(+M)                    5.600E+12     .000    2400.00
     LOW  /  3.800E+40   -7.270   7220.00/
     TROE/   .7507   98.50  1302.00  4167.00 /
H2/2.00/ H2O/6.00/ CH4/2.00/ CO/1.50/ CO2/2.00/ C2H6/3.00/ AR/ .70/
H+C2H3(+M)<=>C2H4(+M)                    6.080E+12     .270     280.00
     LOW  /  1.400E+30   -3.860   3320.00/
     TROE/   .7820  207.50  2663.00  6095.00 /
H2/2.00/ H2O/6.00/ CH4/2.00/ CO/1.50/ CO2/2.00/ C2H6/3.00/ AR/ .70/
H+C2H3<=>H2+C2H2                         3.000E+13     .000        .00
H+C2H4(+M)<=>C2H5(+M)                    0.540E+12     .454    1820.00
     LOW  /  0.600E+42   -7.620   6970.00/
     TROE/   .9753  210.00   984.00  4374.00 /
H2/2.00/ H2O/6.00/ CH4/2.00/ CO/1.50/ CO2/2.00/ C2H6/3.00/ AR/ .70/
H+C2H4<=>C2H3+H2                         1.325E+06    2.530   12240.00
H+C2H5(+M)<=>C2H6(+M)                    5.210E+17    -.990    1580.00
     LOW  /  1.990E+41   -7.080   6685.00/
     TROE/   .8422  125.00  2219.00  6882.00 /
H2/2.00/ H2O/6.00/ CH4/2.00/ CO/1.50/ CO2/2.00/ C2H6/3.00/ AR/ .70/
H+C2H5<=>H2+C2H4                         2.000E+12     .000        .00
H+C2H6<=>C2H5+H2                         1.150E+08    1.900    7530.00
H+HCCO<=>CH2(S)+CO                       1.000E+14     .000        .00
H+CH2CO<=>HCCO+H2                        5.000E+13     .000    8000.00
H+CH2CO<=>CH3+CO                         1.130E+13     .000    3428.00
H+HCCOH<=>H+CH2CO                        1.000E+13     .000        .00
H2+CO(+M)<=>CH2O(+M)                     4.300E+07    1.500   79600.00
     LOW  /  5.070E+27   -3.420  84350.00/
```

```
     TROE/   .9320  197.00  1540.00 10300.00 /
H2/2.00/ H2O/6.00/ CH4/2.00/ CO/1.50/ CO2/2.00/ C2H6/3.00/ AR/ .70/
OH+H2<=>H+H2O                             2.160E+08    1.510    3430.00
2OH(+M)<=>H2O2(+M)                        7.400E+13    -.370        .00
     LOW  /  2.300E+18    -.900  -1700.00/
     TROE/   .7346   94.00  1756.00  5182.00 /
H2/2.00/ H2O/6.00/ CH4/2.00/ CO/1.50/ CO2/2.00/ C2H6/3.00/ AR/ .70/
2OH<=>O+H2O                               3.570E+04    2.400   -2110.00
OH+HO2<=>O2+H2O                           1.450E+13     .000    -500.00
 DUPLICATE
OH+H2O2<=>HO2+H2O                         2.000E+12     .000     427.00
 DUPLICATE
OH+H2O2<=>HO2+H2O                         1.700E+18     .000   29410.00
 DUPLICATE
OH+C<=>H+CO                               5.000E+13     .000        .00
OH+CH<=>H+HCO                             3.000E+13     .000        .00
OH+CH2<=>H+CH2O                           2.000E+13     .000        .00
OH+CH2<=>CH+H2O                           1.130E+07    2.000    3000.00
OH+CH2(S)<=>H+CH2O                        3.000E+13     .000        .00
OH+CH3(+M)<=>CH3OH(+M)                    2.790E+18   -1.430    1330.00
     LOW  /  4.000E+36   -5.920   3140.00/
     TROE/   .4120  195.0  5900.00  6394.00/
H2/2.00/ H2O/6.00/ CH4/2.00/ CO/1.50/ CO2/2.00/ C2H6/3.00/
OH+CH3<=>CH2+H2O                          5.600E+07    1.600    5420.00
OH+CH3<=>CH2(S)+H2O                       6.440E+17   -1.340    1417.00
OH+CH4<=>CH3+H2O                          1.000E+08    1.600    3120.00
OH+CO<=>H+CO2                             4.760E+07    1.228      70.00
OH+HCO<=>H2O+CO                           5.000E+13     .000        .00
OH+CH2O<=>HCO+H2O                         3.430E+09    1.180    -447.00
OH+CH2OH<=>H2O+CH2O                       5.000E+12     .000        .00
OH+CH3O<=>H2O+CH2O                        5.000E+12     .000        .00
OH+CH3OH<=>CH2OH+H2O                      1.440E+06    2.000    -840.00
OH+CH3OH<=>CH3O+H2O                       6.300E+06    2.000    1500.00
OH+C2H<=>H+HCCO                           2.000E+13     .000        .00
OH+C2H2<=>H+CH2CO                         2.180E-04    4.500   -1000.00
OH+C2H2<=>H+HCCOH                         5.040E+05    2.300   13500.00
OH+C2H2<=>C2H+H2O                         3.370E+07    2.000   14000.00
OH+C2H2<=>CH3+CO                          4.830E-04    4.000   -2000.00
OH+C2H3<=>H2O+C2H2                        5.000E+12     .000        .00
OH+C2H4<=>C2H3+H2O                        3.600E+06    2.000    2500.00
OH+C2H6<=>C2H5+H2O                        3.540E+06    2.120     870.00
OH+CH2CO<=>HCCO+H2O                       7.500E+12     .000    2000.00
2HO2<=>O2+H2O2                            1.300E+11     .000   -1630.00
 DUPLICATE
2HO2<=>O2+H2O2                            4.200E+14     .000   12000.00
 DUPLICATE
HO2+CH2<=>OH+CH2O                         2.000E+13     .000        .00
HO2+CH3<=>O2+CH4                          1.000E+12     .000        .00
HO2+CH3<=>OH+CH3O                         3.780E+13     .000        .00
HO2+CO<=>OH+CO2                           1.500E+14     .000   23600.00
HO2+CH2O<=>HCO+H2O2                       5.600E+06    2.000   12000.00
C+O2<=>O+CO                               5.800E+13     .000     576.00
C+CH2<=>H+C2H                             5.000E+13     .000        .00
C+CH3<=>H+C2H2                            5.000E+13     .000        .00
```

```
CH+O2<=>O+HCO                             6.710E+13     .000        .00
CH+H2<=>H+CH2                             1.080E+14     .000    3110.00
CH+H2O<=>H+CH2O                           5.710E+12     .000    -755.00
CH+CH2<=>H+C2H2                           4.000E+13     .000        .00
CH+CH3<=>H+C2H3                           3.000E+13     .000        .00
CH+CH4<=>H+C2H4                           6.000E+13     .000        .00
CH+CO(+M)<=>HCCO(+M)                      5.000E+13     .000        .00
     LOW  /  2.690E+28   -3.740   1936.00/
     TROE/   .5757  237.00  1652.00  5069.00 /
H2/2.00/ H2O/6.00/ CH4/2.00/ CO/1.50/ CO2/2.00/ C2H6/3.00/ AR/ .70/
CH+CO2<=>HCO+CO                           1.900E+14     .000   15792.00
CH+CH2O<=>H+CH2CO                         9.460E+13     .000    -515.00
CH+HCCO<=>CO+C2H2                         5.000E+13     .000        .00
CH2+O2=>OH+H+CO                           5.000E+12     .000    1500.00
CH2+H2<=>H+CH3                            5.000E+05    2.000    7230.00
2CH2<=>H2+C2H2                            1.600E+15     .000   11944.00
CH2+CH3<=>H+C2H4                          4.000E+13     .000        .00
CH2+CH4<=>2CH3                            2.460E+06    2.000    8270.00
CH2+CO(+M)<=>CH2CO(+M)                    8.100E+11     .500    4510.00
     LOW  /  2.690E+33   -5.110   7095.00/
     TROE/   .5907  275.00  1226.00  5185.00 /
H2/2.00/ H2O/6.00/ CH4/2.00/ CO/1.50/ CO2/2.00/ C2H6/3.00/ AR/ .70/
CH2+HCCO<=>C2H3+CO                        3.000E+13     .000        .00
CH2(S)+N2<=>CH2+N2                        1.500E+13     .000     600.00
CH2(S)+AR<=>CH2+AR                        9.000E+12     .000     600.00
CH2(S)+O2<=>H+OH+CO                       2.800E+13     .000        .00
CH2(S)+O2<=>CO+H2O                        1.200E+13     .000        .00
CH2(S)+H2<=>CH3+H                         7.000E+13     .000        .00
CH2(S)+H2O(+M)<=>CH3OH(+M)                4.820E+17   -1.160    1145.00
     LOW  /  1.880E+38   -6.360   5040.00/
     TROE/   .6027  208.00  3922.00  10180.0 /
H2/2.00/ H2O/6.00/ CH4/2.00/ CO/1.50/ CO2/2.00/ C2H6/3.00/
CH2(S)+H2O<=>CH2+H2O                      3.000E+13     .000        .00
CH2(S)+CH3<=>H+C2H4                       1.200E+13     .000    -570.00
CH2(S)+CH4<=>2CH3                         1.600E+13     .000    -570.00
CH2(S)+CO<=>CH2+CO                        9.000E+12     .000        .00
CH2(S)+CO2<=>CH2+CO2                      7.000E+12     .000        .00
CH2(S)+CO2<=>CO+CH2O                      1.400E+13     .000        .00
CH2(S)+C2H6<=>CH3+C2H5                    4.000E+13     .000    -550.00
CH3+O2<=>O+CH3O                           3.560E+13     .000   30480.00
CH3+O2<=>OH+CH2O                          2.310E+12     .000   20315.00
CH3+H2O2<=>HO2+CH4                        2.450E+04    2.470    5180.00
2CH3(+M)<=>C2H6(+M)                       6.770E+16   -1.180     654.00
     LOW  /  3.400E+41   -7.030   2762.00/
     TROE/   .6190  73.20  1180.00  9999.00 /
H2/2.00/ H2O/6.00/ CH4/2.00/ CO/1.50/ CO2/2.00/ C2H6/3.00/ AR/ .70/
2CH3<=>H+C2H5                             6.840E+12     .100   10600.00
CH3+HCO<=>CH4+CO                          2.648E+13     .000        .00
CH3+CH2O<=>HCO+CH4                        3.320E+03    2.810    5860.00
CH3+CH3OH<=>CH2OH+CH4                     3.000E+07    1.500    9940.00
CH3+CH3OH<=>CH3O+CH4                      1.000E+07    1.500    9940.00
CH3+C2H4<=>C2H3+CH4                       2.270E+05    2.000    9200.00
CH3+C2H6<=>C2H5+CH4                       6.140E+06    1.740   10450.00
HCO+H2O<=>H+CO+H2O                        1.500E+18   -1.000   17000.00
```

```
HCO+M<=>H+CO+M                            1.870E+17   -1.000   17000.00
H2/2.00/ H2O/ .00/ CH4/2.00/ CO/1.50/ CO2/2.00/ C2H6/3.00/
HCO+O2<=>HO2+CO                           13.45E+12     .000     400.00
CH2OH+O2<=>HO2+CH2O                       1.800E+13     .000     900.00
CH3O+O2<=>HO2+CH2O                        4.280E-13    7.600   -3530.00
C2H+O2<=>HCO+CO                           1.000E+13     .000    -755.00
C2H+H2<=>H+C2H2                           5.680E+10    0.900    1993.00
C2H3+O2<=>HCO+CH2O                        4.580E+16   -1.390    1015.00
C2H4(+M)<=>H2+C2H2(+M)                    8.000E+12     .440   86770.00
     LOW  /  1.580E+51   -9.300  97800.00/
     TROE/   .7345  180.00  1035.00  5417.00 /
H2/2.00/ H2O/6.00/ CH4/2.00/ CO/1.50/ CO2/2.00/ C2H6/3.00/ AR/ .70/
C2H5+O2<=>HO2+C2H4                        8.400E+11     .000    3875.00
HCCO+O2<=>OH+2CO                          3.200E+12     .000     854.00
2HCCO<=>2CO+C2H2                          1.000E+13     .000        .00
N+NO<=>N2+O                               2.700E+13     .000     355.00
N+O2<=>NO+O                               9.000E+09    1.000    6500.00
N+OH<=>NO+H                               3.360E+13     .000     385.00
N2O+O<=>N2+O2                             1.400E+12     .000   10810.00
N2O+O<=>2NO                               2.900E+13     .000   23150.00
N2O+H<=>N2+OH                             3.870E+14     .000   18880.00
N2O+OH<=>N2+HO2                           2.000E+12     .000   21060.00
N2O(+M)<=>N2+O(+M)                        7.910E+10     .000   56020.00
     LOW  /  6.370E+14     .000  56640.00/
H2/2.00/ H2O/6.00/ CH4/2.00/ CO/1.50/ CO2/2.00/ C2H6/3.00/ AR/ .625/
HO2+NO<=>NO2+OH                           2.110E+12     .000    -480.00
NO+O+M<=>NO2+M                            1.060E+20   -1.410        .00
H2/2.00/ H2O/6.00/ CH4/2.00/ CO/1.50/ CO2/2.00/ C2H6/3.00/ AR/ .70/
NO2+O<=>NO+O2                             3.900E+12     .000    -240.00
NO2+H<=>NO+OH                             1.320E+14     .000     360.00
NH+O<=>NO+H                               4.000E+13     .000        .00
NH+H<=>N+H2                               3.200E+13     .000     330.00
NH+OH<=>HNO+H                             2.000E+13     .000        .00
NH+OH<=>N+H2O                             2.000E+09    1.200        .00
NH+O2<=>HNO+O                             4.610E+05    2.000    6500.00
NH+O2<=>NO+OH                             1.280E+06    1.500     100.00
NH+N<=>N2+H                               1.500E+13     .000        .00
NH+H2O<=>HNO+H2                           2.000E+13     .000   13850.00
NH+NO<=>N2+OH                             2.160E+13    -.230        .00
NH+NO<=>N2O+H                             3.650E+14    -.450        .00
NH2+O<=>OH+NH                             3.000E+12     .000        .00
NH2+O<=>H+HNO                             3.900E+13     .000        .00
NH2+H<=>NH+H2                             4.000E+13     .000    3650.00
NH2+OH<=>NH+H2O                           9.000E+07    1.500    -460.00
NNH<=>N2+H                                3.300E+08     .000        .00
NNH+M<=>N2+H+M                            1.300E+14    -.110    4980.00
H2/2.00/ H2O/6.00/ CH4/2.00/ CO/1.50/ CO2/2.00/ C2H6/3.00/ AR/ .70/
NNH+O2<=>HO2+N2                           5.000E+12     .000        .00
NNH+O<=>OH+N2                             2.500E+13     .000        .00
NNH+O<=>NH+NO                             7.000E+13     .000        .00
NNH+H<=>H2+N2                             5.000E+13     .000        .00
NNH+OH<=>H2O+N2                           2.000E+13     .000        .00
NNH+CH3<=>CH4+N2                          2.500E+13     .000        .00
H+NO+M<=>HNO+M                            4.480E+19   -1.320     740.00
```

```
H2/2.00/ H2O/6.00/ CH4/2.00/ CO/1.50/ CO2/2.00/ C2H6/3.00/ AR/ .70/
HNO+O<=>NO+OH                             2.500E+13     .000        .00
HNO+H<=>H2+NO                             9.000E+11     .720     660.00
HNO+OH<=>NO+H2O                           1.300E+07    1.900    -950.00
HNO+O2<=>HO2+NO                           1.000E+13     .000   13000.00
CN+O<=>CO+N                               7.700E+13     .000        .00
CN+OH<=>NCO+H                             4.000E+13     .000        .00
CN+H2O<=>HCN+OH                           8.000E+12     .000    7460.00
CN+O2<=>NCO+O                             6.140E+12     .000    -440.00
CN+H2<=>HCN+H                             2.950E+05    2.450    2240.00
NCO+O<=>NO+CO                             2.350E+13     .000        .00
NCO+H<=>NH+CO                             5.400E+13     .000        .00
NCO+OH<=>NO+H+CO                          0.250E+13     .000        .00
NCO+N<=>N2+CO                             2.000E+13     .000        .00
NCO+O2<=>NO+CO2                           2.000E+12     .000   20000.00
NCO+M<=>N+CO+M                            3.100E+14     .000   54050.00
H2/2.00/ H2O/6.00/ CH4/2.00/ CO/1.50/ CO2/2.00/ C2H6/3.00/ AR/ .70/
NCO+NO<=>N2O+CO                           1.900E+17   -1.520     740.00
NCO+NO<=>N2+CO2                           3.800E+18   -2.000     800.00
HCN+M<=>H+CN+M                            1.040E+29   -3.300  126600.00
H2/2.00/ H2O/6.00/ CH4/2.00/ CO/1.50/ CO2/2.00/ C2H6/3.00/ AR/ .70/
HCN+O<=>NCO+H                             2.030E+04    2.640    4980.00
HCN+O<=>NH+CO                             5.070E+03    2.640    4980.00
HCN+O<=>CN+OH                             3.910E+09    1.580   26600.00
HCN+OH<=>HOCN+H                           1.100E+06    2.030   13370.00
HCN+OH<=>HNCO+H                           4.400E+03    2.260    6400.00
HCN+OH<=>NH2+CO                           1.600E+02    2.560    9000.00
H+HCN(+M)<=>H2CN(+M)                      3.300E+13     .000        .00
      LOW /  1.400E+26   -3.400    1900.00/
H2/2.00/ H2O/6.00/ CH4/2.00/ CO/1.50/ CO2/2.00/ C2H6/3.00/ AR/ .70/
H2CN+N<=>N2+CH2                           6.000E+13     .000     400.00
C+N2<=>CN+N                               6.300E+13     .000   46020.00
CH+N2<=>HCN+N                             3.120E+09    0.880   20130.00
CH+N2(+M)<=>HCNN(+M)                      3.100E+12     .150        .00
     LOW  /  1.300E+25   -3.160    740.00/
     TROE/   .6670  235.00  2117.00  4536.00 /
H2/2.00/ H2O/6.00/ CH4/2.00/ CO/1.50/ CO2/2.00/ C2H6/3.00/ AR/ 1.0/
CH2+N2<=>HCN+NH                           1.000E+13     .000   74000.00
CH2(S)+N2<=>NH+HCN                        1.000E+11     .000   65000.00
C+NO<=>CN+O                               1.900E+13     .000        .00
C+NO<=>CO+N                               2.900E+13     .000        .00
CH+NO<=>HCN+O                             4.100E+13     .000        .00
CH+NO<=>H+NCO                             1.620E+13     .000        .00
CH+NO<=>N+HCO                             2.460E+13     .000        .00
CH2+NO<=>H+HNCO                           3.100E+17   -1.380    1270.00
CH2+NO<=>OH+HCN                           2.900E+14    -.690     760.00
CH2+NO<=>H+HCNO                           3.800E+13    -.360     580.00
CH2(S)+NO<=>H+HNCO                        3.100E+17   -1.380    1270.00
CH2(S)+NO<=>OH+HCN                        2.900E+14    -.690     760.00
CH2(S)+NO<=>H+HCNO                        3.800E+13    -.360     580.00
CH3+NO<=>HCN+H2O                          9.600E+13     .000   28800.00
CH3+NO<=>H2CN+OH                          1.000E+12     .000   21750.00
HCNN+O<=>CO+H+N2                          2.200E+13     .000        .00
HCNN+O<=>HCN+NO                           2.000E+12     .000        .00
```

```
HCNN+O2<=>O+HCO+N2                        1.200E+13     .000        .00
HCNN+OH<=>H+HCO+N2                        1.200E+13     .000        .00
HCNN+H<=>CH2+N2                           1.000E+14     .000        .00
HNCO+O<=>NH+CO2                           9.800E+07    1.410    8500.00
HNCO+O<=>HNO+CO                           1.500E+08    1.570   44000.00
HNCO+O<=>NCO+OH                           2.200E+06    2.110   11400.00
HNCO+H<=>NH2+CO                           2.250E+07    1.700    3800.00
HNCO+H<=>H2+NCO                           1.050E+05    2.500   13300.00
HNCO+OH<=>NCO+H2O                         3.300E+07    1.500    3600.00
HNCO+OH<=>NH2+CO2                         3.300E+06    1.500    3600.00
HNCO+M<=>NH+CO+M                          1.180E+16     .000   84720.00
H2/2.00/ H2O/6.00/ CH4/2.00/ CO/1.50/ CO2/2.00/ C2H6/3.00/ AR/ .70/
HCNO+H<=>H+HNCO                           2.100E+15    -.690    2850.00
HCNO+H<=>OH+HCN                           2.700E+11     .180    2120.00
HCNO+H<=>NH2+CO                           1.700E+14    -.750    2890.00
HOCN+H<=>H+HNCO                           2.000E+07    2.000    2000.00
HCCO+NO<=>HCNO+CO                         0.900E+13     .000        .00
CH3+N<=>H2CN+H                            6.100E+14    -.310     290.00
CH3+N<=>HCN+H2                            3.700E+12     .150     -90.00
NH3+H<=>NH2+H2                            5.400E+05    2.400    9915.00
NH3+OH<=>NH2+H2O                          5.000E+07    1.600     955.00
NH3+O<=>NH2+OH                            9.400E+06    1.940    6460.00
NH+CO2<=>HNO+CO                           1.000E+13     .000   14350.00
CN+NO2<=>NCO+NO                           6.160E+15   -0.752     345.00
NCO+NO2<=>N2O+CO2                         3.250E+12     .000    -705.00
N+CO2<=>NO+CO                             3.000E+12     .000   11300.00
O+CH3=>H+H2+CO                            3.370E+13     .000        .00
O+C2H4<=>H+CH2CHO                         6.700E+06    1.830     220.00
O+C2H5<=>H+CH3CHO                         1.096E+14     .000        .00
OH+HO2<=>O2+H2O                           0.500E+16     .000   17330.00
  DUPLICATE
OH+CH3=>H2+CH2O                           8.000E+09     .500   -1755.00
CH+H2(+M)<=>CH3(+M)                       1.970E+12     .430    -370.00
   LOW/ 4.820E+25  -2.80  590.0 /
   TROE/ .578  122.0  2535.0  9365.0 /
H2/2.00/ H2O/6.00/ CH4/2.00/ CO/1.50/ CO2/2.00/ C2H6/3.00/ AR/ .70/
CH2+O2=>2H+CO2                            5.800E+12     .000    1500.00
CH2+O2<=>O+CH2O                           2.400E+12     .000    1500.00
CH2+CH2=>2H+C2H2                          2.000E+14     .000   10989.00
CH2(S)+H2O=>H2+CH2O                       6.820E+10     .250    -935.00
C2H3+O2<=>O+CH2CHO                        3.030E+11     .290      11.00
C2H3+O2<=>HO2+C2H2                        1.337E+06    1.610    -384.00
O+CH3CHO<=>OH+CH2CHO                      2.920E+12     .000    1808.00
O+CH3CHO=>OH+CH3+CO                       2.920E+12     .000    1808.00
O2+CH3CHO=>HO2+CH3+CO                     3.010E+13     .000   39150.00
H+CH3CHO<=>CH2CHO+H2                      2.050E+09    1.160    2405.00
H+CH3CHO=>CH3+H2+CO                       2.050E+09    1.160    2405.00
OH+CH3CHO=>CH3+H2O+CO                     2.343E+10    0.730   -1113.00
HO2+CH3CHO=>CH3+H2O2+CO                   3.010E+12     .000   11923.00
CH3+CH3CHO=>CH3+CH4+CO                    2.720E+06    1.770    5920.00
H+CH2CO(+M)<=>CH2CHO(+M)                  4.865E+11    0.422   -1755.00
    LOW/ 1.012E+42  -7.63  3854.0/
    TROE/ 0.465  201.0  1773.0  5333.0 /
H2/2.00/ H2O/6.00/ CH4/2.00/ CO/1.50/ CO2/2.00/ C2H6/3.00/ AR/ .70/
```

```
O+CH2CHO=>H+CH2+CO2                       1.500E+14     .000       .00
O2+CH2CHO=>OH+CO+CH2O                     1.810E+10     .000       .00
O2+CH2CHO=>OH+2HCO                        2.350E+10     .000       .00
H+CH2CHO<=>CH3+HCO                        2.200E+13     .000       .00
H+CH2CHO<=>CH2CO+H2                       1.100E+13     .000       .00
OH+CH2CHO<=>H2O+CH2CO                     1.200E+13     .000       .00
OH+CH2CHO<=>HCO+CH2OH                     3.010E+13     .000       .00
CH3+C2H5(+M)<=>C3H8(+M)                   .9430E+13     .000       .00
     LOW/ 2.710E+74  -16.82  13065.0 /
     TROE/ .1527  291.0  2742.0  7748.0 /
H2/2.00/ H2O/6.00/ CH4/2.00/ CO/1.50/ CO2/2.00/ C2H6/3.00/ AR/ .70/
O+C3H8<=>OH+C3H7                          1.930E+05    2.680   3716.00
H+C3H8<=>C3H7+H2                          1.320E+06    2.540   6756.00
OH+C3H8<=>C3H7+H2O                        3.160E+07    1.800    934.00
C3H7+H2O2<=>HO2+C3H8                      3.780E+02    2.720   1500.00
CH3+C3H8<=>C3H7+CH4                       0.903E+00    3.650   7154.00
CH3+C2H4(+M)<=>C3H7(+M)                   2.550E+06    1.600   5700.00
      LOW/ 3.00E+63  -14.6  18170./
      TROE/ .1894  277.0  8748.0  7891.0 /
H2/2.00/ H2O/6.00/ CH4/2.00/ CO/1.50/ CO2/2.00/ C2H6/3.00/ AR/ .70/
O+C3H7<=>C2H5+CH2O                        9.640E+13     .000       .00
H+C3H7(+M)<=>C3H8(+M)                     3.613E+13     .000       .00
      LOW/ 4.420E+61  -13.545  11357.0/
      TROE/ .315  369.0  3285.0  6667.0 /
H2/2.00/ H2O/6.00/ CH4/2.00/ CO/1.50/ CO2/2.00/ C2H6/3.00/ AR/ .70/
H+C3H7<=>CH3+C2H5                         4.060E+06    2.190    890.00
OH+C3H7<=>C2H5+CH2OH                      2.410E+13     .000       .00
HO2+C3H7<=>O2+C3H8                        2.550E+10    0.255   -943.00
HO2+C3H7=>OH+C2H5+CH2O                    2.410E+13     .000       .00
CH3+C3H7<=>2C2H5                          1.927E+13   -0.320       .00
END
```